

PREPARATION AND CHARACTERIZATION OF MATRIMID/P84 BLEND FILMS

by

SHUZHEN QIU

B.S., China University of Petroleum (East China), 2012

A THESIS

submitted in partial fulfillment of the requirements for the degree

MASTER OF SCIENCE

Department of Chemical Engineering
College of Engineering

KANSAS STATE UNIVERSITY
Manhattan, Kansas

2015

Approved by:

Major Professor
Mary Rezac

Abstract

Polymeric membranes have been playing important roles in gas or liquid separations. Polyimide polymers are of interest due to their commercial availability along with good transport, thermal and mechanical properties. In this study, two common commercial polyimide polymers, Matrimid and P84 were blended, to combine the good transport property of Matrimid with the plasticization resistance of P84. Matrimid/P84 blend solutions ranging from 0-100 wt. % Matrimid were prepared to make blend films. Physical properties (density, d-spacing, thickness), transport properties (permeability of H₂, N₂, CH₄, Ar, He, CO₂, and gas pairs selectivity), thermal property (mass loss curves of TGA), and liquid solutes (water, methanol, toluene, butanol, 1-propanol, 2-propanol) desorption behavior were measured or characterized.

Rules of changing behavior of the properties with mass fraction of Matrimid were investigated, summarized, and interpreted mathematically. As Matrimid mass fraction increases, there are more mobility and space between polymer chains, therefore there are smaller density, larger d-spacing, larger fractional free volume (FFV) and larger permeability. The selectivity-permeability relationship follows the trade-off line. Thermal mass loss curve of the blend films in air have presented intermediate characteristic with rising fraction of Matrimid compared to individual polymers. A partial-miscible behavior has been found from the correlation between permeability and FFV. The desorption behavior was found to be reasonably described by the case III model, where the diffusion rate is similar with relaxation rate of polymers.

Table of Contents

List of Figures	vi
List of Tables	x
Acknowledgements	xi
Chapter 1 - Introduction	1
1.1 Gas Separation Membrane	1
1.2 Polymer Blends	7
1.3 This Study	11
Chapter 2 - Characterization of Physical and Thermal Properties of Matrimid/P84 Blend Films	12
2.1 Introduction	12
2.2 Experimental	13
2.2.1 Materials	13
2.2.2 Preparation of Matrimid/P84 Blend Films	14
2.2.3 Density Measurement	14
2.2.4 Thickness Measurement	16
2.2.5 X-ray Diffraction Characterization	16
2.2.6 Thermogravimetric Analysis	17
2.3 Results and Discussion	18
2.3.1 Observation of Stamps of Matrimid/P84 Blend Films	18
2.3.2 Density of Matrimid/P84 Blend Films	18
2.3.3 d-spacing of Matrimid/P84 Blend Films	20
2.3.4 TGA of Matrimid/P84 Blend Films in Air	21
2.3.5 TGA of Matrimid/P84 Blend Films in N ₂	23

2.4 Conclusion	24
Chapter 3 - Transport Property of Matrimid/P84 Blend Films.....	25
3.1 Introduction.....	25
3.2 Experimental.....	26
3.2.1 Materials	26
3.2.2 Preparation of Matrimid/P84 Blend Films.....	27
3.2.3 Gas Permeability Measurement	28
3.3 Results and Discussion	30
3.3.1 Permeability and Mass Fraction of Matrimid	30
3.3.2 Selectivity and Permeability	31
3.3.3 Permeability and Polymer Volume Fraction.....	33
3.3.4 Permeability and Fractional Free Volume (FFV)	40
3.4 Conclusion	42
Chapter 4 - Desorption of Liquid Solutes in Matrimid/P84 Blend Films.....	43
4.1 Introduction.....	43
4.2 Experimental.....	46
4.2.1 Materials	46
4.2.2 Preparation of Matrimid/P84 Blend Films.....	46
4.2.3 Desorption Measurement of Liquid Solutes in Matrimid/P84 Blend Films	47
4.2 Mathematical Models for Desorption.....	48
4.2.1 Crank's Model	48
4.2.2 Wang's Model.....	48
4.2.3 Variable Surface-Concentration Model	49

4.3 Results and Discussion	50
4.3.1 Investigation of Experimental Data	50
4.3.2 General Comparison of Three Models.....	52
4.3.3 Mass Fraction of Matrimid and Diffusion Coefficients in Three Models	56
4.3.4 Diffusion Coefficients and Relaxation Rate Constant k	60
4.4 Conclusion	63
Chapter 5 - Conclusion	64
References.....	66
Appendix A - Physical Properties of Matrimid/P84 Blend Films	75
Appendix B - Permeability of Matrimid/P84 Blend Films.....	83
Appendix C - Matrimid/PBI Blend Films.....	94

List of Figures

Figure 1.1 Membrane.....	1
Figure 1.2 Simple Module Structure of Membrane Reactor.....	2
Figure 1.3 SEM Cross-Section of PEI Membrane.....	2
Figure 1.4 Free Energy of Mixing for Binary Mixtures. A: completely immiscible;.....	8
Figure 1.5 Phase Diagram Showing LCST and UCST Behavior for Polymer Blends.....	10
Figure 2.1 Chemical Structures of Matrimid and P84	13
Figure 2.2 Measured Spots Distribution on a Sample Film Stamp.....	16
Figure 2.3 Photos of Stamps of Matrimid/P84 Blend Films.....	18
Figure 2.4 Correlation of Film Density with Mass Fraction of Matrimid	19
Figure 2.5 FFV of Matrimid/P84 Blend Films from Two Groups of Calculations	19
Figure 2.6 An Example of Raw XRD Data of Pure Matrimid Film.....	20
Figure 2.7 d-spacing of Matrimid/P84 Blend Films	20
Figure 2.8 TGA Mass Loss Curves of Matrimid/P84 in Air Flow	22
Figure 2.9 TGA Mass Loss Curves of Matrimid/P84 in N ₂ flow	23
Figure 3.1 Chemical Structures of Matrimid and P84	26
Figure 3.2 Schematic Diagram of Gas Permeability Measurement Apparatus	28
Figure 3.3 Detailed Structure of Diffusion Cell.....	28
Figure 3.4 Permeability of Matrimid/P84 Blend Films	30
Figure 3.5 Permselectivity of H ₂ /N ₂ versus H ₂ permeability. 10 atm, 35 °C	32
Figure 3.6 Permselectivity of CO ₂ /CH ₄ versus CO ₂ permeability. 10 atm, 35 °C	33
Figure 3.7 Correlation of P(CH ₄) with Matrimid vol. % with Six Models for Matrimid/P84 Blend Films	36

Figure 3.8 Correlation of P(N ₂) with Matrimid vol. % with Series Model for Matrimid/P84 Blend Films	37
Figure 3.9 Correlation of P(Ar) with Matrimid vol. % with Series Model for Matrimid/P84 Blend Films	37
Figure 3.10 Correlation of P(CO ₂) with Matrimid vol. % with Series Model for Matrimid/P84 Blend Films	38
Figure 3.11 Correlation of P(H ₂) with Matrimid vol. % with Series Model for Matrimid/P84 Blend Films	39
Figure 3.12 Correlation of P(He) with Matrimid vol. % with Series Model for Matrimid/P84 Blend Films	39
Figure 3.13 Correlation of CH ₄ , N ₂ , Ar CO ₂ , He, and H ₂ permeability with 1/FFV. For each gas, from left to right, the data points represent films of 100, 75, 50, 25, 0wt% Matrimid. FFV is calculated from Resource I [52].....	41
Figure 3.14 Correlation of CH ₄ , N ₂ , Ar CO ₂ , He, and H ₂ permeability with 1/FFV. For each gas, from left to right, the data points represent films of 100, 75, 50, 25, 0wt% Matrimid. FFV is calculated from Resource II [53]	41
Figure 4.1 Desorption Data of Water in Matrimid/P84 Blend Films. Room temperature, 1 atm..	50
Figure 4.2 Polymerization of Penetrants in the Films.....	51
Figure 4.3 Skinning Trapping.....	51
Figure 4.4 Modelling of the Experimental Data for Water Desorption in 50 Matrimid % Blend Film. (a) Short time range (b) Whole time range. Room temperature, 1 atm.....	55
Figure 4.5 Comparison of Butanol Diffusion Coefficients of Three Models versus Mass Fraction of Matrimid. Room temperature, 1 atm.	56

Figure 4.6 Comparison of Water Diffusion Coefficients of Three Models versus Mass Fraction of Matrimid. Room temperature, 1 atm.....	57
Figure 4.7 Comparison of Toluene Diffusion Coefficients of Three Models versus Mass Fraction of Matrimid. Room temperature, 1 atm.	57
Figure 4.8 Comparison of Methanol Diffusion Coefficients of Three Models versus Mass Fraction of Matrimid. Room temperature, 1 atm.	59
Figure 4.9 Comparison of 1-Propanol Diffusion Coefficients of Three Models versus Mass Fraction of Matrimid. Room temperature, 1 atm.	59
Figure 4.10 Comparison of 2-Propanol Diffusion Coefficients of Three Models versus Mass Fraction of Matrimid. Room temperature, 1 atm.	60
Figure 4.11 Values of k for 1-Propanol, 2-Propanol, and Toluene.....	61
Figure 4.12 Values of k for Methanol.....	62
Figure 4.13 Values of k for Water	62
Figure 4.14 Values of k for Butanol	62
Figure A.1 Calibration of Density Gradient Column.....	75
Figure A.2 Density of Matrimid/P84 Blend Films	76
Figure B.1 Permeability of H ₂ vs. Matrimid Mass Fraction for Matrimid/P84 Blend Film.....	84
Figure B.2 Permeability of He vs. Matrimid Mass Fraction for Matrimid/P84 Blend Film	85
Figure B.3 Permeability of CO ₂ vs. Matrimid Mass Fraction for Matrimid/P84 Blend Film	86
Figure B.4 Permeability of Ar vs. Matrimid Mass Fraction for Matrimid/P84 Blend Film.....	87
Figure B.5 Permeability of N ₂ vs. Matrimid Mass Fraction for Matrimid/P84 Blend Film.....	88
Figure B.6 Permeability of CH ₄ vs. Matrimid Mass Fraction for Matrimid/P84 Blend Film	89

Figure B.7 Selectivity vs. $P(H_2)$ for H_2/N_2 Gas Pair in Comparison with Reference and Robeson Upper Limit Line. Each data in this study is the average value with error bars, from left to right, the content is from 0% Matrimid to 100% Matrimid..... 91

Figure B.8 Selectivity vs. $P(CO_2)$ for $CO_2/CH_4 N_2$ Gas Pair in Comparison with Reference and Robeson Upper Limit Line. Each data in this study is the average value with error bars, from left to right, the content is from 0% Matrimid to 100% Matrimid..... 92

Figure B.9 Permeability versus Kinetic Diameter of Gas Molecules 93

Figure C.1 Chemical Structure of PBI..... 94

Figure C.2 TGA Mass Loss Curve in air for Matrimid/PBI Blend Film. The mass loss shifts at 200, 250, 300 °C were because of the samples had been hold at those temperature for half an hour 95

Figure C.3 TGA Mass Loss Curve in air for Matrimid/PBI Blend Film. The mass loss of Figure C.2 was normalized to be 1 at 300 °C..... 96

List of Tables

Table 3.1 Comparison of Two Methods of Calculation of Volume Fraction.....	34
Table 4.1 Summary of Diffusion Coefficients Calculated from Model I.....	53
Table 4.2 Summary of Diffusion Coefficients Calculated from Model II.....	53
Table 4.3 Summary of Diffusion Coefficients Calculated from Model III	53
Table 4.4 Parameters of Model III.....	54
Table A.1 Calibration of Density Gradient Column with Standard Density Beans	75
Table A.2 Density of Matrimid/P84 Blend Films.....	76
Table A.3 V_w and MW of Groups in Matrimid (Resource I)	78
Table A.4 V_w and MW of Groups in P84 (Resource I)	79
Table A.5 FFV of Matrimid/P84 Blend Films (Resource I).....	80
Table A.6 FFV of Matrimid/P84 Blend Films (Resource II)	80
Table A.7 V_w and MW of Groups in Matrimid (Resource II)	81
Table A.8 V_w and MW of Groups in P84 (Resource II).....	82
Table B.1 Kinetic Diameters and Molecular Weights of Gases	83
Table B.2 Summary of Permeability of H_2 in Matrimid/P84 Blend Films.....	84
Table B.3 Summary of Permeability of He in Matrimid/P84 Blend Films	85
Table B.4 Summary of Permeability of CO_2 in Matrimid/P84 Blend Films	86
Table B.5 Summary of Permeability of Ar in Matrimid/P84 Blend Films.....	87
Table B.6 Summary of Permeability of N_2 in Matrimid/P84 Blend Films.....	88
Table B.7 Summary of Permeability of CH_4 in Matrimid/P84 Blend Films	89
Table B.8 Summary of Selectivity for Matrimid/P84 Blend Films	90

Acknowledgements

First and mostly, my sincerest gratitude goes to my advisor Dr. Mary Rezac, for her constructive advice and huge support in my study. And my gratitude also goes to the other two professors in my supervisory committee: Dr. Peter Pfromm and Dr. John Schlup who have shown great patience and given me valuable suggestions in the process of completing my master's thesis. Also, I want to appreciate my group members for their generous favors in the lab, in the class and in my daily life. And they are: Leslie Schulte, John Stanford, Michael Wales, Matthew Young, Michael Heidlage, and Yixao Li. Especially, the SEM photo of PEI membrane in Chapter 1 was provided by Matthew Young. In the last but not least, I want to express my deepest love to my family and my friends for their unconditional love and company during all the time.

Chapter 1 - Introduction

1.1 Gas Separation Membrane

A membrane, is defined as a selective barrier that allows the passage of certain constituents and retains others [1]. The schematic diagram of a membrane is shown in Figure 1.1. Membranes have gained an important place in chemical technology and are used in a broad range of applications, such as artificial kidney, gas separation, pervaporation, carrier-facilitated transport [2] and fuel cells.

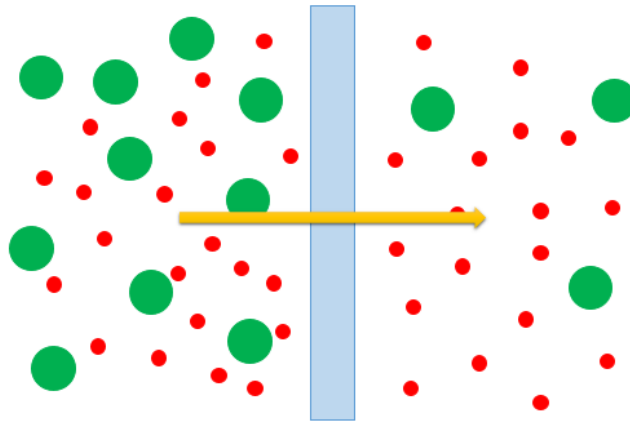


Figure 1.1 Membrane

Membrane reactor for biomass derived biofuels is a promising application for two reasons. In terms of reactor, membrane reactors are increasingly replacing conventional separation, process and conversion technologies across a wide range of applications. The enhanced efficiency and great economic potential have brought increasing interest in the study of membrane [3]. As shown in Figure 1.2, membrane reactors achieve efficiencies by combining in one unit a reactor that generates a product with a semipermeable membrane that extracts the product. What's more, removal of a product increases the residence time for a given volume of reactor and drives equilibrium-limited reactions towards completion, and finally a higher conversion is obtained [4].

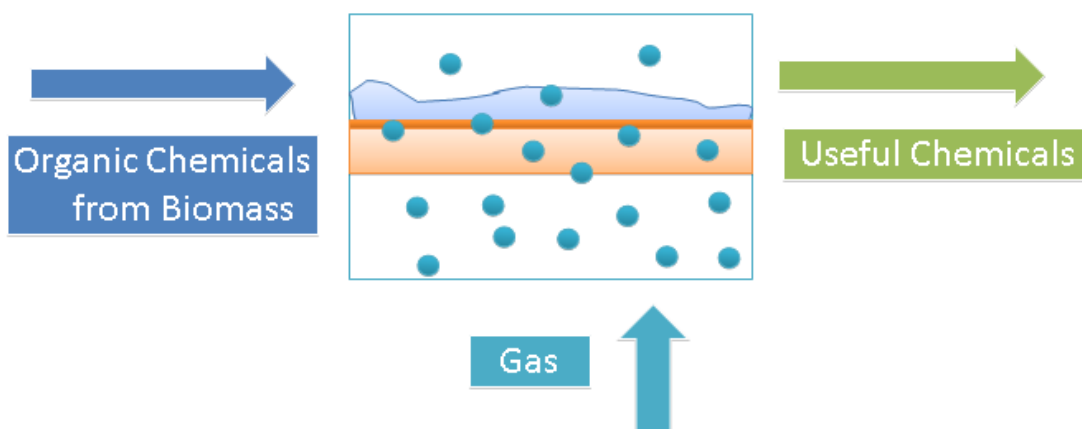


Figure 1.2 Simple Module Structure of Membrane Reactor

Gas separation membranes in this study are of interest for the high selectivity, and asymmetric structure of the membrane is of interest for the great transport properties. The asymmetric membrane was made with Loeb-Sourirajan method [2] and form a two-layer structure as shown in Figure 1.3. The asymmetric membranes have a very thin surface layer which greatly enhances separation properties and permeation rates, and a much thicker and porous substructure which is used as mechanical support.

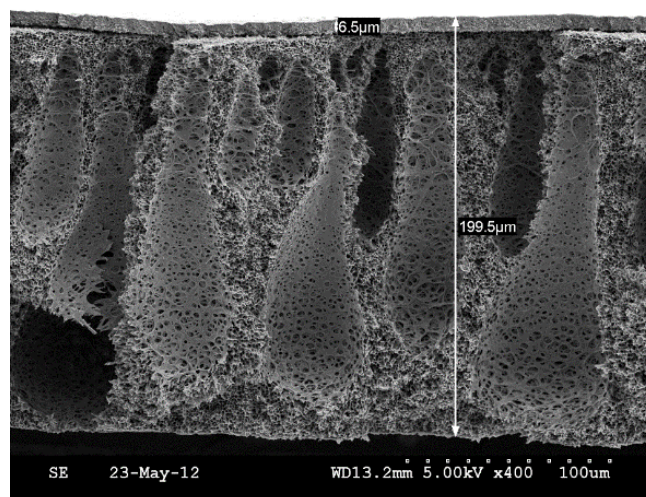


Figure 1.3 SEM Cross-Section of PEI Membrane.

Ideal gas separation membranes are supposed to have pores as small as 3-5 Å, which is within the range of thermal motion of the polymer chains in which situation, the transport mechanism can be best described by solution-diffusion model. In this model, permeants dissolve in the membrane material and then diffuse through the membrane down a concentration gradient. Permeants are separated because of differences in their solubilities in the membrane [2]. This model is based on Fick's Law. But in real processes, this model can not apply to all situations. When the pore is larger than 5 Å, Knudsen diffusion model will apply for membranes. The Knudsen diffusion model is considered when the pore radius decreases to be smaller than the mean free path (commonly 500-2000 Å) of gas molecules. Diffusion gas molecules will have more collision with the pore walls other with each other. At every collision with the pore walls, the gas molecules are momentarily adsorbed and then reflected in a random direction [2]. The Knudsen selectivity equals the inverse square root ratio of the molecular weights of the gases [5], which is a simple judgment of the existence of Knudsen diffusion pores. Molecular sieving, or pore-flow model are suitable for membranes with pores size larger than 10-15 Å. In this model, permeants are transported by pressure-driven convective flow through tiny pores. Separation occurs because smaller molecules have higher diffusion rates than larger molecules. Membranes that fit solution-diffusion model are desired in this study.

Properties of membrane desired in this study are high transport performance, high mechanical strength, strong thermal stability, strong chemical stability, as well as commercial availability. In general, polymeric materials do not simultaneously meet all of these criteria. For example, highly permeable polymers exhibit moderate to low selectivity values while materials with high resistance to harsh chemical environments or plasticizing gases are either difficult to process or are very expensive. Compared with other modification techniques such as crosslinking

[6] or even with the synthesis of entirely new materials, polymer blending is preferred due to simplicity, reproducibility, and commercial benefits [7]. Membrane blending has been widely used for the property improvement of pure membranes for various applications.

Sulfonated polyimide (SPI) was blended with sulfonated poly(phenylene arylene) (SPA) to enhance the membrane's stability in water and methanol solution to make proton exchange membrane for fuel cell application [8]. Polybenzimidazole (PBI) was blended into Nafion proton conduction membrane in order to reduce methanol permeability for a direct methanol fuel cell membrane [9]. In the cross-linked sulfonated poly(arylene ether sulfone) (cSPAES)/sulfonated polyimide (SPI) blend membranes for fuel cell application, the stability of blend membranes in water and methanol solutions was significantly improved by the introduction of SPI [10]. Proton conductive membranes made from sulphonated poly(ether ether ketone) (SPEEK) /Matrimid showed that the addition of polyimide has decreased the methanol crossover [11]. Poly(styrene-b-vinylbenzylphosphonic acid) (PS-b-PVBPA) were blended with poly(2,6-dimethyl-1,4-phenylene oxide) (PPO) to obtained polymer electrolyte membranes (PEM) for higher temperature applications because of the high glass transition temperature of PPO [12]. SPESc was reported to be able to reduce the water uptake caused by the sulfonation, which is a process to enhance the conductivity of SPEEK membrane for the fuel cell application [13]. The PES/PVP membrane for water electrolysis application possesses combined advantages of the hydrophobic and hydrophilic components; specifically, both good mechanical strength and excellent hydrophilicity have been achieved simultaneously [14]. Blend membranes for polymer electrolyte fuel cell applications prepared from sulfonated poly(arylene ether sulfone) (SPAES) and sulfonated polynaphthalimide (SPI), were moderately anisotropic and had the advantages of the smaller in-plane membrane swelling and the larger through plane conductivity compared to SPAES and SPI, respectively [15].

Polysulphone (PSF) was blended with Matrimid to increase the critical plasticization pressure of polyimide based membrane for CO₂/CH₄ separations [16]. PIM-1/Torlon blend membranes were prepared to enhance plasticization resistance of pure PIM-1 membrane [17, 18] for gas separation application. Polyethersulfone (PES) was blended with Matrimid for gas separation, because PES exhibits high chemical resistance thermal and dimensional stability and high selectivity values while Matrimid have good transport performance but have low chemical resistance [19, 20, 21, 22]. Polyimide was added to enhance the mechanical strength of thermal rearranged poly (benzoxazole) (PBO) for CO₂ separation [23]. In polysulfone/polyimide (PSF/PI) blended for CO₂/CH₄ separation, thermal stability was improved with the addition of PI [24]. PEEK of excellent anti-plasticization properties and Matrimid of superior gas separation properties, good mechanical properties and thermal stability were blended for CO₂ separation [25]. The high selectivity of PES and high permeability of Matrimid were combined for O₂/N₂ gas separation [26]. With the introduction of multitrifluoromethylated polyimide (12F-PI) to sulfophenylated polyetheretherketone (Ph-SPEEK), an obvious improvement in dimension stability, oxidative stability, mechanical properties, and proton conductivity could be observed in the blend membrane in comparison with pure Ph-SPEEK [27]. Considerable increments in gas permeability were observed by adding only 5 or 10 wt% PIM-1 to Ultem polyetherimide without much compromising gas pair selectivity [28].

For toluene/iso-octane separation, PBI was added to Matrimid due to its enhanced chemical stability, diffusivity and solubility selectivity for toluene [29]. A small amount of addition of PBI was demonstrated to significantly stabilize Matrimid's polymeric chains for high-temperature pervaporation and remarkably enhance the selectivity and permeance for the dehydration of tert-butanol/water mixtures [30]. PBI and Matrimid were also blended for N₂/CH₄,

CO₂/CH₄ gas separation [31, 32]. Novel solvent resistant nanofiltration (SRNF) membranes from blends of polyphenylsulfone (PPSU)/Matrimid showed potential for filtrations in organic solvents, including alcohols, alkanes, ketones and alkyl acetates, for most of which they showed a reasonable or good solvent stability [33]. Polydimethylsiloxane (PDMS)/polyimide blended interpenetrating polymer network (IPN) pervaporation membrane for methanol/toluene azeotrope separation, had demonstrated higher performance than the pristine PDMS membrane, in terms of thermal and mechanical stability and selectivity [34].

The carbon molecular sieving membranes were prepared from the polymer blend of polyphenylene oxide (PPO) and polypyrrolidone (PVP) as thermally stable and labile polymer, respectively. And the blend membrane showed higher permeation performance in comparison with those of the PPO derived carbon membrane [35, 36]. In the polyetherimide (PEI)/multi-wall carbon nanotubes (MWCNTs) composite carbon membrane, MWCNTs offered a favorable effect on increasing gas permeability by decreasing the gas diffusion resistance [37]. Introduction of thermally labile polymer PVP to PI carbon molecular sieve (CMS) membrane had improved gas permeation performance [38].

Polyimide polymers are of interest because polyimide membranes are used as functional materials for gas separation because they have better permeability-selectivity balance compared with conventional glassy polymers [39]. Matrimid is considered as the membrane polymer, for its relatively high gas permeability and selectivity, along with excellent mechanical properties, solubility in non-hazard organic solvents as well as commercial availability [40]. However, Matrimid is easy to be plasticized by CO₂ and swollen by organic chemicals. Blending a polymer (Matrimid in this study) with weak plasticization resistance with another polymer with high plasticization resistance is expected to enhance the plasticization resistance of the former polymer.

Therefore, P84, another commercial polyimide membrane, which has lower gas permeability yet much stronger plasticization resistance than Matrimid, is a good choice in the consideration of blending. Wessling's group [41] and Koops' group [42] showed that the resistance of Matrimid against plasticization induced by CO₂ can be increased by blending Matrimid with P84, which also increased CO₂/CH₄ selectivity. To the knowledge of the author, there is no complete study of the physical, thermal, transport properties of Matrimid/P84 blend membrane yet.

1.2 Polymer Blends

In the study of polymer blends, the miscibility of the polymers are of vital important and desired for improving the properties of membrane. As defined [43], a *miscible* polymer blend is a blend of two or more amorphous polymers homogeneous down to the molecular level and fulfilling the thermodynamic conditions for a miscible multicomponent system. An *immiscible* polymer blend is the blend that does not comply with the thermodynamic conditions of phase stability. The term *compatible* polymer blend indicates a commercially attractive polymer mixture that is visibly homogeneous, frequently with improved physical properties compared with the constituent polymers. In this section, the thermodynamic behaviors of polymer blends have been discussed.

In systems of miscible blend, the various components have the thermodynamic ability to be mixed at the molecular level. Since these systems form only one miscible amorphous phase, interphase stress transfer is not an issue and the physical properties of miscible blends approach and frequently exceed those expected for a random copolymer comprised of the same chemical constituents. Only in this way can the component physical properties be efficiently utilized to give blends with the desired properties.

Homogeneous miscibility in polymer blends requires a negative free energy of mixing [44]:

$$\Delta G_{mix} = \Delta H_{mix} - T\Delta S_{mix} \quad (1.1)$$

Where ΔH_{mix} is the enthalpy change of mixing and ΔS_{mix} is the entropy change of mixing.

As shown in Figure 1.4 which was modified from the diagram in reference [45], there are three possible ways in which the free energy of mixing may vary with the composition of the overall mixture (ϕ_i = volume fraction of component i). Case A represents completely immiscible blends of which the free energy of mixing is above zero for the whole content range. But a negative free energy of mixing does not assure complete miscibility as Case C illustrates. Here the free energy of mixing shows a reversed curvature in the mid-composition range, and thus the mixture can develop an even lower free energy in this range by splitting into two phases with compositions given by the two minima. This results in a miscibility gap or partial miscibility.

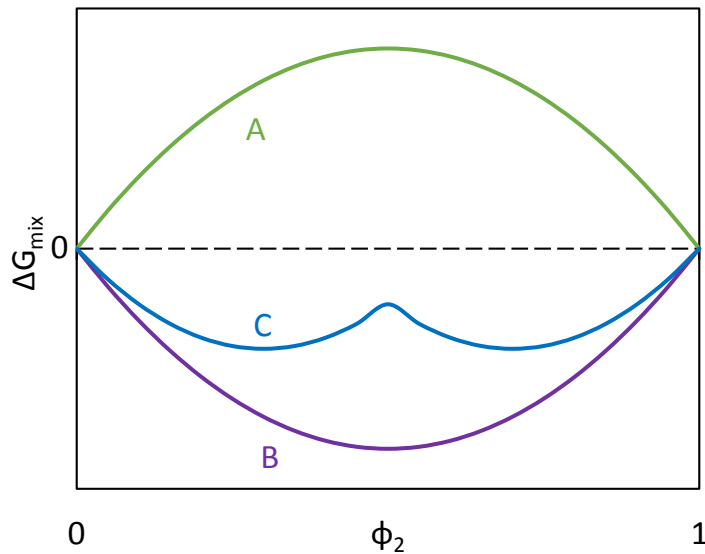


Figure 1.4 Free Energy of Mixing for Binary Mixtures. A: completely immiscible; B: completely miscible; C: partially miscible

A complete statement of the thermodynamic criteria for miscibility is that Eq. (1.2) is satisfied over the range of concentration of interest [46]. This is the only thermodynamically valid definition of miscibility. While there are no direct means of measuring free energy, many experimental observations can be related to it.

$$\left[\frac{\partial^2 \Delta G_{mix}}{\partial \phi_2^2} \right]_{T,p} > 0 \quad (1.2)$$

The simplest model for polymer-polymer mixtures is the Flory-Huggins theory. This assumes that the heat of mixing follows a quadratic dependence on composition, i.e., a van Laar type expression,

$$\Delta H_{mix} = BV\phi_1\phi_2 \quad (1.3)$$

Where V is the volume of the mixture and B is the mixing energy density characteristic of polymer-polymer segmental interactions in the blend.

From the calculation of a lattice model, the entropy of mixing ΔS_{mix} is negligible when polymers have very high molecular weights [45]. Therefore it is suggested and certificated that polymer pairs which show exothermic heats of mixing ($\Delta H_{mix} < 0$) are miscible.

Thermodynamically, there are three important temperatures related to the miscible behavior of polymer blends, which are the glass transition temperature (T_g), lower critical solution temperature (LCST) and upper critical solution temperature (UCST), as shown in Figure 1.5.

When the temperature is above T_g , the polymer is in rubbery state. The polymer has very high free volume, which is the space not occupied by polymer chains. The structure of rubbery polymer is not rigid and transport of permeates through the polymer is also very fast. As the temperature goes down, free volume is decreased and structure is more rigid. The transport rate through polymer is smaller than before. At T_g , there is a rapid change of the state of polymer. The free volume is rapidly decreased and mobility of polymer chains has been also reduced rapidly. The structure of polymer is very rigid and transport rate is very slow. At this time, the polymer is in the state of glass. Each polymer has a unique glass transition temperature. And a completely miscible blends is supposed to have a unique glass transition temperature. It is a most commonly used way to test the miscibility of polymer blends by observing the glass transition temperature.

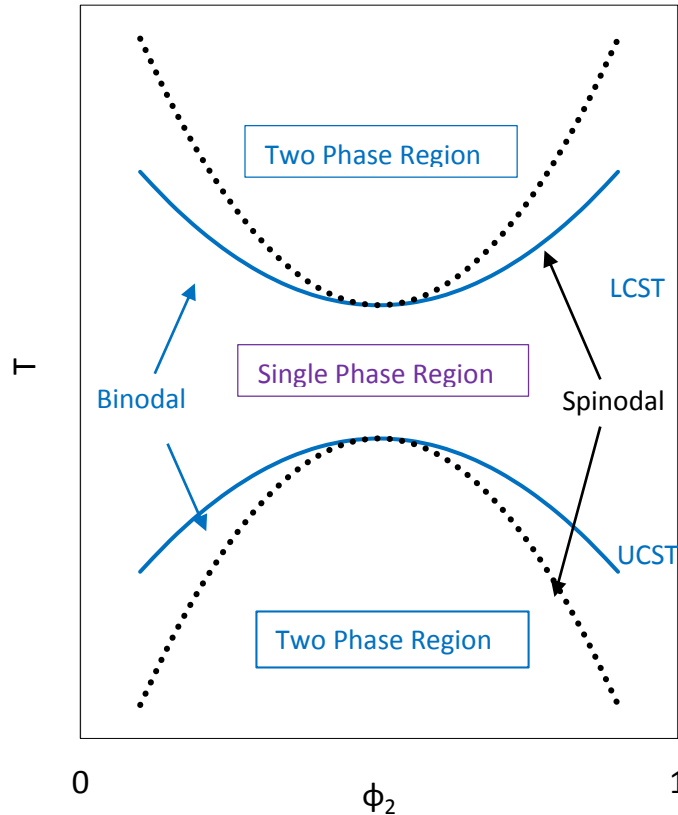


Figure 1.5 Phase Diagram Showing LCST and UCST Behavior for Polymer Blends

Figure 1.5 was modified from the diagram in reference [47], and shows the phase diagram for polymer blends. Binodal curves define the two-phase region. The spinodal curve defines the region of absolute instability of the polymer blend. The point common to the binodal and spinodal curves is the critical point. The region between a binodal curve and a spinodal curve is the metastable region. The region between the two binodal lines represents a single phase.

Highly miscible polymers exhibit single phase behavior over the entire temperature-volume fraction space available for experimental verification. But if UCST or LCST behavior exists, the miscibility cannot be determined. At low temperatures, the UCST cannot be determined due to the glassy state restricting molecular motion (phase separation); and at higher temperatures, polymer degradation occurs before phase separation can be observed. With highly immiscible polymer

blends, the phase diagram is virtually all in the two phase region with the binodal curves virtually overlapping the y axis at 0 and 1.0 volume fraction.

Matrimid and P84, which are polymer materials studied in this thesis, have similar glass transition temperatures from the characterization of differential scanning calorimetry (DSC). Therefore, it is very difficult to tell the miscibility of the blends from the glass transition temperature. In the other side, the miscibility was discussed in the view of the transport behavior of the blends. When two polymer are completely miscible, there is a linear relationship between logarithmic permeability of a certain gas and reciprocal fractional free volume of the membrane. The detailed discussion of transport behavior could be found in Chapter 3.

1.3 This Study

To study blend membranes, what is of vital important is the characterization of blend dense films, which could provide fundamental information of physical, thermal, and transport properties of polymers. Therefore, in this study, Matrimid/P84 blend solutions have been prepared and cast carefully into dense films. The physical properties (density and d-spacing) was measured and the changing rules with polymer composition has been discussed. And the thermal degradation behavior of blends was measured by TGA. Gas flux tests of CH₄, N₂, Ar, CO₂, H₂, He were processed with a constant volume apparatus and the permeability and selectivity were calculated. Mathematical models have been applied to explain the relationship between permeability and selectivity, permeability and fractional free volume, permeability and volume composition. The transport behavior of the blend films has a partial miscible characteristic.

Desorption of water, methanol, 1-propanol, 2-propanol, butanol, toluene in blend films have been processed at room temperature. Diffusion coefficients of desorption of diffusion coefficients were calculated with three mathematical models.

Chapter 2 - Characterization of Physical and Thermal Properties of Matrimid/P84 Blend Films

2.1 Introduction

Polyimide gas separation membranes are promising in the application of membrane reactors transferring biomass into biofuels or biochemical. Polyimide (Matrimid, P84, etc.) membranes have the advantage of better permeability-selectivity balance than conventional glassy polymers [39]. Matrimid is a common commercial polyimide polymer with relatively high gas permeability and selectivity, along with excellent mechanical properties, solubility in non-hazard organic solvents as well as commercial availability [48]. However, good solubility of Matrimid in organic solvents makes it easy to swell in the environment of organic chemicals, thus deteriorating the separation performance of membranes. The presence of solvent plasticization causes the transport rates of all penetrants in a mixture to increase, which may result in significant selectivity losses because the increase for the slower permeating component is larger than for the faster permeating component [49]. P84 is another commercial polyimide polymer which shows ability against plasticization but lower permeability than Matrimid. Blending Matrimid with P84 can increase the resistance of Matrimid against plasticization induced by CO₂ as well as increasing CO₂/CH₄ selectivity [41, 42]. Also Matrimid/P84 blend membrane was found to achieve H₂/N₂ selectivity comparable with pure Matrimid membranes [50]. Therefore, it is reasonable to expect a blended Matrimid/P84 membrane which combines the advantages of two current commercial polymers as well as avoiding the cost of synthesizing new polymers.

The study of properties of dense films can provide fundamental data for further research of membranes. In this chapter, a series of mass ratios of Matrimid/P84 blended films were

prepared. Physical and thermal properties were measured with TGA. Density, d-spacing, and FFV have apparent trend of changing with mass fraction of Matrimid. Rules between TGA curves and film composition were also discussed and interpreted.

2.2 Experimental

2.2.1 Materials

Matrimid 5218 (poly [3, 3',4, 4'-benzophenone tetracarboxylic dianhydride and 5(6)-amino-1-(4'-aminophenyl-1, 3-trimethylindane)], BTDA-DAPI) was supplied by Huntsman Advanced Materials Americas Inc. P84 (copolyimide of 3, 3',4, 4'-benzophenone tetracarboxylic dianhydride and 80% methylphenylenediamine + 20% methylenediamine) was provided by HP Polymer Inc. NMP (N-Methyl-2-pyrrolidone, purity 99%) was supplied by Sigma-Aldrich. Methanol (purity 99.9%) was supplied by Fisher Scientific

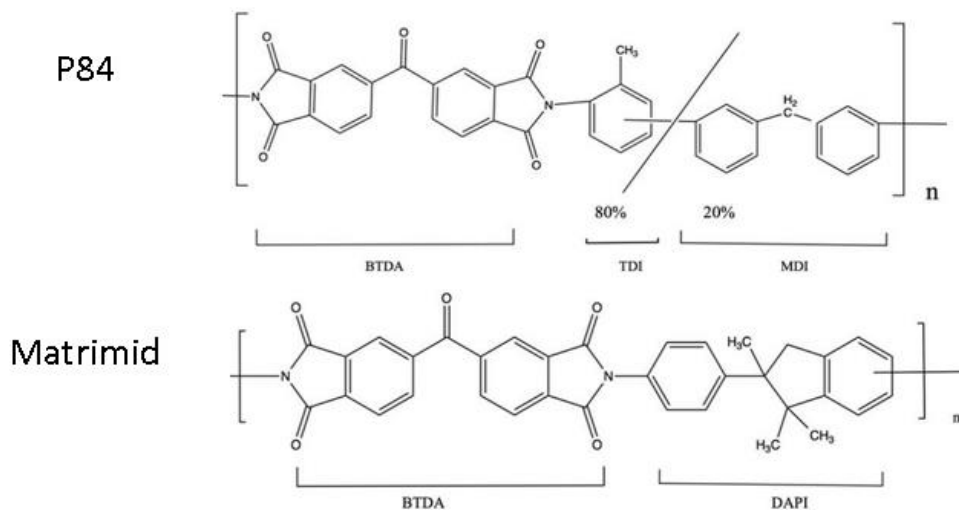


Figure 2.1 Chemical Structures of Matrimid and P84

Figure 2.1 represents chemical structures of Matrimid and P84. The similar aromatic structures indicate the strong chemical stability of both the two polymers. As shown below, both polymers have a BTDA structure on the left side. While on the right side, Matrimid have an extra

pentacyclic ring with three methyl groups, which could occupy more space than P84. It is reasonable to expect that Matrimid have a larger fractional free volume.

2.2.2 Preparation of Matrimid/P84 Blend Films

The films were prepared by a casting method. Polymer solutions (20 wt. % polymer/80 wt. % NMP) with various compositions of 0/100, 10/90, 25/75, 50/50, 75/25, 90/10, 100/0 g/g were prepared from Matrimid and P84 according to the following steps.

Firstly, polymer powders were dissolved by NMP in glass jars under room temperature. The jars were capped and settled in the hood under room temperature without stirring for at least a week until totally dissolved (there were no visible polymer powder particles and the solution is visibly transparent while the color is evenly distributed).

The solutions were poured on a glass plate and cast with a casting knife with a very slow rate under room temperature, with the thickness set to 50 μ m. Subsequently, films were dried in a vacuum oven at 50°C for 12 hours, and then at 100°C for 12 hours, and finally 150 °C for 48 hours to get rid of the solvent residues.

The films were taken out of the oven, and peeled off the glass plate with a bit of water after cooling down to room temperature. The films were wiped with soft tissues and kept in the oven at 100 °C overnight to remove any water residues. Naturally cooled films were conserved in a container with drierite (anhydrous Calcium Sulfate) inside.

2.2.3 Density Measurement

Density of films were measured with a density gradient column. A metal bucket was loaded at the bottom of the column before a soft tube was inserted to the bottom of the column. A series of Ca(NO₃)₂·4H₂O solutions in water were prepared with the density range from 1.0 g/cm³ to 1.5

g/cm³ (density step is 0.05 g/cm³). The solutions were slowly added to the bottom of the column through the soft tube at the sequence from smaller density to bigger density. Standard density beans were wetted with water before dropped into the column from the top. Positions of the beans were recorded after 24 hours of settlement. A linear equation was calculated from bean density and bean position ($y = 0.0025x + 1.1164, R^2 = 0.9981$), the value of R^2 is reliable for the density measurement (Details of the calibration of density gradient column can be viewed in Appendix A.1.). Sample films of different polymer compositions into small pieces of an area $< 1\text{ cm}^2$ and of different shapes. The positions of samples were recorded and transferred into density values from the density-position relationship equation. Detailed calibration of the density gradient column is shown in Appendix A.1.

Fractional free volume (FFV) is an important semi-empirical parameter that correlates the permeation properties of polymers with their chemical structure. It is the fraction of the space filled by the polymer that is not occupied by the atoms that make up the polymer chains [2], and is usually defined as

$$FFV = \frac{V - V_0}{V} \quad (2.1)$$

Where $V = 1/\rho$ is the specific volume of the polymer (cm³/g), V_0 is the volume occupied by the molecules themselves (cm³/g). A common approach to get V_0 is Bondi's group contribution method [51] where the occupied volume is computed from the van der Waals volumes, $(V_w)_k$, of the various groups in the polymer structure by

$$V_0 = 1.3V_w \quad (2.2)$$

$$V_w = \sum (V_w)_k \times n_k \quad (2.3)$$

Where n_k is the number of group k in one repeat unit of the polymer, and $(V_w)_k$ (cm^3/g) is the van der Waals volume of group k. The values of $(V_w)_k$ were obtained from two resources: Park and Paul [52] (Resource I), van Krevelen and Nijenhuis [53] (Resource II). Therefore there were two groups of calculations of FFV and the detailed calculation process can be viewed in Appendix A.2.

2.2.4 Thickness Measurement

The films were cut into 13.8 cm^2 round stamps as below. Thickness was measured with a Mitutoyo digital micrometer (accuracy: 0.001mm) at five spots distributed evenly on each sample stamp, as shown in Figure 2.2.

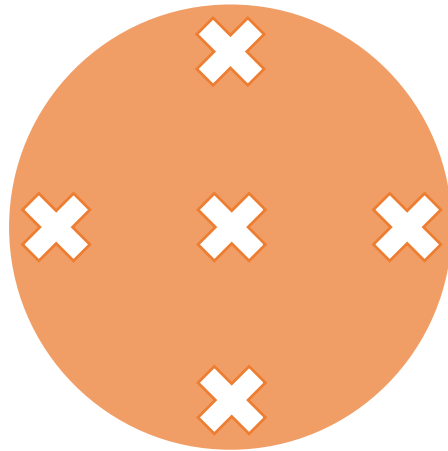


Figure 2.2 Measured Spots Distribution on a Sample Film Stamp

2.2.5 X-ray Diffraction Characterization

Film d-spacing was determined by X-ray diffraction analysis (XRD) using a MiniFlex II X-ray diffractometer using $\text{Cu K}\alpha$ radiation with a wavelength (λ) = 1.54 \AA at room temperature. XRD was run from 4-40 degree at the speed of 0.5.

Average d-spacing was determined based on Bragg's Law:

$$n\lambda = 2d\sin\theta \quad (2.4)$$

Where n is an integral number (1, 2, 3 ...), λ denotes the X-ray wavelength, d stands for the intersegmental spacing between two polymer chains and θ indicates the diffraction angle. The value of 2θ can be obtained by capturing the peak of the scanning curve generated by XRD. In this study, n was 1 in the calculation.

2.2.6 Thermogravimetric Analysis

Thermogravimetric analysis (TGA) was conducted with a Pyris 1 TGA analyzer. TGA characterizations were run under air flow and nitrogen flow separately.

For TGA in air flow, the films were pretreated as the following: The pure Matrimid and 50%Matrimid films were heated in a vacuum oven at 200 °C for a week, immersed in methanol for 5 days and dried in the vacuum oven at 200 °C for 3 hours. The pure P84, 10%Matrimid, 25%Matrimid, and 75%Matrimid films were heated in a vacuum oven at 200 °C for two weeks, immersed in methanol for three times with each time being three hours, and then dried in the vacuum oven over night.

For each time of TGA measurement run in air flow, 5-10 mg of samples were weighed and added to a platinum pan. The pan was heated from room temperature to 100 °C at a heating rate of 10 °C/min to remove any water residues, held at 100 °C for 10 min, and then heated to 800 °C at 10 °C/min and allowed to cool down to room temperature under an air atmosphere at a flow rate of 20ml/min. The mass loss curve versus temperature were generated by Pyris TGA software. And the mass loss was normalized to be 1 at 100 °C.

For TGA in nitrogen flow, all the samples were dried in a vacuum oven at 150 °C overnight to remove solvent residues. And TGA measurement steps were conducted as above except that some of the samples were only heated to 500 °C.

2.3 Results and Discussion

2.3.1 Observation of Stamps of Matrimid/P84 Blend Films

Figure 2.3 provided photos of stamps of Matrimid/P84 Blend Films of five compositions. The background of the photos are white paper with green grids. As can be observed from the photos, all the films have a color of light yellow and transparent. Words under the films can be clearly seen through the films. Only the 50% Matrimid film is a little more turbid than the others, which might not be observed from the photos due to photographic technique limitations. What's more, the films are pliable with smooth surface.

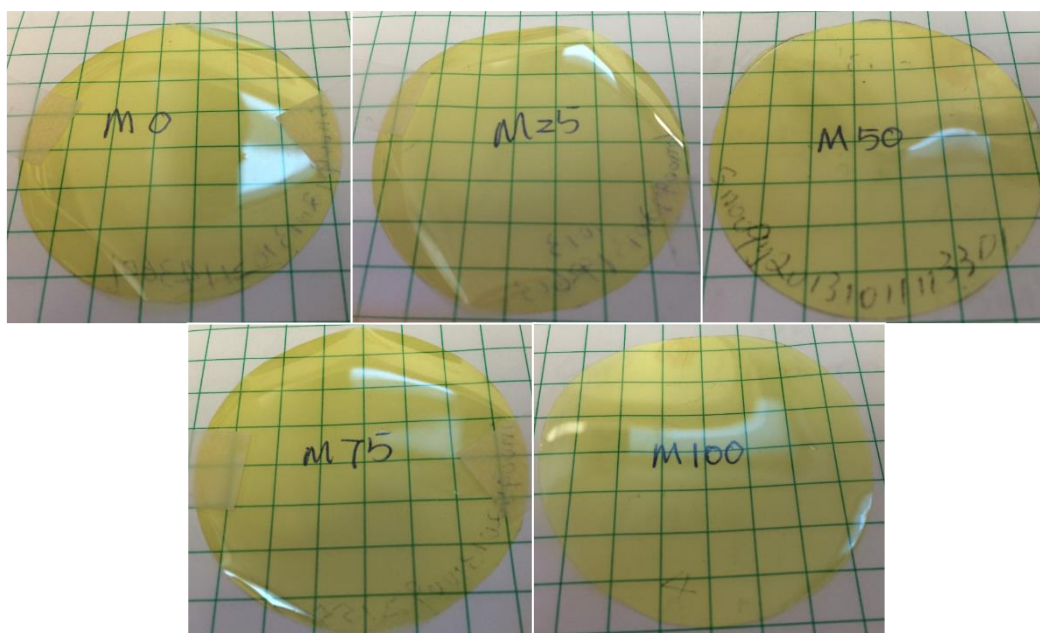


Figure 2.3 Photos of Stamps of Matrimid/P84 Blend Films

2.3.2 Density of Matrimid/P84 Blend Films

Figure 2.4 shows the density of blend films from 0 wt. % to 100 wt. % Matrimid. The density presents a linear relationship with mass fraction of Matrimid. This is reasonable since P84 has a larger density than Matrimid compared with reference density of pure Matrimid and pure

P84. The density of pure Matrimid has a range of 1.17~1.262 g/cm³ [16, 39, 54, 55]. Pure P84 is 1.355, 1.336g/cm³ [56, 57]. Figure 2.5 presents the calculated FFV values from equation (4) from two groups of calculations. Both groups of FFV increase with Matrimid mass fraction, which is reasonable because denser polymer should have smaller d-spacing.

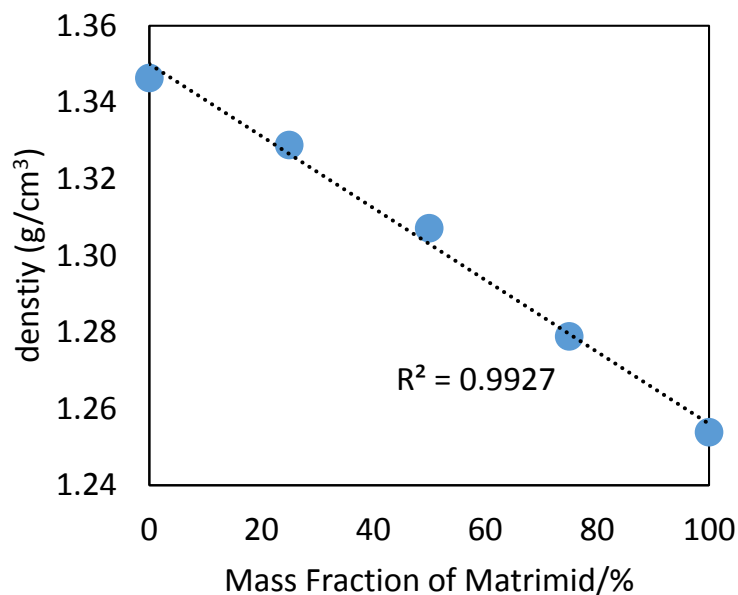


Figure 2.4 Correlation of Film Density with Mass Fraction of Matrimid

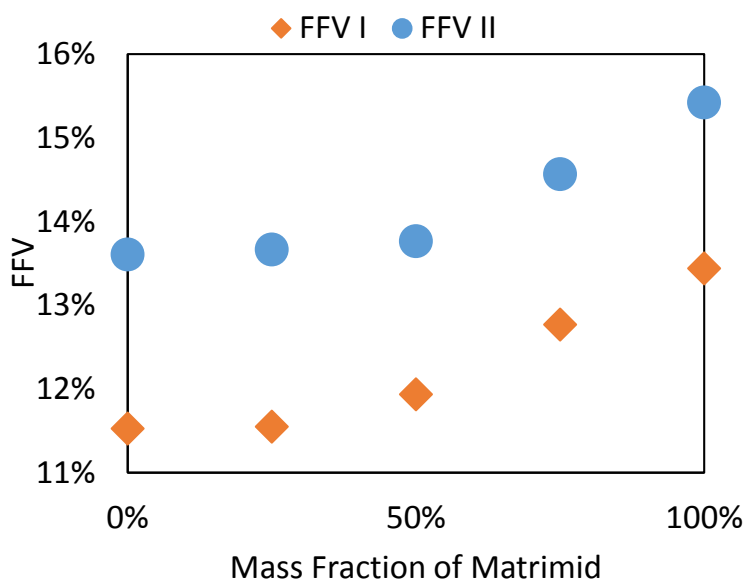


Figure 2.5 FFV of Matrimid/P84 Blend Films from Two Groups of Calculations

2.3.3 d-spacing of Matrimid/P84 Blend Films

An example of raw data for pure Matrimid is shown as Figure 2.6. The d-spacing can be visualized as the average spacing between the centers of the chains in the molecular matrix [58] and it is calculated with Bragg's Equation (Eq. 2.4).

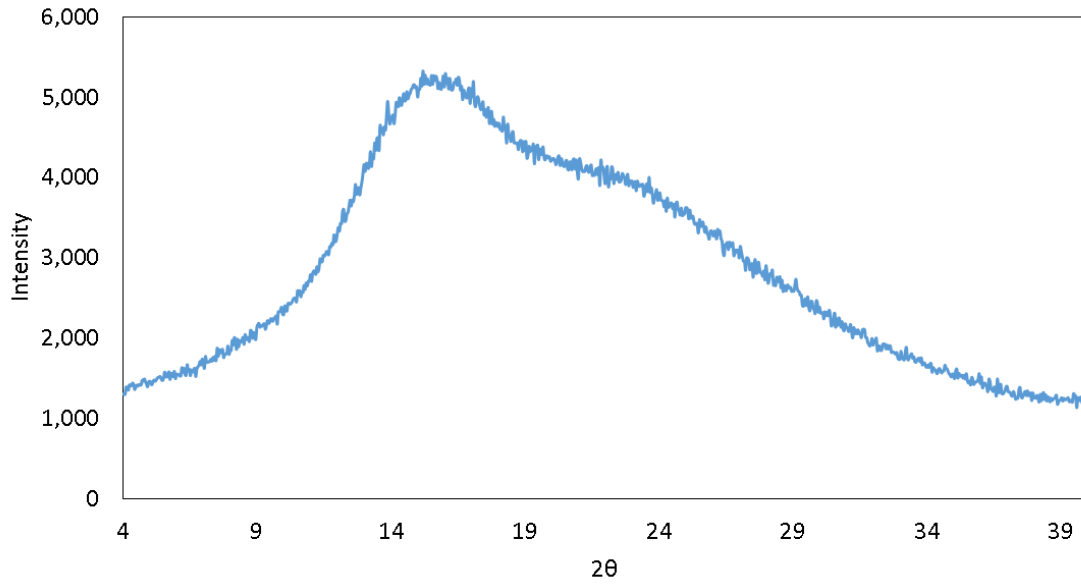


Figure 2.6 An Example of Raw XRD Data of Pure Matrimid Film

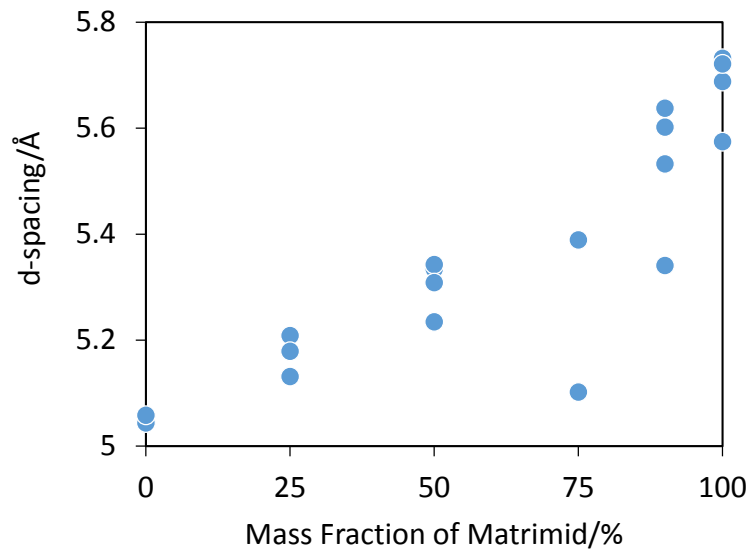


Figure 2.7 d-spacing of Matrimid/P84 Blend Films

Figure 2.7 indicates the d-spacing of Matrimid/P84 Blend Films. Each point represents the d-spacing value of one single sample. There is a trend that d-spacing increases with mass fraction of Matrimid, which is consistent with density versus Matrimid mass fraction, and FFV versus Matrimid mass fraction. P84 has more compact structure and smaller d-spacing than Matrimid. With decreasing Matrimid (or increasing P84) mass fraction, the shift in d-spacing indicates a reduction in the polymer inter-chain distance and free volume, leading towards a tighter and narrower structure.

2.3.4 TGA of Matrimid/P84 Blend Films in Air

Figure 2.8 shows TGA data of Matrimid/P84 blend films in air flow. Pure Matrimid mass loss curve stays stable before 500 °C, and after 500 °C, the mass loss decreases at a rapid rate, which is in agreement with reference [39]. For pure P84, the mass loss curve represent a “three-stage” characteristic: stable when $T < 300$ °C; slowly decreases when 300 °C $< T < 500$ °C; rapidly decreases when $T > 500$ °C, which is also in agreement with reference [59, 60]. The mass loss curves of blend films present intermediate characteristics from pure Matrimid to pure P84.

From Figure 2.8, the blend curves are mostly within the range of individual polymer curves in the temperature range of 300-550 °C. The 75%Matrimid film curve is almost the same as pure Matrimid until 500 °C from where the 75 % curve decreases quicker than the pure Matrimid curve. Except for 50% Matrimid, mass loss rate during 300-550 °C is in the order of pure P84 > 10% Matrimid > 25% Matrimid > 75% Matrimid > pure Matrimid. 50% Matrimid films have an abnormal larger mass loss from 100-200 °C, and the possible reason would be some residual solvent.

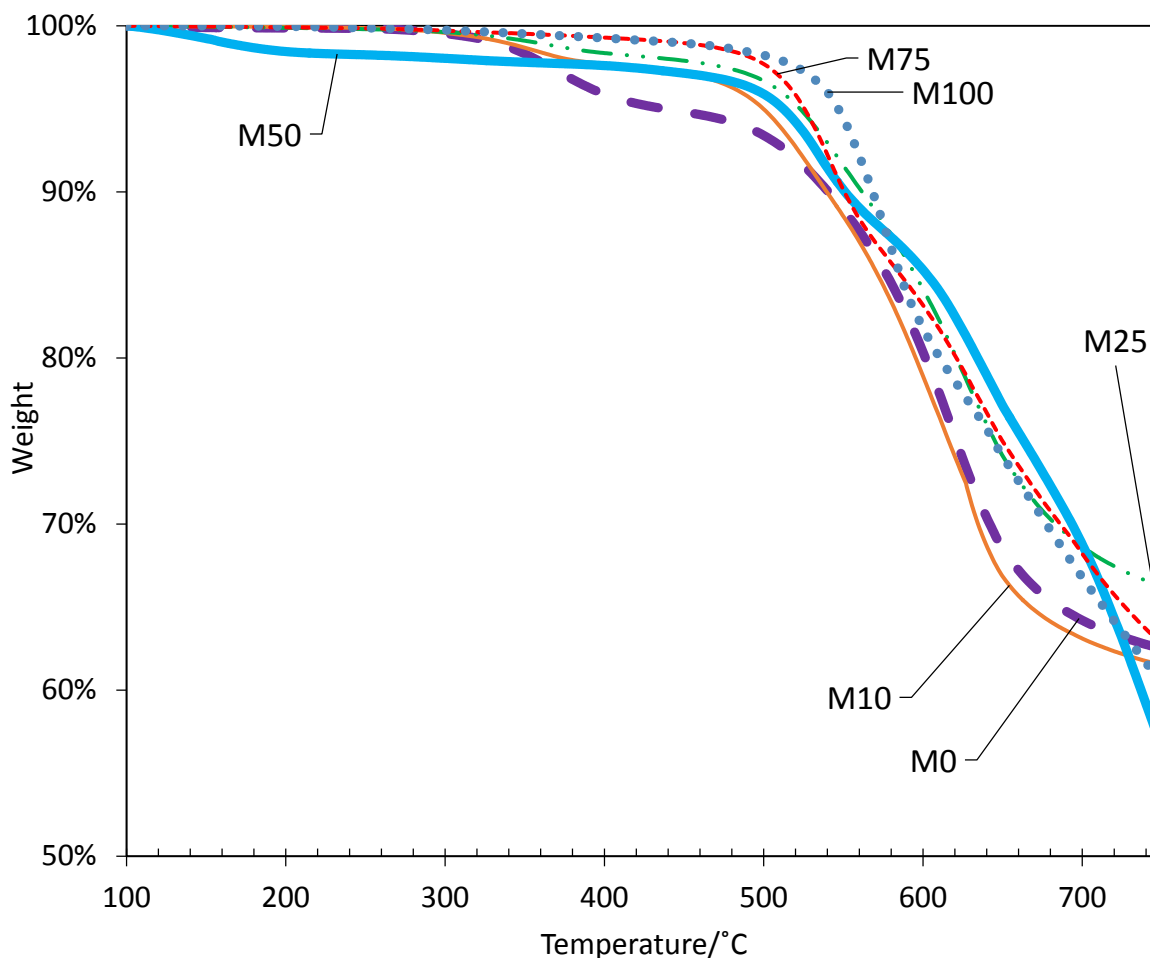


Figure 2.8 TGA Mass Loss Curves of Matrimid/P84 in Air Flow

Pyrolysis process of polyimide films consists of two processes [61]: carbonization at a low-temperature range of 300-700 °C and graphitization at a high temperature of pyrolysis (>700 °C). In the carbonization process, the most weight loss of polyimides is induced by the expelling of noncarbon atoms (N, O) as different gases. The rates of weight loss are related to the chemical structures of polyimide. However, the chain conformation of carbonized materials will be retained as that of polyimide in the carbonization process. When the pyrolysis temperature increases up to 700 °C, the linkage of independent aromatic rings is induced by dehydrogenization and

denitrogenization. The amorphous carbon will move toward to the graphitic state which is more thermodynamically stable.

2.3.5 TGA of Matrimid/P84 Blend Films in N₂

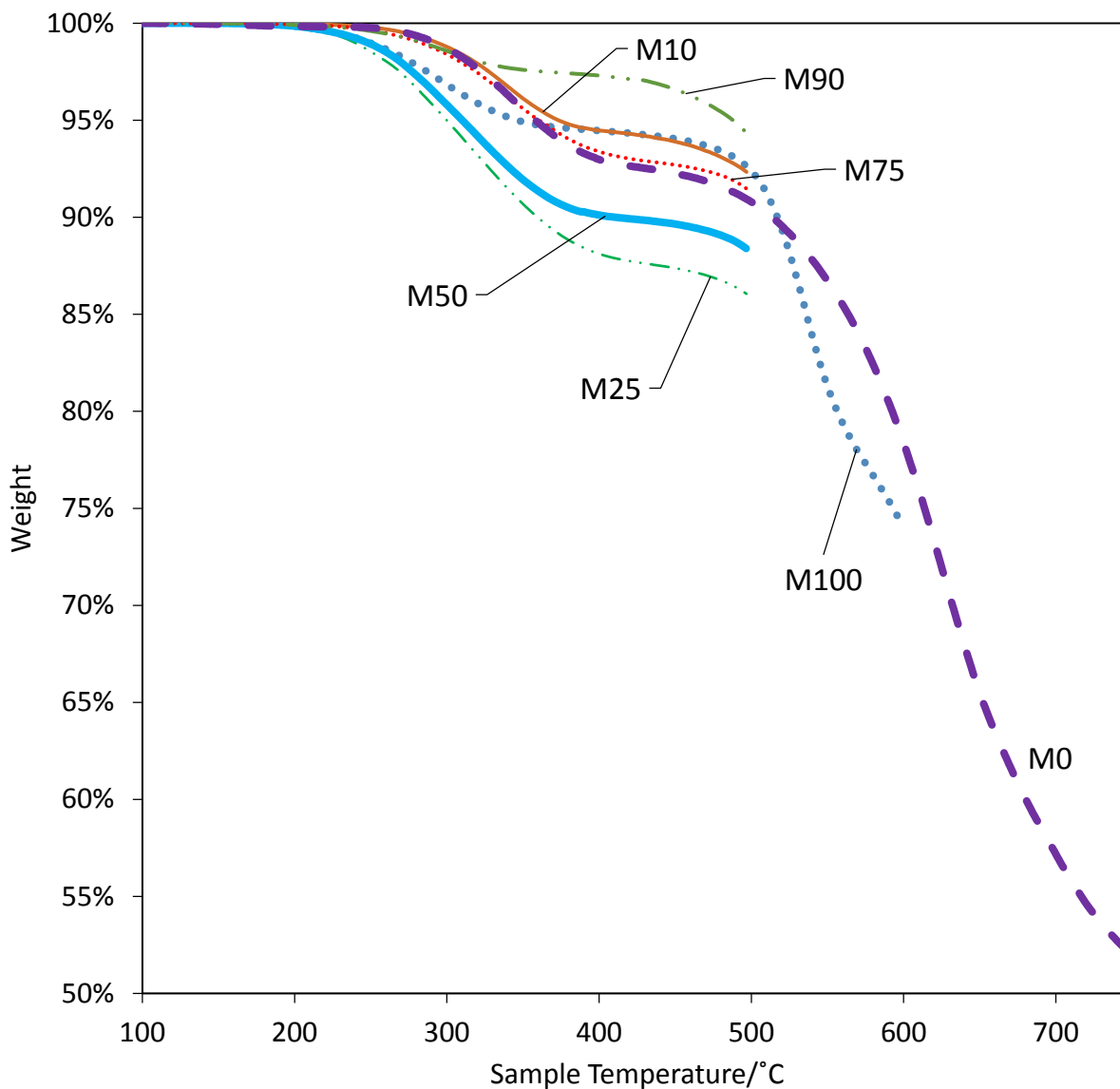


Figure 2.9 TGA Mass Loss Curves of Matrimid/P84 in N₂ flow

Figure 2.9 is TGA curve of Matrimid/P84 blend films in Nitrogen flow. All the curves have similar characteristics of “three-stage”, but there is no apparent correlation between the mass loss

and polymer composition. TGA mass fraction curves of samples in nitrogen decrease at a relative low temperature ($<300\text{ }^{\circ}\text{C}$), which is abnormal compared with TGA in air and as shown in a reference [39], both of which have a slope change at about $500\text{ }^{\circ}\text{C}$ for pure Matrimid.

One should compare the pretreatment of films for TGA in air and TGA in nitrogen. The films test in nitrogen flow were not preheated and solvent exchanged as samples tested in air flow. It is possible that a considerable amount of mass loss at the first stage is contributed by residual solvent.

2.4 Conclusion

In this study, the measurement of density, and characterization of XRD, TGA in N_2 , and TGA in air have been applied to Matrimid/P84 blend films. FFV and d-spacing have been calculated.

Density, d-spacing, and FFV of blend films follow the same pattern: more rigid (high P84 content) films, have less space, higher density, and smaller FFV.

For TGA in air, pure Matrimid mass loss curve is stable until 500°C , while pure P84 presents a three-stage characteristic, and begins to have slow mass loss from $300\text{-}500\text{ }^{\circ}\text{C}$, and rapid mass loss from $500\text{ }^{\circ}\text{C}$. Both are consistent with reported studies. And the blend films are presenting an intermediate characteristic with rising mass fraction of Matrimid compared to individual polymers.

For TGA in nitrogen, there is no apparent rationale. All the films present a three-stage characteristic in the mass loss curves. The larger mass loss at the first stage is possibly caused by residual solvent due to differences in pre-treatment.

Chapter 3 - Transport Property of Matrimid/P84 Blend Films

3.1 Introduction

Polyimide gas separation membranes are promising in the application of membrane reactors transferring biomass into biofuels or biochemical. Polyimide (Matrimid, P84, etc.) membranes have the advantage of better permeability-selectivity balance than conventional glassy polymers [39]. Matrimid is a common commercial polyimide polymer with relatively high gas permeability and selectivity, along with excellent mechanical properties, solubility in non-hazard organic solvents as well as commercial availability [48]. However, good solubility of Matrimid in organic solvents makes it easy to swell in the environment of organic chemicals, thus deteriorating the separation performance of membranes. The presence of solvent plasticization causes the transport rates of all penetrants in a mixture to increase, which may result in significant selectivity losses because the increase for the slower permeating component is larger than for the faster permeating component [49]. P84 is another commercial polyimide polymer which shows ability against plasticization but lower permeability than Matrimid. Blending Matrimid with P84 can increase the resistance of Matrimid against plasticization induced by CO₂ as well as increasing CO₂/CH₄ selectivity [41, 42]. Also Matrimid/P84 blend membrane was found to achieve H₂/N₂ selectivity comparable with pure Matrimid membranes [50]. Therefore, it is reasonable to expect a blended Matrimid/P84 membrane which combines the advantages of two current commercial polymers as well as avoiding the cost of synthesizing new polymers.

The study of properties of dense films can provide fundamental data for further research of membranes. In this chapter, a series of ratios of Matrimid/P84 blended films were prepared before the single gas permeability was measured. The relationship of permeability-selectivity, permeability-FFV, and permeability-volume fraction of Matrimid have been discussed and applied

to available mathematical models. The Matrimid/P84 blend films in this study present the behavior of partial-miscible blends.

3.2 Experimental

3.2.1 Materials

Matrimid 5218 (poly [3, 3'4, 4'-benzophenone tetracarboxylic dianhydride and 5(6)-amino-1-(4'-aminophenyl-1, 3-trimethylindane)], BTDA-DAPI) was supplied by Huntsman Advanced Materials Americas Inc. P84 (copolyimide of 3, 3'4, 4'-benzophenone tetracarboxylic dianhydride and 80% methylphenylenediamine + 20% methylenediamine) was provided by HP Polymer Inc. NMP (N-Methyl-2-pyrrolidone, purity 99%) was supplied by Sigma-Aldrich.

Figure 3.1 represents chemical structures of Matrimid and P84. The similar aromatic structures indicate the strong chemical stability of both the two polymers.

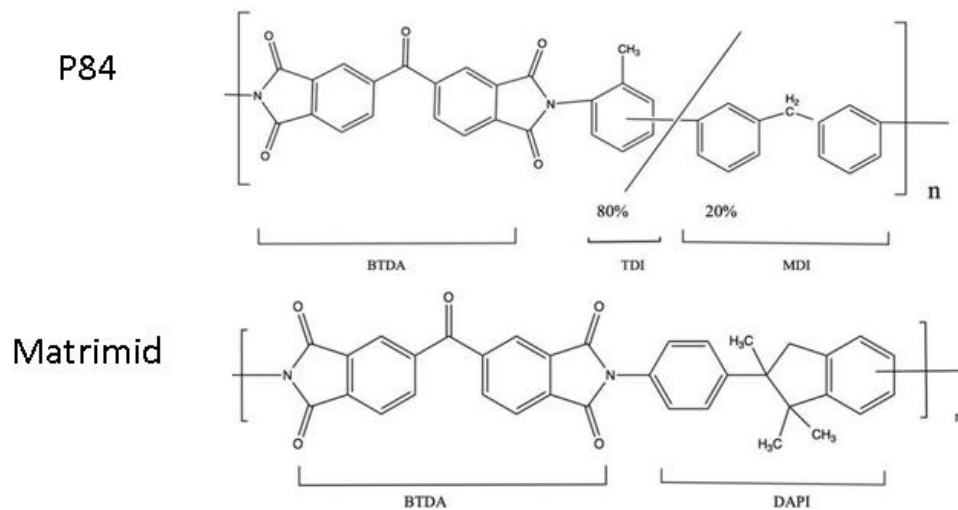


Figure 3.1 Chemical Structures of Matrimid and P84

3.2.2 Preparation of Matrimid/P84 Blend Films

The films were prepared by a casting method. Polymer solutions (20 wt. % polymer/80 wt. % NMP) with various compositions of 0/100, 10/90, 25/75, 50/50, 75/25, 90/10, 100/0 g/g were prepared from Matrimid and P84 according to the following steps.

Firstly, polymer powders were dissolved by NMP in glass jars under room temperature. The jars were capped and settled in the hood under room temperature without stirring for at least a week until totally dissolved (there were no visible polymer powder particles and the solution is visibly transparent while the color is evenly distributed).

The solutions were poured on a glass plate and cast with a casting knife with a very slow rate under room temperature, with the thickness set to 50 μ m. Subsequently, films were dried in a vacuum oven at 50°C for 12 hours, and then at 100°C for 12 hours, and finally 150 °C for 48 hours to get rid of the solvent residues.

The films were taken out of the oven, and peeled off the glass plate with a bit of water after cooling down to room temperature. The films were wiped with soft tissues and kept in the oven at 100 °C overnight to remove any water residues. Naturally cooled films were conserved in a container with drierite (anhydrous Calcium Sulfate) inside.

3.2.3 Gas Permeability Measurement

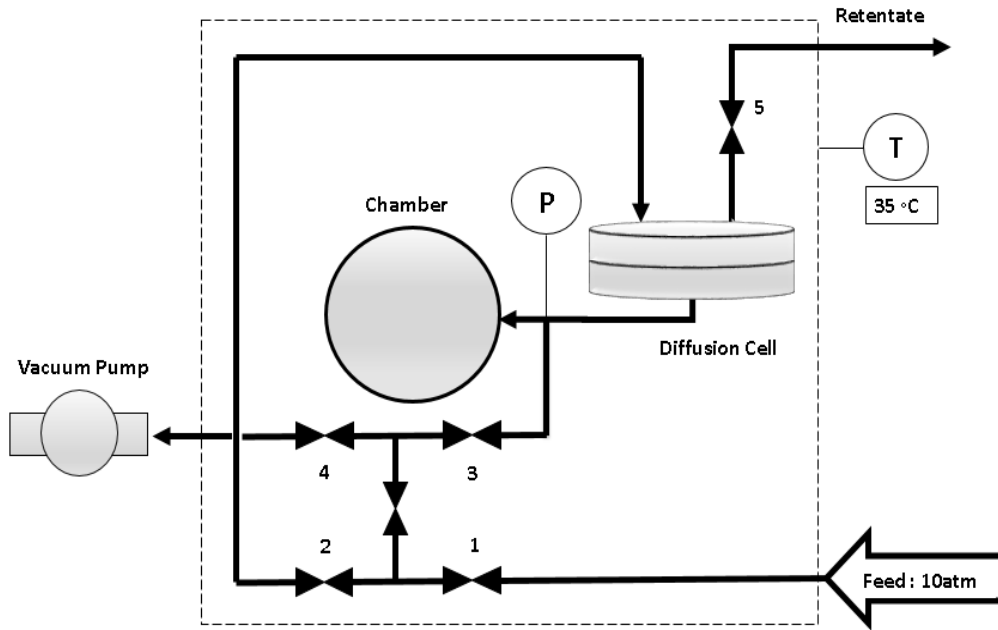


Figure 3.2 Schematic Diagram of Gas Permeability Measurement Apparatus

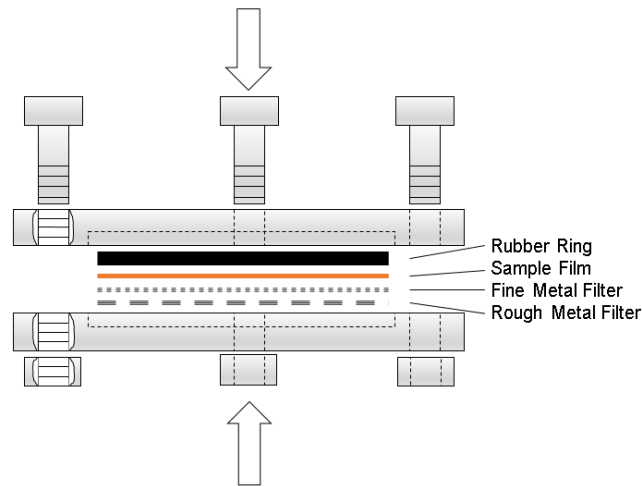


Figure 3.3 Detailed Structure of Diffusion Cell

The permeability was measured using variable-pressure constant-volume method. Figure 3.2 shows the schematic diagram of gas permeability measurement apparatus. The diffusion cell was employed that was separated into two compartments by a sample film (see in Figure3.3).

Before measuring gas flux, the system was kept under vacuum to remove residual air or other gases to obtain accurate measurements. The sample film, totally devoid of adsorbed gases, came in contact with the test gas at the top surface. The upstream pressure P_0 of input feed was kept constant, while an increase in downstream pressure P of the permeation chamber was directly measured by a pressure transducer (reading range 0-10 torr, accuracy 0.001 torr).

Each sample was tested for 3 times for each kind of gas.

The downstream pressure increase rate dp/dt was measured under the temperature of 35°C, and upstream pressure of 132 psig (10atm). The measurement sequence of single gas permeability was according to the sequence of the kinetic diameter of the gas molecules: CH₄ (3.80 Å) > N₂ (3.64 Å) > Ar (3.40Å) > CO₂ (3.30 Å) > H₂ (2.89 Å) > He (2.60 Å) [62, 63]. And the permeability is calculated from the following relationship

$$P_A = \frac{273.15 \times 10^{10} V l}{760 A T \left(\frac{P_0 \times 76}{14.7} \right)} \times \left(\frac{dp}{dt} \right) \quad (3.1)$$

Where P_A is permeability of gas A through films in Barrer (1Barrer= 1×10^{-10} cm³(STP)-cm/cm²sec cmHg), and V is the volume of downstream chamber (cm³). l is the average film thickness (cm). T is the operating temperature (K). A is the effective area of film (cm²), P_0 is upstream pressure (psia). The ideal selectivity from gas A to gas B is defined as below:

$$\alpha_{A/B} = \frac{P_A}{P_B} \quad (3.2)$$

3.3 Results and Discussion

3.3.1 Permeability and Mass Fraction of Matrimid

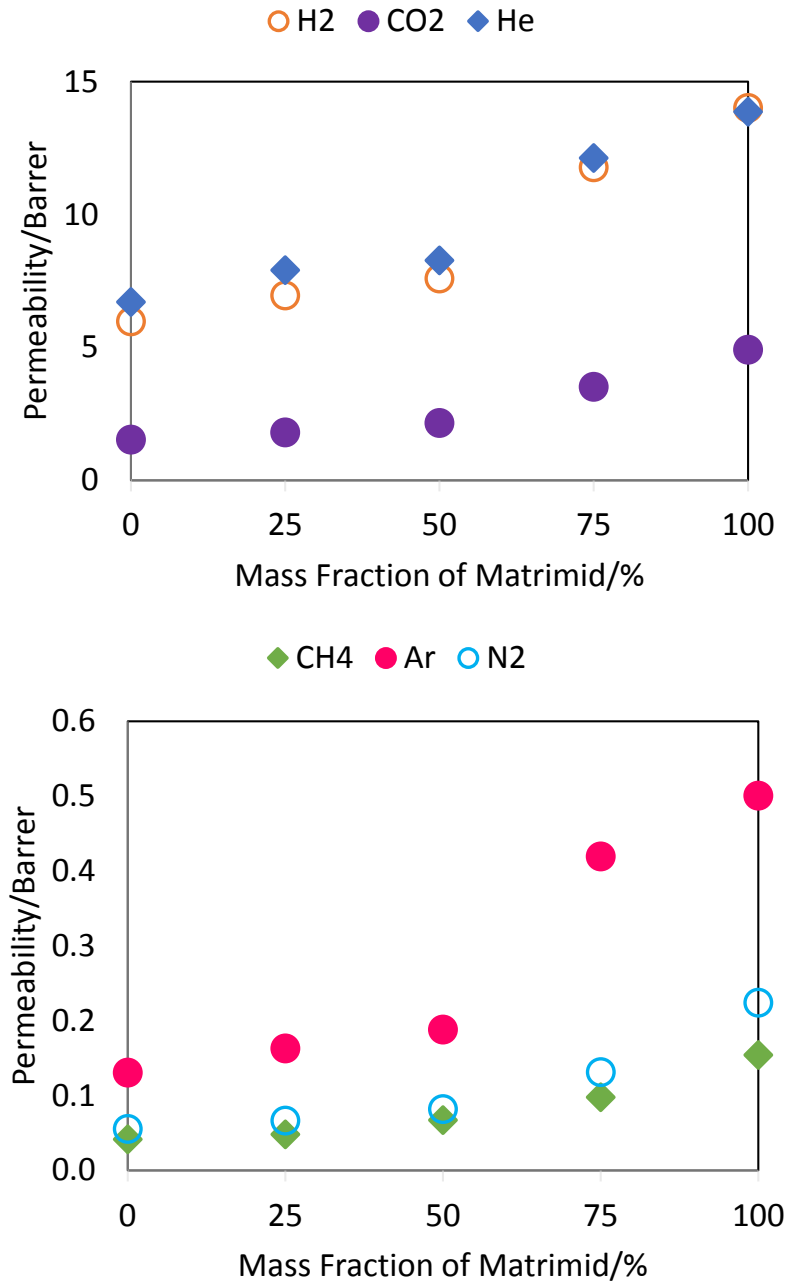


Figure 3.4 Permeability of Matrimid/P84 Blend Films

Figure 3.4 is a summary of permeabilities of each single gas for Matrimid/P84 blend films. It is apparent that for all gases, the permeability of pure Matrimid films is larger than that of pure P84 films, and the permeability of blend films are bracketed by pure polymers. And there is an apparent trend that the permeability of each gas increases with Matrimid content.

For smaller gas molecules He, H₂, CO₂ and Ar, from 0-50 Matrimid wt. %, the rate of increase is slower than that for 50-100 Matrimid wt. %. It demonstrates that the permeability of 50/50 blend films is more like that of pure P84 film than that of pure Matrimid.

For larger gas molecules CH₄ and N₂, there is no sudden change in the rate of increase. The permeability increases smoothly as Matrimid wt. % increases. But the permeability of 50/50 blend film is still more similar to pure P84 than that pure Matrimid.

For each sample film, the permeability values of gases follow the sequence of CH₄<N₂<Ar<CO₂<H₂<He, which is the opposite of gas molecular kinetic diameters.

In conclusion, permeability of each gas has an apparent increasing trend when Matrimid mass fraction increases. For small molecule gases H₂, He, CO₂, Ar, there are two stages where the increasing rate of the first stage is slower than that of the second stage. For large molecules N₂ and CH₄, the increase is smooth with Matrimid mass fraction.

3.3.2 Selectivity and Permeability

A plot of selectivity versus permeability in relation to Robeson's upper bound limit line [64] to show the tradeoff between permeability and permselectivity is presented in Figure 3.5 and Figure 3.6 for the gas pair H₂/N₂ and CO₂/CH₄, separately. Each point in the figure represent the transport data for one sample stamp.

Figure 3.5 indicates transport properties for gas pair H₂/N₂. The selectivity-permeability relationship follows generally follows the trend of the trade-off line of Robeson. Similar to

reference [31, 65] , pure P84 films have lower permeability but higher selectivity than pure Matrimid films. Both this study and reports in the literature have results in the same general range, and all below the Robeson upper limit line.

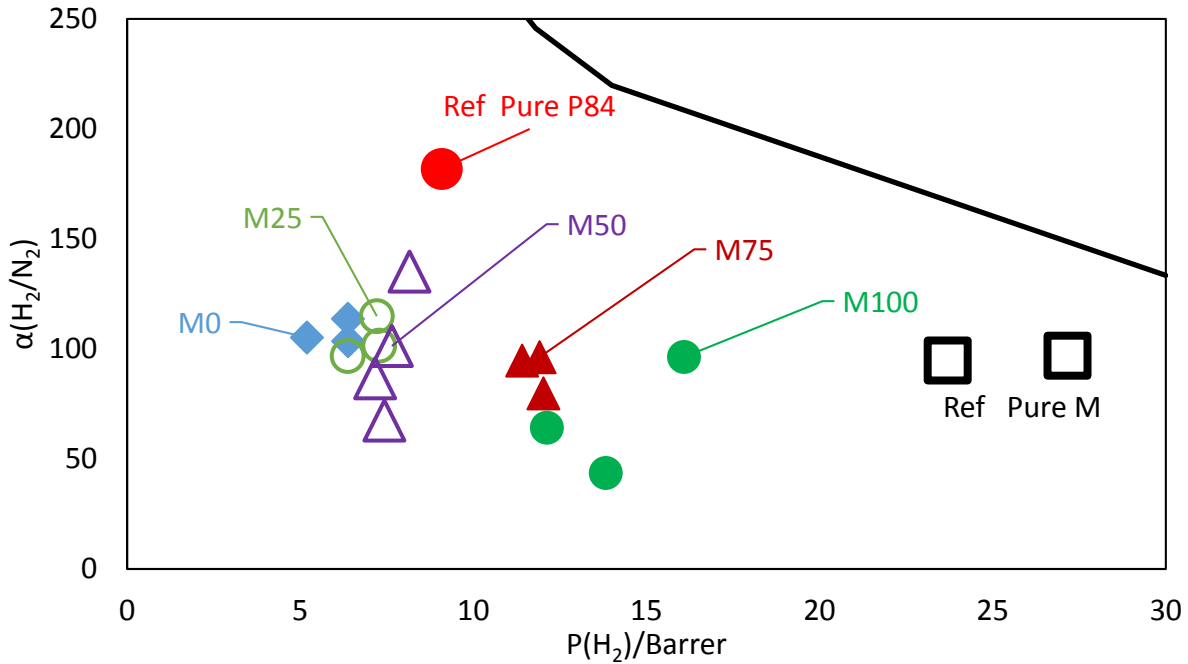


Figure 3.5 Permselectivity of H₂/N₂ versus H₂ permeability. 10 atm, 35°C

Figure 3.6 indicates transport properties for gas pair CO₂/CH₄. There is no apparent relation between permselectivity and permeability of the films. The selectivity-permeability relationship generally follows the trend of the trade-off line of Robeson. CO₂/CH₄ selectivity is closer to other groups [66, 67, 68, 69, 31, 70, 65] than that of H₂/N₂. Pure P84 film has been reported elsewhere to have a smaller permeability but higher selectivity than in this study. Pure Matrimid films reported elsewhere have larger permeability but the selectivity is comparable to this study. Both this study and reports in the literature have results in the same general range, and all below the Robeson upper limit line.

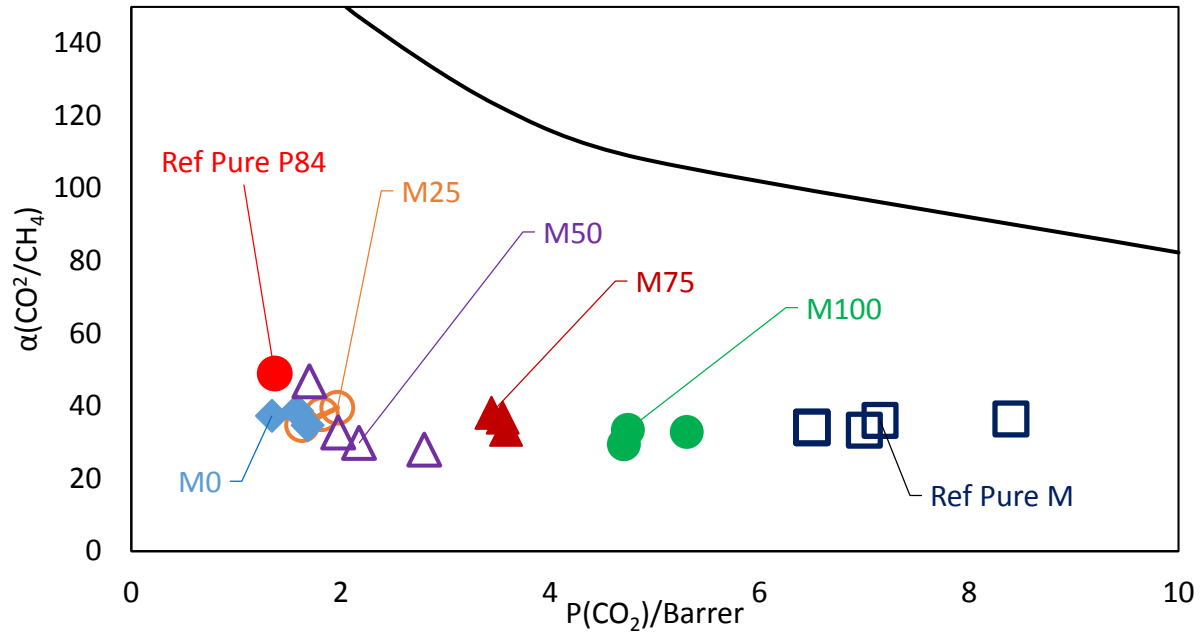


Figure 3.6 Permselectivity of CO₂/CH₄ versus CO₂ permeability. 10 atm, 35 °C

A complete summary of permeability and selectivity of Matrimid/P84 blend films was shown in Appendix B.

3.3.3 Permeability and Polymer Volume Fraction

In Robeson's paper [71], models have been talked about to predict the permeability of miscible blends and partial-miscible blends. For miscible blends, a mostly commonly used equation was applied

$$\ln P_b = \phi_1 \ln P_1 + \phi_2 \ln P_2 \quad (3.3)$$

Where P_b , P_1 , and P_2 are the permeability of the blend, pure Matrimid and pure P84. ϕ_1 and ϕ_2 are the respective volume fractions of Matrimid and P84. The volume fraction was calculated from the following equation [72, 73]:

$$\phi_1 = \frac{\frac{w_1}{\rho_1}}{\frac{w_1}{\rho_1} + \frac{w_2}{\rho_2}} \quad (3.4)$$

Where ρ_1, ρ_2 are the densities of pure Matrimid and pure P84 films, and w_1, w_2 are the mass fraction of pure Matrimid and pure P84 films. Volume fraction can be calculated by [74]

$$\phi_1 = w_1 \times \frac{\rho_{blend}}{\rho_1} \quad (3.5)$$

The comparison of volume fractions calculated from two methods is shown in Table 3.1. The results have very small difference which won't influence the discussion in this part. In the following discussion, the volume fraction calculated from equation (3.5) is employed.

Table 3.1 Comparison of Two Methods of Calculation of Volume Fraction

Matrimid	Density	Matrimid ¹	Matrimid ²
wt. %	g/cc	vol. %	vol.%
0.00	1.35	0.000	0.000
0.25	1.33	0.265	0.266
0.50	1.31	0.519	0.524
0.75	1.28	0.764	0.768
1.00	1.25	1.000	1.000

¹ is calculated from equation (3.4); ² is calculated from equation (3.5).

For partial-miscible blends, there were four models talked about in Robeson's paper [71]: parallel model, series model, Maxwell model and EBM model, with the equations in the below

Parallel Model $P_b = \phi_1 P_1 + \phi_2 P_2$ (3.6)

Series Model

$$P_b = \frac{P_1 P_2}{\phi_1 P_2 + \phi_2 P_1} \quad (3.7)$$

Maxwell's Model

$$P_b = P_m \frac{P_b + 2P_m - 2\phi_b(P_m - P_b)}{P_b + 2P_m + \phi_b(P_m + P_b)} \quad (3.8)$$

Where b is the blend, m is the continuous phase, and d is the dispersed phase.

EBM model (the Equivalent Box Model)

$$P_b = P_1\phi_{1p} + P_2\phi_{2p} + \frac{(\phi_{1s} + \phi_{2s})^2}{\frac{\phi_{1s}}{P_1} + \frac{\phi_{2s}}{P_2}} \quad (3.9)$$

Where b is for blend, m is for continuous phase, d is for dispersed phase, P is for permeability, and ϕ is for volume fraction, 1 and 2 are for two components. $\phi_{1p}, \phi_{2p}, \phi_{1s}, \phi_{2s}$ are defined by the expressions

$$\phi_{1p} = [(\phi_1 - \phi_{1cr})/(1 - \phi_{1cr})]^{T_1} \quad \phi_{1s} = \phi_1 - \phi_{1p} \quad (3.10)$$

$$\phi_{2p} = [(\phi_2 - \phi_{2cr})/(1 - \phi_{2cr})]^{T_2} \quad \phi_{2s} = \phi_2 - \phi_{2p} \quad (3.11)$$

Where ϕ_{1cr}, ϕ_{2cr} are critical threshold percolation values of component 1 and 2, and T_1, T_2 are the critical universal exponents for the components. For discrete spherical domains,

$$\phi_{1cr} = \phi_{2cr} = 0.156$$

$$T_1 = T_2 = 1.833$$

But in the regions of low concentration

$$\phi_{1p} = 0 \quad \phi_{1s} = \phi_1 \quad (\text{when } 0 < \phi_1 < \phi_{1cr})$$

$$\phi_{2p} = 0 \quad \phi_{2s} = \phi_2 \quad (\text{when } 0 < \phi_2 < \phi_{2cr})$$

Figure 3.7 is a summary of the six models applied to correlate permeability of CH₄ and volume fraction of Matrimid. And apparently the Series Model has the best simulation of the real experimental data. All the data fits in the series model and the blend films present a partial-miscible characteristic here. Therefore, the series model has been selected as the model to describe the relationship between P and volume fraction for other gases.

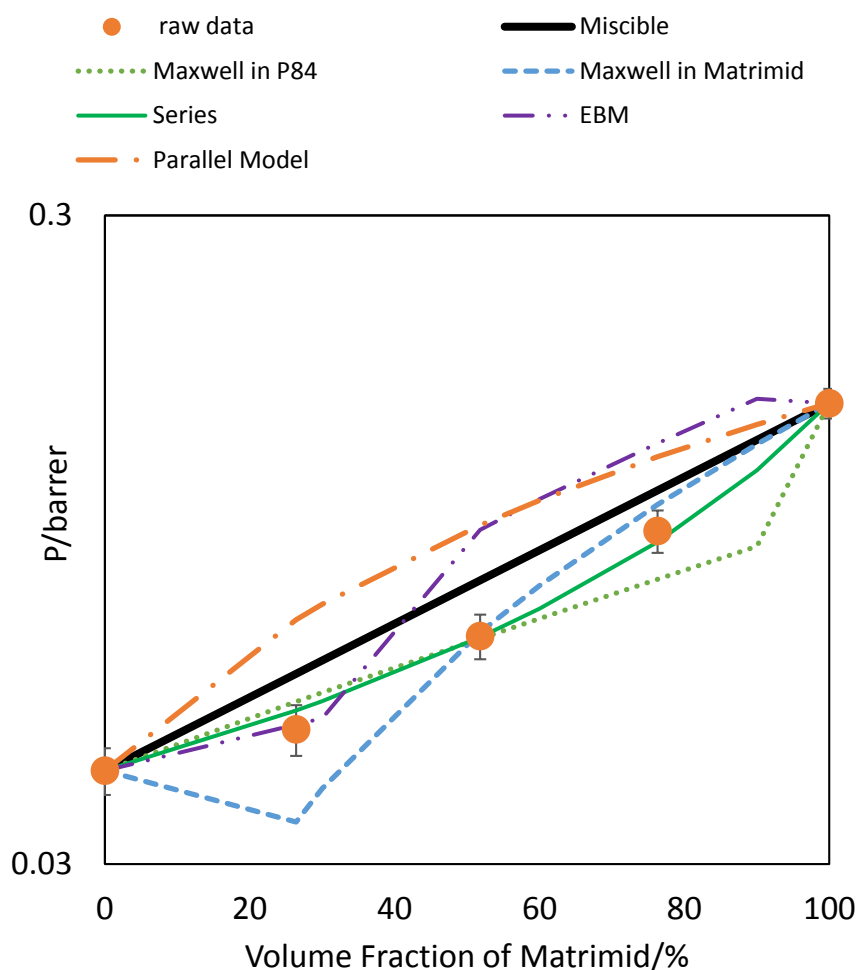


Figure 3.7 Correlation of $P(\text{CH}_4)$ with Matrimid vol. % with Six Models for Matrimid/P84 Blend Films

Figure 3.8 is the correlation of permeability of N_2 with volume fraction of Matrimid. Similar as the performance of N_2 , the experimental data fits in the series model quite well with the consideration of error bars and the polymer blends present partial-miscible behavior.

Figure 3.9 is the correlation of permeability of Ar with volume fraction of Matrimid. The average value of permeability is above but near the miscible line at 76.3 vol. %. While at 51.8 vol. %, the average permeability is below but near the series model line. But considering the error bars, the permeability of Ar generally follows the Series Model line. And the blends represent partial-miscible characteristic.

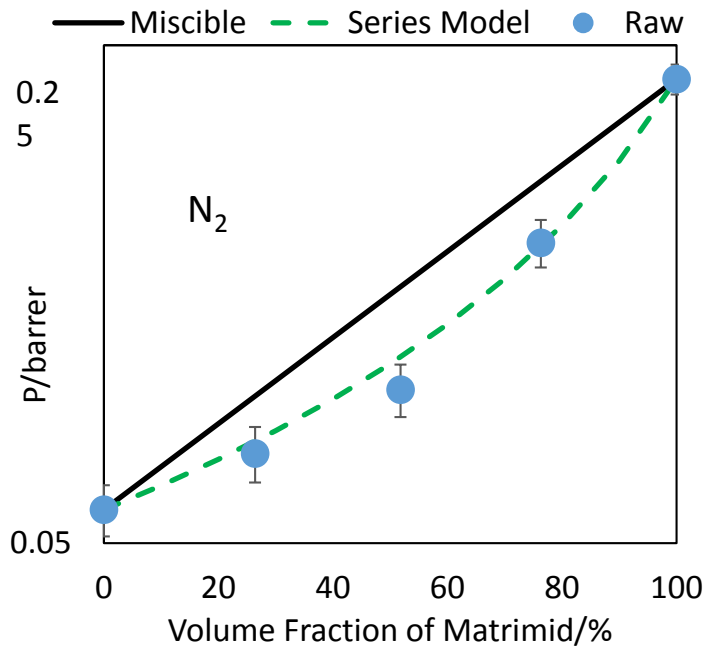


Figure 3.8 Correlation of $P(N_2)$ with Matrimid vol. % with Series Model for Matrimid/P84 Blend Films

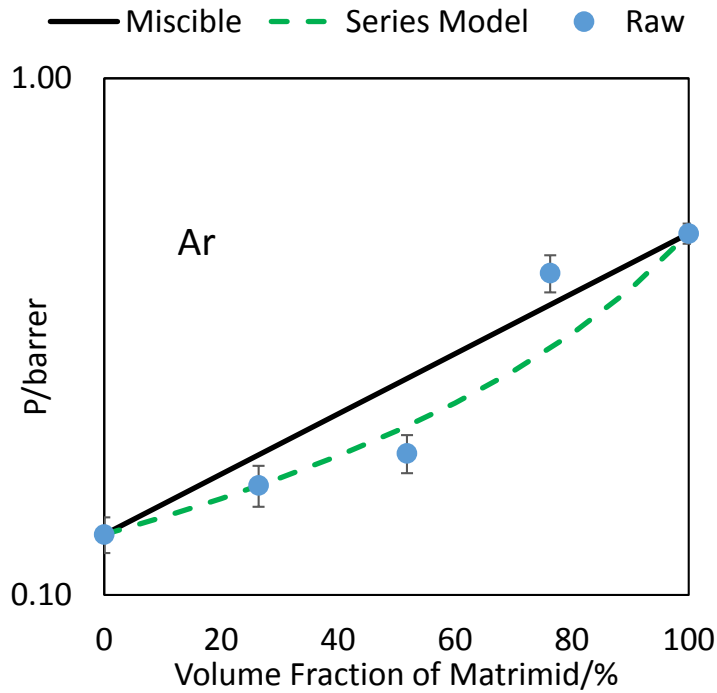


Figure 3.9 Correlation of $P(Ar)$ with Matrimid vol. % with Series Model for Matrimid/P84 Blend Films

Figure 3.10 is the correlation of permeability of CO₂ with volume fraction of Matrimid. The average value of permeability is above but near the series line at 76.3 vol. %. While at 51.8 vol. %, the average permeability is slightly below but near the series model line. But considering the error bars, the permeability of CO₂ can fit in the series model. And the blends represent partial-miscible characteristic. In reference [75], the correlation of permeability of CO₂ and volume fraction also fits the Series Model.

H₂ and He have very similar transport behavior, as shown in Figure 3.11 and 3.12. The average value of permeability is above but near the miscible line at 76.3 vol. %. While at 51.8 vol. %, the average permeability is slightly below but near the series model line. But taking the error bars into account, the permeability of H₂ and He can be considered to fit in the series model. And the blends represent partial-miscible characteristic.

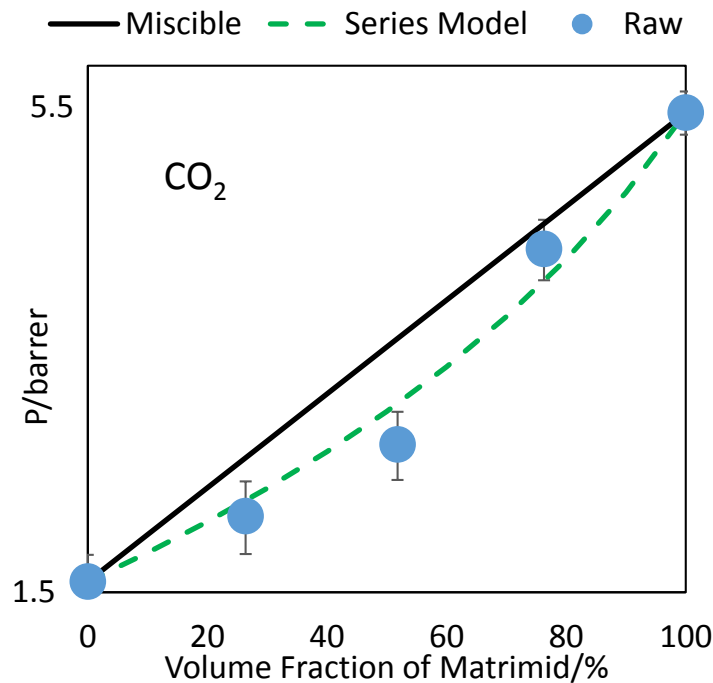


Figure 3.10 Correlation of P(CO₂) with Matrimid vol. % with Series Model for Matrimid/P84 Blend Films

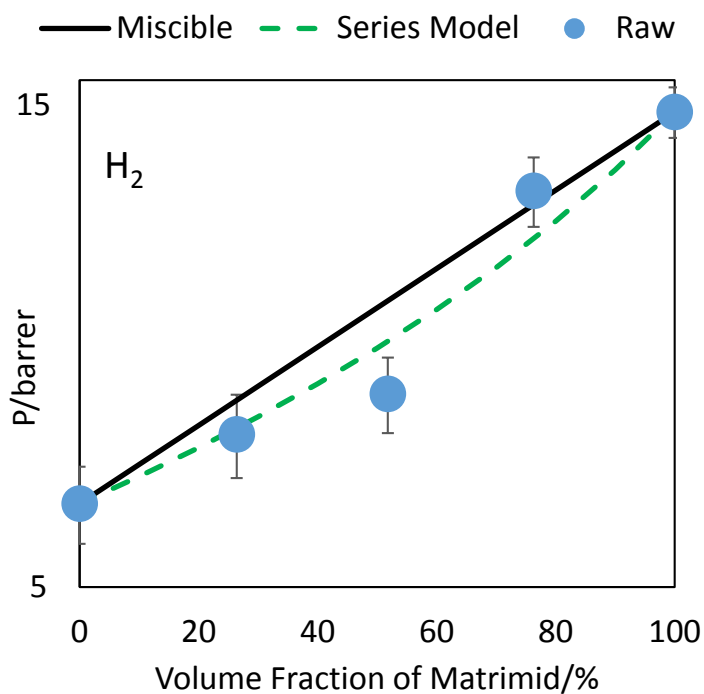


Figure 3.11 Correlation of $P(H_2)$ with Matrimid vol. % with Series Model for Matrimid/P84 Blend Films

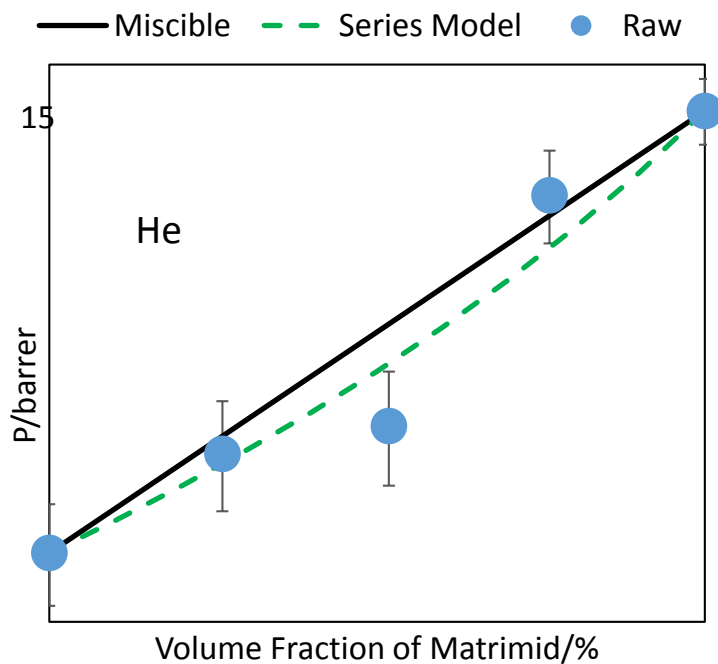


Figure 3.12 Correlation of $P(He)$ with Matrimid vol. % with Series Model for Matrimid/P84 Blend Films

3.3.4 Permeability and Fractional Free Volume (FFV)

Free volume is an intrinsic property of the polymer matrix and arises from the gaps left between entangled polymers chains [76]. Permeability is defined as the product of the diffusion coefficient and the sorption coefficient, as shown in equation (3.3).

$$P = D \cdot S \quad (3.12)$$

Where P is permeability, D is the diffusion coefficient and S is the sorption coefficient. It has been indicated that free volume is among the most important factors that influence the diffusion coefficient, and the solubility also depends on free volume [2, 52, 76]. Greater free volume always means higher capacity of absorption and higher mobility of the molecules within matrix. The gas permeability is often correlated with the fractional free volume (FFV) in an amorphous polymer through the following equation [52]

$$P = A \exp\left(-\frac{B}{FFV}\right) \quad (3.13)$$

Which can be transformed into

$$\ln P = m + n \times \frac{1}{FFV} \quad (3.14)$$

Where A , B , m , and n are adjustable constants.

The calculation of fractional free volume has been discussed in Chapter 2 and there are two groups of FFV which were calculated from two different database of van der Waal's volumes, and for convenience, the two database were referred as Resource I [52] and Resource II [53].

The algorithm of the permeability as a function of reciprocal fractional free volume is shown in Figure 3.13 (Resource I) and Figure 3.14 (Resource II). Dashed lines are simulated linear trend lines. Figure 3.13 shows that except for small deviations for Argon, a linear relation exists between $\ln P$ and $1/FFV$, which is in agreement with equation (3.13). The permeability decreases

with increasing reciprocal fractional free volume, in another word, the permeability increases with increasing fractional free volume. Same rules appeared in Figure 3.14.

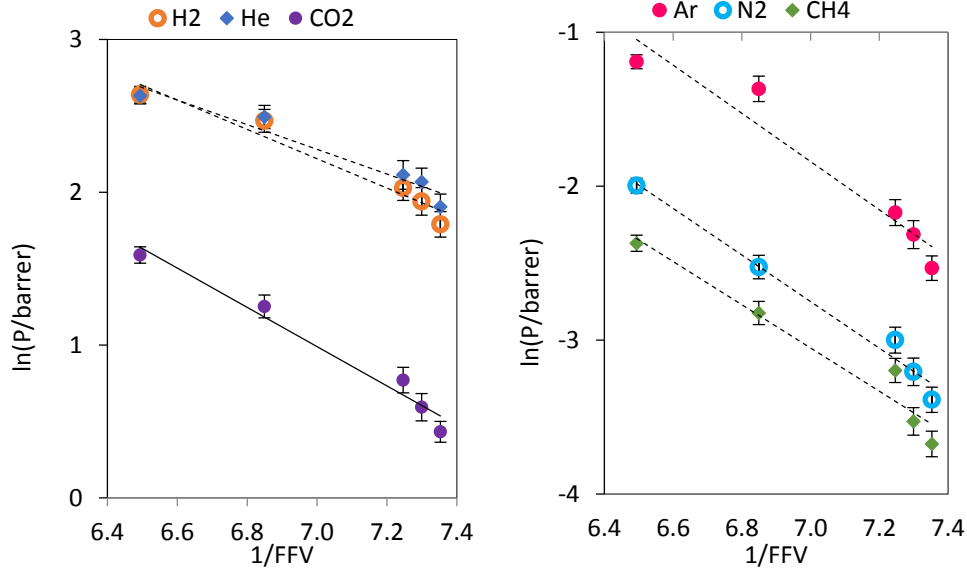


Figure 3.13 Correlation of CH₄, N₂, Ar CO₂, He, and H₂ permeability with 1/FFV. For each gas, from left to right, the data points represent films of 100, 75, 50, 25, 0wt%Matrimid. FFV is calculated from Resource I [52]

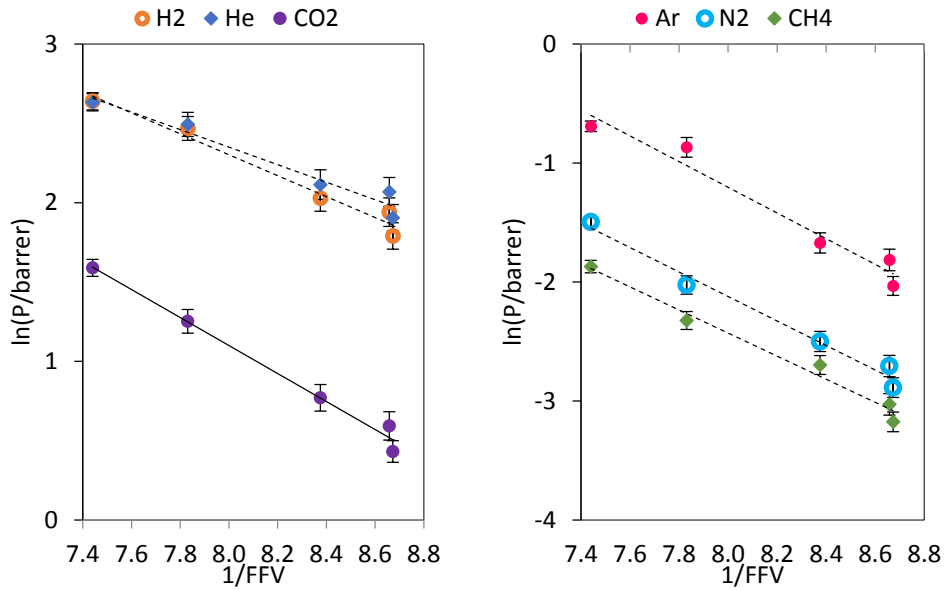


Figure 3.14 Correlation of CH₄, N₂, Ar CO₂, He, and H₂ permeability with 1/FFV. For each gas, from left to right, the data points represent films of 100, 75, 50, 25, 0wt%Matrimid. FFV is calculated from Resource II [53]

3.4 Conclusion

In this chapter, transport properties of Matrimid/P84 blend films were measured and discussed. The blend films exhibit partial-miscibility behavior.

Permeability of each gas has an apparent increasing trend when Matrimid mass fraction increases. For small molecule gases H_2 , He, CO_2 , Ar, there are two stages where the increasing rate of the first stage is slower than that of the second stage. For large molecules N_2 and CH_4 , the increase is smooth with Matrimid mass fraction.

The selectivity-permeability relationship for gas pair H_2/N_2 and CO_2/CH_4 followed the trend of the trade off line of Robeson. The transport data in this study is in a reasonable range in comparison with reference. Both the data points in this study and in reference are below the Robeson's upper limit line. Therefore, there is still large space for the enhancement of the transport properties of the Matrimid/P84 blend films.

The relationship between permeability and Matrimid volume fraction has been rationalized by applying a logarithmic relationship and the experimental data generally fits the series model line indicating that the blend films are partial-miscible.

The correlation of logarithm of permeability and reciprocal FFV indicates a linear relationship between the two parameters, which leads to a conclusion that permeability strongly depends on FFV. As $1/FFV$ increases, or as FFV decreases, the mobility of polymer is decreased and the structure is more rigid, and the space between polymer chains is reduced, therefore the permeability decreases.

Chapter 4 - Desorption of Liquid Solutes in Matrimid/P84 Blend

Films

4.1 Introduction

Polyimide membrane is of interest because of the commercial availability and great transport properties. Combination of Matrimid which has higher permeability and selectivity, and P84 which has plasticization resistance, can hopefully develop blend membranes with a combination of the advantages of the two polymers. The sorption behavior of water or organic solvents in polymeric membrane materials such as polyimide, has a strong effect on the separation efficiency of the dense polymeric membranes.

There are three modes of transport to explain the mechanism of desorption in this study [77]:

- (I) case I or Fick diffusion, occurred when the diffusion rate of penetrant molecules is much slower than the polymer chain relaxation; the flux follows the Fick's Law and the solute dissolves into the polymer matrix and subsequently diffuses across the membrane due to the concentration gradient [78]
- (II) case II diffusion, occurred when the penetrant diffusion rate is much faster than the polymer chain relaxation; the diffusion has a sharp front and a linear kinetics and essentially no concentration gradient behind the front
- (III) case III or anomalous diffusion, occurred when the penetrant mobility and polymer chain relaxation rates are similar and two-stage sorption behavior can be observed sometimes.

In Wang's paper [79], a combination of Fickian and case II mechanism were applied to study vapor desorption of dense films and the model used can fit the experimental data well. In Sun's paper [80], a two-stage sorption models (case III) was used to describe the desorption behavior of water vapor in PHEMA membrane and can simulate the experimental data in an almost perfect way.

In Sun's model, the slow relaxation of the polymer chains due to sorption of penetrant is used to interpret the anomalies in the sorption kinetics. When a penetrant enters the polymer matrix, motions of whole or portions of glassy polymer chains are not sufficiently rapid to completely homogenize the penetrant's environment. Penetrants can thus potentially rest the holes or irregular cavities with very different intrinsic diffusional mobilities.

The relative magnitude of the rates of diffusion and relaxation processes is a major factor determining the anomalous effects in polymer-penetrant diffusion. A diffusion Deborah number ($(DEB)_D$) [77, 81] was proposed to characterize this quantity:

$$(DEB)_D = \frac{t_{relaxation}}{t_{diffusion}} = \frac{\lambda_m}{\theta_D} \quad (4.1)$$

Where λ_m is the characteristic time of the relaxation and

$$\theta_D = \frac{L_0^2}{D} \quad (4.2)$$

Where L_0 is the sample dimension in the direction of transport and D is the diffusion coefficient.

If the relaxation follows a first-order kinetics [82], the characteristic time λ_m is represented by the reciprocal of the first-order rate constant k :

$$\lambda_m = \frac{1}{k} \quad (4.3)$$

Therefore the diffusion Deborah number can be expressed as

$$(DEB)_D = \frac{D}{kL_0^2} \quad (4.4)$$

Which is proportional to the ratio of the diffusion rate of a penetrant to the relaxation rate of the polymer system. When both the rate of diffusion and relaxation are similar in magnitude, anomalous diffusion dominate. On the other hand, when one of them is much larger than the other, Fickian diffusion will be in domain.

When $(DEB)_D \gg 1$, the diffusion is much faster than the rate of the polymer relaxation and the glassy state is preserved, the ‘elastic’ Fickian diffusion prevails. While for $(DEB)_D \ll 1$, the polymer relaxes to a rubbery state in a speed much faster than the diffusion of the penetrant, the ‘viscous’ Fickian diffusion is expected. If $(DEB)_D$ is of the order of unity, the diffusion process can be described as ‘viscoelastic’.

Two-stage sorption is one of the notable non-Fickian features of glassy polymer system [82, 83, 84]. In this study, two-stage desorption from a desorption experimental of different solvent in Matrimid/P84 blend films were observed. Correlation of the data with mathematical models to track down the kinetic and equilibrium parameters of the system. The variable surface-concentration model proposed by Long and Richman gave a satisfactory fitting of the experimental data.

In this chapter, a series of mass ratios of Matrimid/P84 blended films were prepared. And the desorption of water, methanol, toluene, 1-propanol, 2-propanol, and butanol for the blend films have been studied experimentally and interpreted mathematically with three models. By comparing some similar and different features of these three models, a general discussion of the advantages and limitations of these models is presented.

4.2 Experimental

4.2.1 Materials

Matrimid 5218 (poly [3, 3'4, 4'-benzophenone tetracarboxylic dianhydride and 5(6)-amino-1-(4'-aminophenyl-1, 3-trimethylindane)], BTDA-DAPI) was supplied by Huntsman Advanced Materials Americas Inc. P84 (copolyimide of 3, 3'4, 4'-benzophenone tetracarboxylic dianhydride and 80% methylphenylenediamine + 20% methylenediamine) was provided by HP Polymer Inc. NMP (N-Methyl-2-pyrrolidone, purity 99%) was supplied by Sigma-Aldrich. 2-propanol (purity 99.9%), 1-butanol (purity 99.9%), toluene (purity 99.9%), methanol (purity 99.9%), and 1-propanol (purity 99.9%) were supplied by Fisher Scientific. All solvents were used as received. Water was deionized water supplied directly to the lab.

4.2.2 Preparation of Matrimid/P84 Blend Films

The films were prepared by a casting method. Polymer solutions (20 wt. % polymer/80 wt. % NMP) with various compositions of 0/100, 10/90, 25/75, 50/50, 75/25, 90/10, 100/0 g/g were prepared from Matrimid and P84 according to the following steps.

Firstly, polymer powders were dissolved by NMP in glass jars under room temperature. The jars were capped and settled in the hood under room temperature without stirring for at least a week until totally dissolved (there were no visible polymer powder particles and the solution is visibly transparent while the color is evenly distributed).

The solutions were poured on a glass plate and cast with a casting knife with a very slow rate under room temperature, with the thickness set to 50 μ m. Subsequently, films were dried in a

vacuum oven at 50 °C for 12 hours, and then at 100 °C for 12 hours, and finally 150 °C for 48 hours to get rid of the solvent residues.

The films were taken out of the oven, and peeled off the glass plate with a bit of water after cooling down to room temperature. The films were wiped with soft tissues and kept in the oven at 100 °C overnight to remove any water residues. Naturally cooled films were conserved in a container with drierite (anhydrous Calcium Sulfate) inside.

4.2.3 Desorption Measurement of Liquid Solutes in Matrimid/P84 Blend Films

Dense films were cut into stamps, dried in the oven at 100 °C overnight and weighed before immersed into solvents (n-butane, water, toluene, methanol, 1-propanol, 2-propanol). The samples were weighed before immersion, then weighed again after a week and maintained in solvent bath for three month.

For each solvent desorption measurement, a sample was taken out of the solvent bath, wiped gently and quickly, and put on the zeroed digital scale (accuracy=0.001g). Consider the time as zero when the sample was put on the scale and record the mass at the initial time. Read the scale for every 10 seconds for the first 1 minutes, every 30 seconds for the following 5 minutes, every 60 seconds for the following 5 minutes, every 5 minutes for the following 30 minutes, every 15~20 minutes for the following time. The total measure time varies from 2 hours to one week.

The sample was dried at 120 °C overnight before taken out. Mass and Thickness measured again.

Because the mathematical models used in this study are all used in the form of sorption, the mass uptake is also presented in the form of sorption. The uptake of desorption has been transferred in to the form of sorption by the way of:

$$\left(\frac{M_t}{M_\infty}\right)_{sorption} = \left(1 - \frac{M_t}{M_\infty}\right)_{desorption} \quad (4.5)$$

Where $(M_t)_{desorption}$ equals to mass at time t deducted by mass of dry film, $(M_t)_{desorption}$ equals to mass at time zero deducted by mass of dry film. And every $\frac{M_t}{M_\infty}$ that appears in the following content represents mass uptake in sorption.

4.2 Mathematical Models for Desorption

4.2.1 Crank's Model

A model from Crank [85] was applied in this paper to calculate diffusion coefficient of desorption:

$$\frac{M_t}{M_\infty} = 1 - \frac{8}{\pi^2} \sum_{m=0}^{\infty} \frac{1}{(2m+1)^2} \exp\left[-\frac{D(2m+1)^2\pi^2 t}{l^2}\right] \quad (4.6)$$

Where M_t is the total amount of penetrant A (solute) absorbed by the polymer at time t, M_∞ is the equilibrium sorption mass and D is the Fickian diffusion coefficient.

4.2.2 Wang's Model

Wang and his coworkers [79] had studied the diffusion of organic vapors in glassy polymers in terms of a combination of Fickian and case II mechanism. The model used is shown below:

$$\frac{M_t}{M_\infty} = 1 - \sum_{N=0}^{\infty} \frac{4n^2\pi^2 \left(1 - (-1)^n \cosh\left(\frac{vl}{2D}\right)\right)}{\left(\left(\frac{vl}{2D}\right)^2 + (n\pi)^2\right)^2} \times \exp\left(-\left(\frac{n^2\pi^2 D}{l^2} + \frac{v^2}{4D}\right)t\right) \quad (4.7)$$

Where M_t is the total amount of penetrant (solute) absorbed by the polymer at time t , M_∞ is the equilibrium uptake mass and D is the Fickian diffusion coefficient. v is the velocity of case II diffusion and has been used as a stress coefficient to represent the effect of the differential stress on transport properties. l is the thickness. The value of $\left(\frac{vl}{2D}\right)$ in the calculation of this study was 1.

4.2.3 Variable Surface-Concentration Model

A model proposed by Long and Richman [83] to provide a reasonable explanation for two-stage sorption behavior. This model was transformed into a more generalized way by Sun [80] as below, assuming that the concentration at the film surface jumps to C_0 as soon as the film contacts the vapor and then reaches a final concentration C_∞ following a first order relaxation process. It is also assumed that the concentration of penetrant is symmetric at the center of the film.

$$\begin{aligned} \frac{M_t}{M_\infty} = & \phi \left(1 - \frac{8}{\pi^2} \sum_{n=0}^{\infty} \frac{\exp\left(\frac{-(2n+1)^2\pi^2\theta}{4}\right)}{(2n+1)^2} \right) \\ & + (1 - \phi) \left(1 - \frac{\tan\sqrt{\psi}\exp(-\psi\theta)}{\sqrt{\psi}} - \frac{8}{\pi^2} \sum_{n=0}^{\infty} \frac{\exp\left(\frac{-(2n+1)^2\pi^2\theta}{4}\right)}{(2n+1)^2 \left(1 - \frac{(2n+1)^2\pi^2}{4\psi}\right)} \right) \end{aligned} \quad (4.8)$$

And the dimensionless variables are

$$\theta = \frac{D_0 t}{L^2} \quad \psi = \frac{kL^2}{D_0} \quad \phi = \frac{C_0}{C_\infty} \quad (4.9)$$

Where L is the half-thickness of the film, k is the rate constant of the relaxation process, θ is the dimensionless time, ψ is the inverse of the diffusion Deborah number and ϕ is the equilibrium ratio constant which represents the ratio of the equilibriums of the first stage to that of the second stage in the sorption. The first part on the right-hand side of equation (4.7) is the

classical Fickian diffusion to the quasi-equilibrium (first stage), and is the weight uptake for the penetrant which enters due to diffusion down the concentration gradient set up by the initial surface concentration. The second part is for the penetrant which enters as a result of the time dependence of the surface concentration change.

4.3 Results and Discussion

4.3.1 Investigation of Experimental Data

The experimental desorption data were first plotted in the form of uptake versus time. As shown in Figure 4.1, curves for blend films of successive desorption data for water in the form of $\frac{M_t}{M_\infty}$ versus the square root of time were plotted as a standard example to show the desorption characteristics of all the solvents. The curves have an obvious two-stage characteristic. The first stage is linear, and the second stage is plateau. All the curves of solvents do not reach 1 (representing complete desorption), and possible reasons could be the polymerization or clustering of solutes due to hydrogen bonding [86] and trapping skinning [87] during desorption.

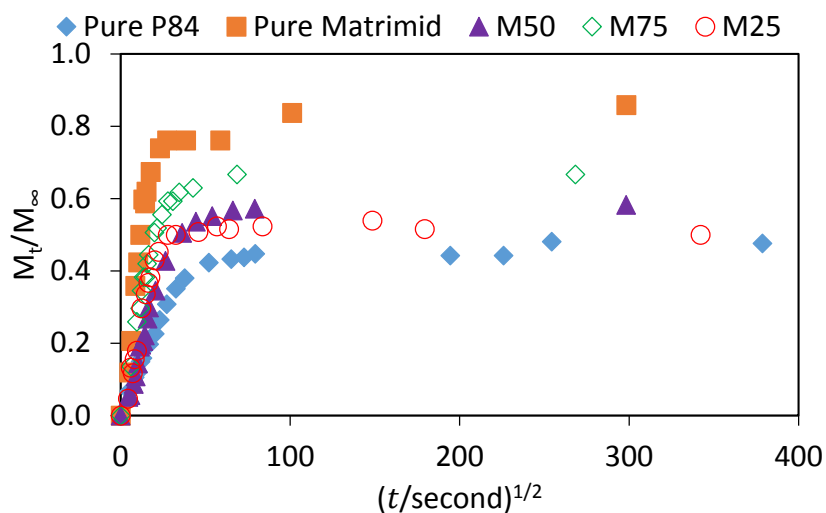


Figure 4.1 Desorption Data of Water in Matrimid/P84 Blend Films. Room temperature, 1atm.

The polymerization process is considered to be a purely random formation of hydrogen bonds. Cavities have been indicated to be present in glassy polymers [86]. As shown in Figure 4.2, penetrant molecules would be preferentially sorbed in cavities rather than the denser region of the matrix considering the need of degree of expansion. Despite the sorptive capacity of polymers, the polar groups of the polymers would also donate centers of nucleation for cluster growth. Formation of clusters would cause the decrease of diffusion coefficient with concentration.

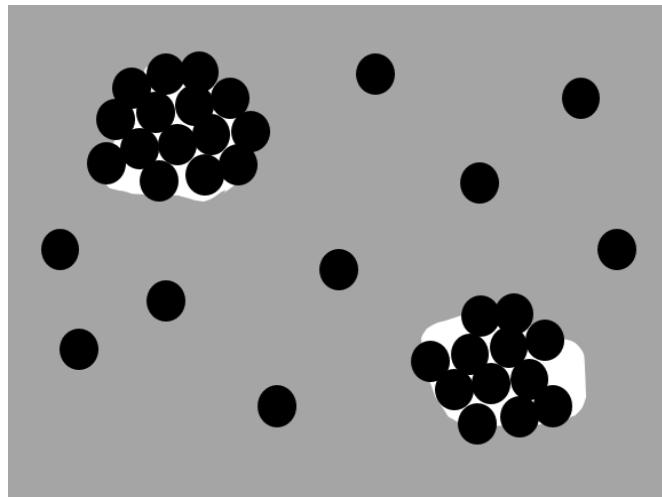


Figure 4.2 Polymerization of Penetrants in the Films

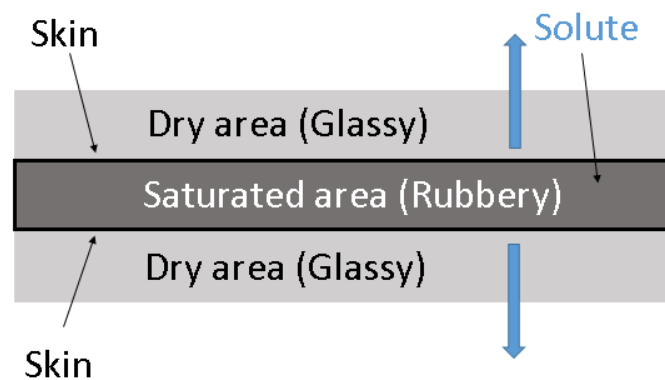


Figure 4.3 Skinning Trapping

As shown in Figure 4.3, Matrimid and P84 are glassy polymers when dried but in a rubbery state when saturated. The penetrates diffuse through glassy polymers in a slow rate but travel through rubbery polymers quickly. During the desorption of such a saturated film, often a glassy

region, or skin, develops at the exposed surface. The phenomenon that the film during desorption may have a glassy skin and rubbery inside material, is called literal skinning [87]. Then desorption process will be slowed by the skin due to the smaller diffusion coefficient of the glassy region. Trapping skinning is an anomalous special case of the skinning effect in which an increase in the force driving the desorption will actually decrease the accumulated flux through the boundary. This process is dominated by the viscoelastic stress, which is related the relaxation time of polymers, which is infinite in glassy polymers and instantaneous in rubbery polymers.

4.3.2 General Comparison of Three Models

Three mathematical models have been applied to fit the experimental data. Diffusion coefficients and relative parameters were calculated from the models and shown as below. From Table 4.1~4.3, the diffusion coefficient of solvent in Matrimid/P84 blend films are in the range of 10^{-8} ~ 10^{-10} cm²/s. The experimental results show significant differences in the sorption speed of solute liquids in the two polyimides. The desorption of toluene, 1-propanol, water, methanol is very fast compared to the desorption of 2-propanol and butanol. Table 4.4 are the parameters for Model III.

Table 4.1 Summary of Diffusion Coefficients Calculated from Model I

Solvents	M0	M10	M25	M50	M75	M90	M100
Water	0.90		1.07	1.84	1.72		3.88
Methanol			2.26	3.46	1.98		6.24
1-Propanol			0.01	4.40	5.11		1.55
Butanol		0.08		0.04	0.10	0.25	0.39
Toluene				2.54	5.23	3.55	
2-Propanol					0.07	0.13	0.08

Unit: $10^8 \text{ cm}^2/\text{s}$

Condition: Room Temperature, 1atm

Table 4.2 Summary of Diffusion Coefficients Calculated from Model II

Solvents	M0	M10	M25	M50	M75	M90	M100
Water	0.23		0.25	0.50	0.50		1.00
Methanol			0.50	0.90	0.50		1.40
1-Propanol			0.002	1.00	1.40		0.40
Butanol		0.04		0.01	0.03	0.05	0.10
Toluene				0.58	1.20	0.08	
2-Propanol					0.02	0.03	0.02

Unit: $10^8 \text{ cm}^2/\text{s}$

Condition: Room Temperature, 1atm

Table 4.3 Summary of Diffusion Coefficients Calculated from Model III

Solvents	M0	M10	M25	M50	M75	M90	M100
Water	1.10		1.20	1.50	2.00		1.50
Methanol			1.50	3.00	1.20		4.00
1-Propanol			0.012	2.50	3.00		1.30
Butanol		0.15		0.035	0.07	0.10	0.25
Toluene				1.50	2.50	2.00	
2-Propanol					0.20	0.30	0.26

Unit: $10^{-8} \text{ cm}^2/\text{s}$

Condition: Room Temperature, 1atm

Table 4.4 Parameters of Model III

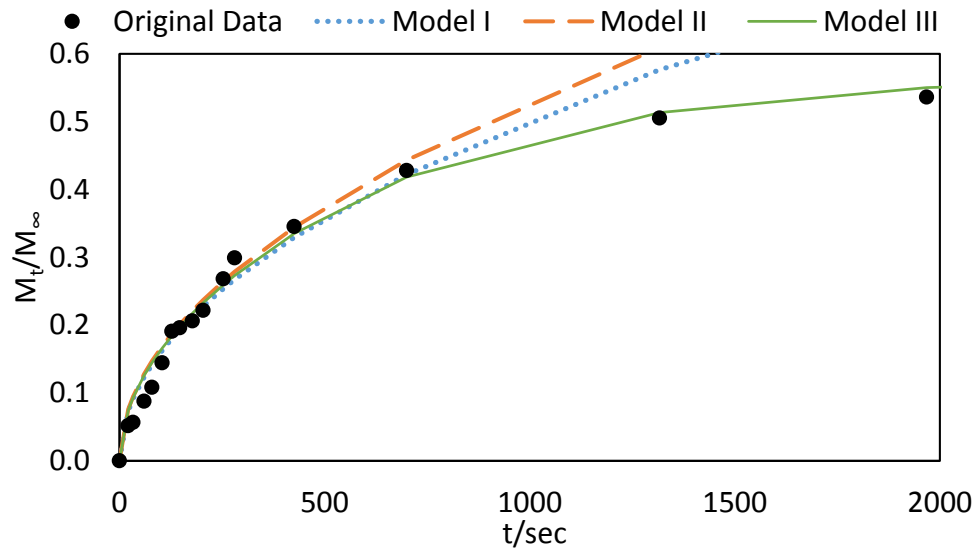
	$k \cdot 10^6 \text{ (s}^{-1}\text{)}$						
	M0	M10	M25	M50	M75	M90	M100
Water	0.00488		0.0158	0.651	2.33		4.03
Methanol			37.2	69.4	51.0		172
1-Propanol			0.281	0.796	52.8		3.36
Butanol		0.619		0.258	0.283	0.434	0.510
Toluene				0.851	2.75	2.70	
2-Propanol					3.20	4.45	4.07

	$\psi = k \cdot L^2 / D_0$						
	M0	M10	M25	M50	M75	M90	M100
Water	0.000001		0.00001	0.001	0.001		0.002
Methanol			0.02	0.05	0.035		0.04
1-Propanol			0.015	0.0007	0.015		0.002
Butanol		0.0023		0.015	0.0034	0.003	0.002
Toluene				0.0012	0.0012	0.004	
2-Propanol					0.011	0.0095	0.011

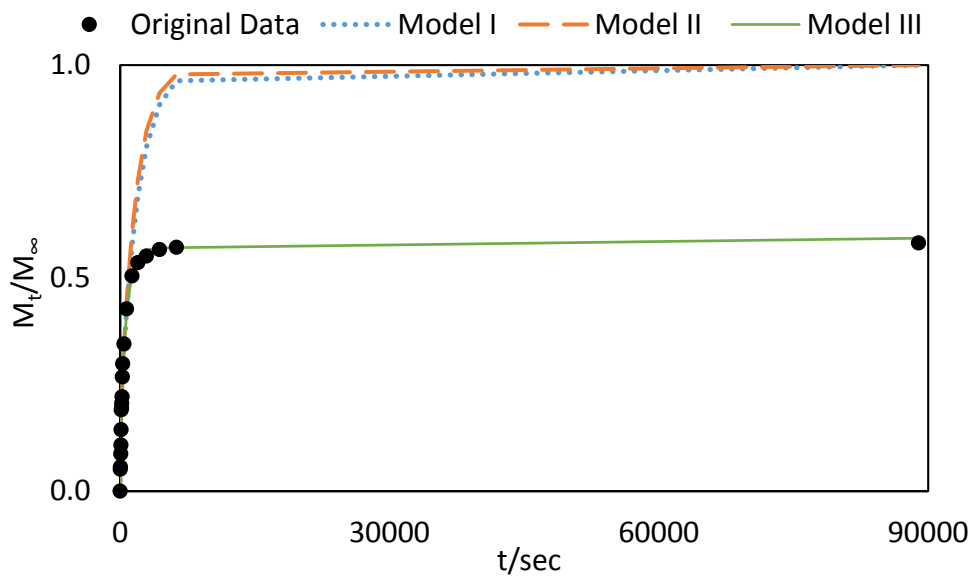
ψ is dimensionless.

	$\phi = C_0 / C_f$						
	M0	M10	M25	M50	M75	M90	M100
Water	0.48		0.52	0.57	0.70		0.80
Methanol			0.55	0.50	0.60		0.65
1-Propanol			0.40	0.50	0.62		0.55
Butanol		0.53		0.36	0.48	0.52	0.52
Toluene				0.62	0.72	0.72	
2-Propanol					0.30	0.32	0.30

ϕ is dimensionless.



(a)



(b)

Figure 4.4 Modelling of the Experimental Data for Water Desorption in 50 Matrimid % Blend Film. (a) Short time range (b) Whole time range. Room temperature, 1atm.

From Figure 4.4, all the three models can simulate the experimental data reasonably well for short time stage. Only Model III can fit the second stage well, which became a plateau before reaching 1.

4.3.3 Mass Fraction of Matrimid and Diffusion Coefficients in Three Models

The values of diffusion coefficients calculated from three models were summarized in Figure 4.5~Figure 4.10, and each figure is for one single solvent with the comparison of three models. I, II, II represent the three mathematical models.

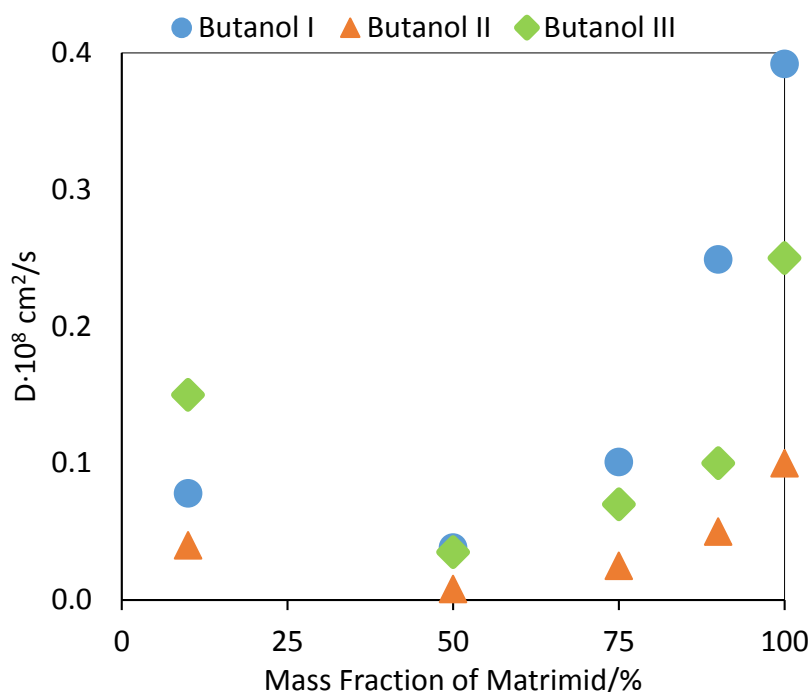


Figure 4.5 Comparison of Butanol Diffusion Coefficients of Three Models versus Mass Fraction of Matrimid. Room temperature, 1 atm.

For the desorption of butanol, as shown in Figure 4.5, for all models diffusion coefficients increase from 50%-100% Matrimid. D has a relatively high value at 10wt% Matrimid. The thickness of samples of 10%, 50%, 75%, 90%, 100% are 0.00472, .00902, 0.0058, 0.00526, 0.00626 cm, and the weights are: 0.0922, 0.4042, 0.2691, 0.2234, 0.3093 g. Considering the thickness and small mass of 10wt% sample, D value at 10wt% may be less reliable.

D values for each fraction are in a sequence of: Model I > Model III > Model II, except that for the 10wt% Matrimid, D of model III is the largest one.

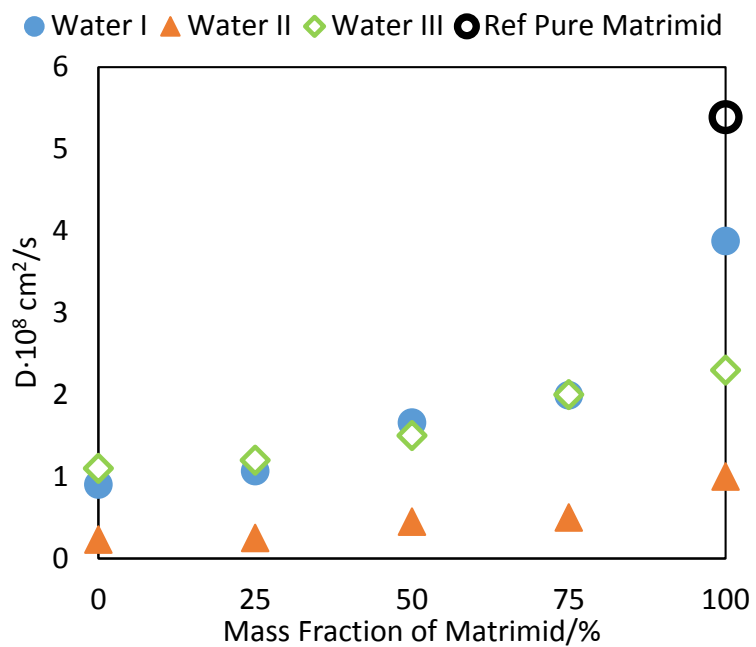


Figure 4.6 Comparison of Water Diffusion Coefficients of Three Models versus Mass Fraction of Matrimid. Room temperature, 1 atm.

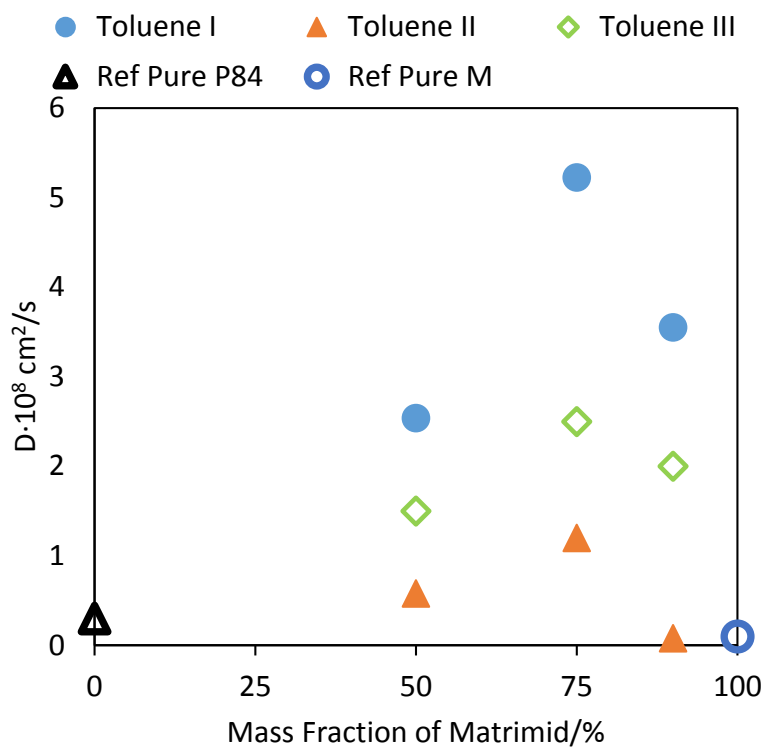


Figure 4.7 Comparison of Toluene Diffusion Coefficients of Three Models versus Mass Fraction of Matrimid. Room temperature, 1 atm.

Figure 4.6 is the desorption diffusion coefficients of water versus Matrimid mass fraction. For model I, II and III, D is increasing with Matrimid. Model II has the lowest values for each mass fraction. The D of Model I is similar to or slightly smaller than the D of Model of II when the Matrimid fraction is 0 and 25wt%. But when Matrimid fraction is 50-100wt%, D of Model I is the largest. The calculated D for pure Matrimid is smaller than reference data [78], but of the same magnitude.

For the desorption of toluene, as shown in Figure 4.7, the changing trend of diffusion coefficient versus Matrimid% has a maximum for each mass fraction, D follows the sequence: 75wt% Matrimid > 50wt% Matrimid > 90wt% Matrimid. For each model, D follows the sequence: Model I > Model III > Model II. Compared with the reference diffusion coefficients of individual polymers, the results in this study for toluene are higher than reference value, but of the same magnitude.

As Figure 4.8 indicates, the diffusion coefficient of methanol increases with mass fraction of Matrimid for all three models, except that D is lower than nearby values at 75% Matrimid. The diffusion coefficient values at each mass fraction is following the sequence: Model I > Model III > Model II. And the Ds of three models for pure P84 are similar.

In Figure 4.9, for all three models, the diffusion coefficient of 1-Propanol increases with mass fraction of Matrimid from 25% to 75% Matrimid, and then falls down to pure Matrimid. The sequence of D values are: Model I > Model III > Model II, except that D of pure Matrimid for Model III is lower than the other two.

In Figure 4.10, for all three models, the diffusion coefficients of 2-propanol increase from 75% to 90% Matrimid and falls down to 100% Matrimid. The sequence of D values are: Model III > Model I > Model II. Reference [88] diffusion coefficients for individual polymer films were

also marked in the figure. It is apparent that results from this study are in the same magnitude with reference values. What's more, D of pure Matrimid calculated from Model I is quite close with reference value.

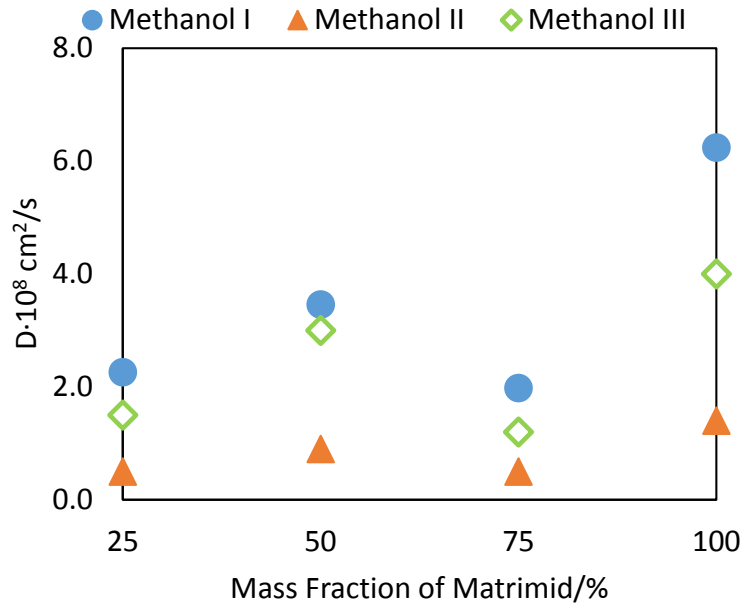


Figure 4.8 Comparison of Methanol Diffusion Coefficients of Three Models versus Mass Fraction of Matrimid. Room temperature, 1 atm.

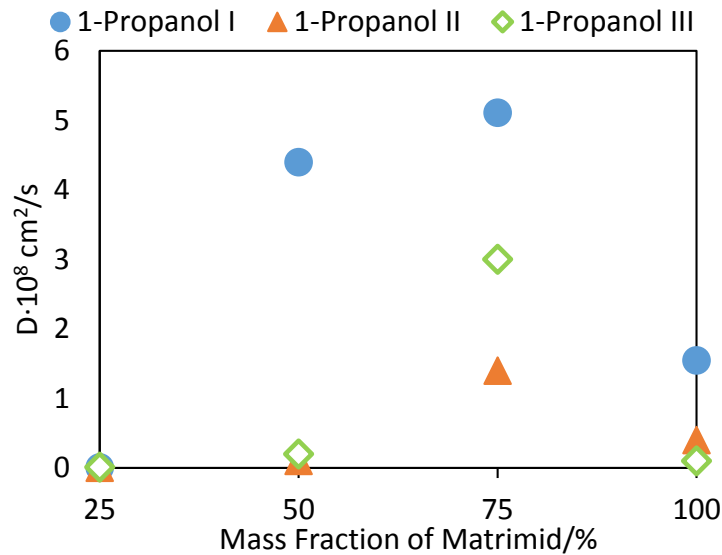


Figure 4.9 Comparison of 1-Propanol Diffusion Coefficients of Three Models versus Mass Fraction of Matrimid. Room temperature, 1 atm.

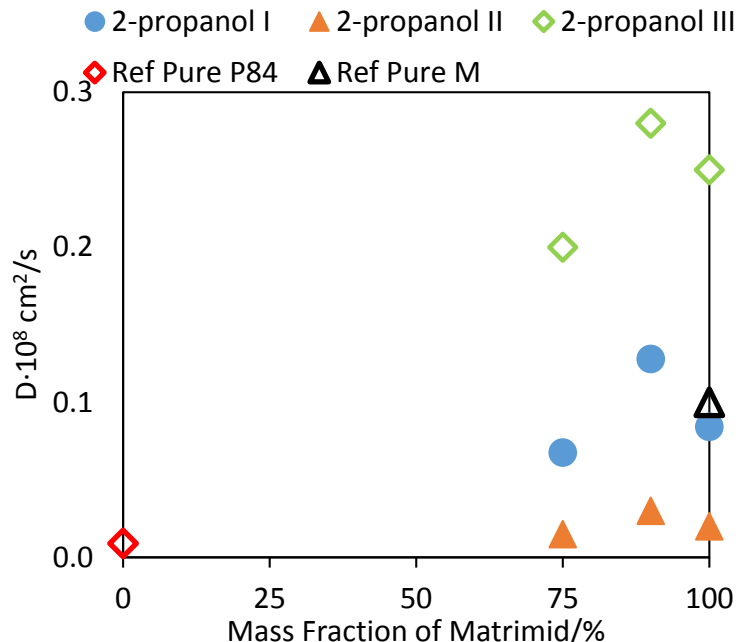


Figure 4.10 Comparison of 2-Propanol Diffusion Coefficients of Three Models versus Mass Fraction of Matrimid. Room temperature, 1 atm.

4.3.4 Diffusion Coefficients and Relaxation Rate Constant k

From section 4.3.3, it is easy to find out water and butanol present similar desorption characteristic, which is that D increases with Matrimid mass fraction, if not considering 10% Matrimid (which is not reliable) for butanol. And methanol also presents similar trend except that a lower D at 75% Matrimid. While different from methanol, the desorption of toluene, 1-propanol, and 2-propanol have larger D at 75% Matrimid. Since it is concluded that Model III is the best of the three models to simulate the desorption behavior of liquid solutes in this study, the theory of Model III is discussed here to explain the behavior. As talked above, when case III applies, the relaxation rate and diffusion rate are similar ($(DEB)_D \approx 1$). Therefore, it is reasonable to predict that the changing rule of diffusion coefficient versus film composition in Model III has a parallel relationship with that of relaxation constant k versus film composition.

Figure 4.11 shows the similar trend of k with Matrimid% for 1-Propanol, 2-Propanol, and Toluene. They all have a larger relaxation constant k at 75% Matrimid than other fraction. The

trend of k is consistent with the trend of diffusion coefficient for Toluene, 1-Propanol, and 2-Propanol, as shown in and Figure 4.7, Figure 4.10, and Figure 4.11.

Figure 4.12 shows that k of methanol increases with Matrimid mass fraction except the lower k at 75% Matrimid, and the same relationship between D of methanol and Matrimid mass fraction has been found.

In Figure 4.13 and Figure 4.14, k for water and butanol increases with mass fraction, and same relationship have been found between D and Matrimid mass fraction, again, as in Figure 4.6 and Figure 4.5.

From the discussion in this section, the changing behavior of D versus Matrimid mass fraction follows the changing behavior of k versus Matrimid mass fraction. This results is in agreement with the prediction made before. Model III is further proved to be an appropriate model to simulate and explain the desorption behavior of the liquid solutes in this study. In conclusion, the diffusion of the desorption in this study follows the mechanism of case III, which is anomalous diffusion, where relaxation rate and diffusion rate are similar.

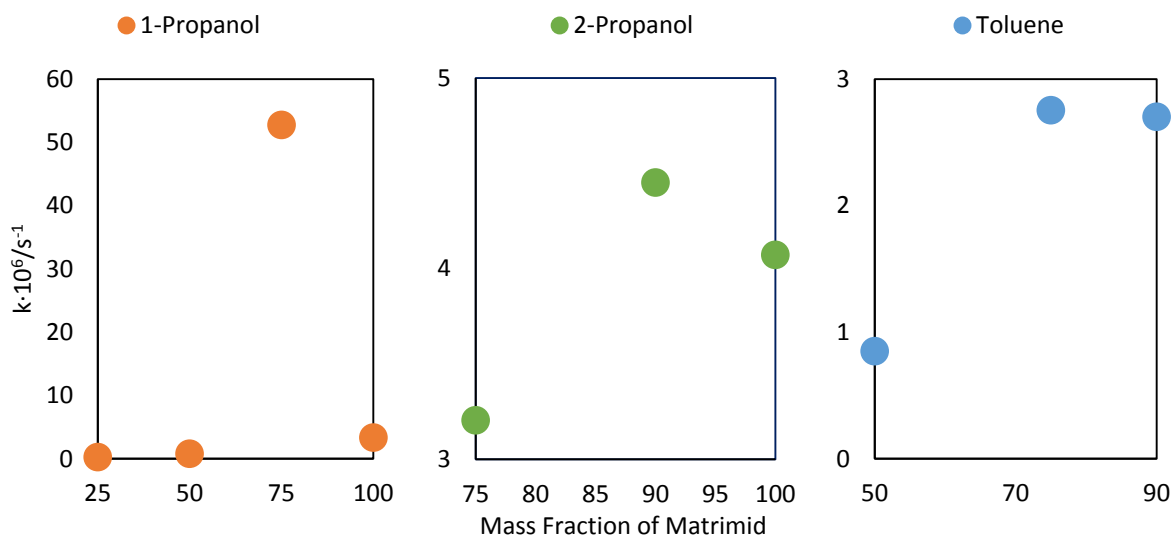


Figure 4.11 Values of k for 1-Propanol, 2-Propanol, and Toluene.

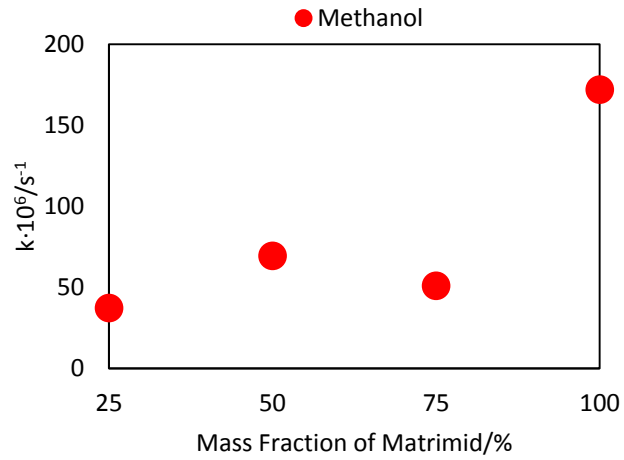


Figure 4.12 Values of k for Methanol

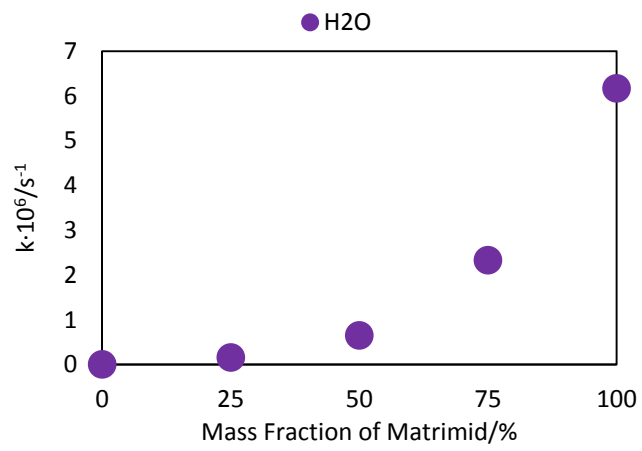


Figure 4.13 Values of k for Water

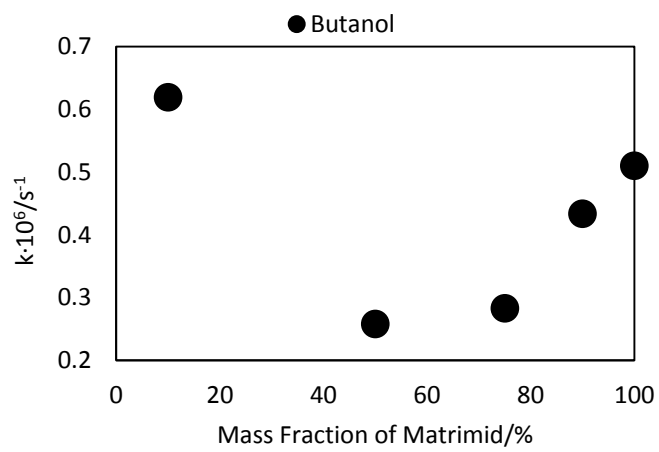


Figure 4.14 Values of k for Butanol

4.4 Conclusion

In this study, desorption data of water, methanol, toluene, 1-propanol, 2-propanol, and butanol were obtained from experiments and simulated with three models of mechanisms of standard Fickian, combination of Fickian and case II, and case III. The third model has been proved to best fit the experimental data.

The desorption uptake versus time have a strong two-stage characteristic, which have a rapid increase at first and then a very slow increase or a plateau. The uptake cannot reach 1 for each solvent, possibly because of penetrant clustering and skinning trapping.

The diffusion coefficients have been calculated with three models. In model III, the changing rule of diffusion coefficient with mass fraction of Matrimid is in consistence with changing rule of relaxation rate constant k with mass fraction. And this is in agreement with the condition of model III that the relaxation rate and diffusion rate are similar. Model III is again been approved to be suitable to explain the desorption behaviors in this study, which is anomalous diffusion.

Chapter 5 - Conclusion

In this study, Matrimid/P84 blend films were prepared and characterized for physical, thermal, and transport properties. Relative mathematical models or equations have been applied to simulate the experimental results and explain the behavior of the blend films.

The blend films were visibly transparent and the color was distributed evenly on the film sheet. As the content of P84 increases, the blend films have less space, smaller d-spacing, higher density and smaller FFV. Thermal mass loss curve of the blend films in air have presented intermediate characteristic with rising fraction of Matrimid compared to individual polymers. But for TGA in nitrogen, no apparent rationale have been found, possibly caused by residual solvent due to differences in pre-treatment.

Permeability of each gas increases with the mass fraction of Matrimid, due to the increasing fractional free volume. A linear relationship has been found between $\ln P$ and $1/FFV$. The selectivity-permeability relationship of gas pair H_2/N_2 and CO_2/CH_4 followed the trend of the trade off line of Robeson. The transport data in this study is in a reasonable range in comparison with reference. Both the data points in this study and in reference are below the Robeson's upper limit line. Therefore, there is still large space for the enhancement of the transport properties of the Matrimid/P84 blend films. The relationship between permeability and Matrimid volume fraction has been rationalized by applying a logarithmic relationship and the experimental data generally fits the series model line indicating that the blend films are partial-miscible. In another word, the blend films exhibited partial-miscibility behavior.

The desorption behavior of water, methanol, toluene, 1-propanol, 2-propanol, and butanol have been simulated with three models and only case III model can reasonably describe the two-stage characteristic of the uptake curve. In this case, the relaxation rate and diffusion rate are

similar, which have been proved by the similar changing behaviors of diffusion coefficient and relaxation rate constant as Matrimid mass fraction increases.

Further study would be the preparation and characterization of the Matrimid/P84 blend membranes. Physical, thermal and transport properties should be measured. Plasticization pressure should be measured. The influence of temperature on the permeability of blend membranes should be studied. And furthermore, crosslinking should be applied to improve the transport behavior of blend membranes.

References

- [1] M. Cheryan, *Ultrafiltration and Microfiltration Handbook*, Lancaster, PA: CRC Press, 1998.
- [2] R. W. Baker, *Membrane Technology and Applications (Third Edition)*, California: John Wiley & Sons, 2012.
- [3] A. Basile, *Handbook of Membrane Reactors*, Cambridge, UK: Woodhead Publishing Limited, 2013.
- [4] R. Buxbaum, "Membrane reactors, fundamental and commercial advantages, e.g. for methanol," in *Canadian AIChE Membrane Separations Meeting*, Calgary, Alberta, 1997.
- [5] W. J. Koros and G. K. Fleming, "Membrane-based gas separation," *Journal of Membrane Science*, vol. 83, no. 1, pp. 1-80, 1993.
- [6] K. Vanherck, P. Vandezande, S. O. Aldea and I. F. J. Vankelecom, "Cross-linked polyimide membranes for solvent resistant nanofiltration in aprotic solvents," *Journal of Membrane Science*, vol. 320, no. 1-2, pp. 468-476, 2008.
- [7] D. Wang, K. Li and W. K. Teo, "Gas Permselection Properties in Silicone-Coated Asymmetric Polyethersulfone Membranes," *Journal of Applied Polymer Science*, vol. 66, no. 5, pp. 837-846, 1997.
- [8] X. Zhang, S. Chen, J. Liu, Z. Hu, S. Chen and L. Wang, "Preparation and properties of sulfonated poly(phenylene arylene)/sulfonated polyimide (SPA/SPI) blend membranes for polymer electrolyte membrane fuel cell applications," *Journal of Membrane Science*, vol. 371, no. 1-2, pp. 276-285, 2011.
- [9] R. Wycisk, J. Chisholm, J. Lee, J. Lin and P. N. Pintauro, "Direct methanol fuel cell membranes from Nafion-polybenzimidazole blends," *Journal of Power Sources*, vol. 163, no. 1, pp. 9-17, 2006.
- [10] H. Bi, J. Wang, S. Chen, Z. Hu, Z. Gao, L. Wang and K.-i. Okamoto, "Preparation and properties of cross-linked sulfonated poly(arylene ether sulfone)/sulfonated polyimide blend membranes for fuel cell application," *Journal of Membrane Science*, vol. 350, no. 1-2, pp. 109-116, 2010.

- [11] H. Maab, M. Schieda, W. Yave, S. Shishatskiy and S. P. Nunes, "SPEEK/Polyimide blends for proton conductive membranes," *Fuel Cells*, vol. 9, no. 4, pp. 401-409, 2009.
- [12] C. G. Cho, S. H. Kim, Y. C. Park, H. Kim and J.-W. Park, "Fuel cell membranes based on blends of PPO with poly(styrene-*b*-vinylbenzylphosphonic acid) copolymers," *Journal of Membrane Science*, vol. 308, no. 1-2, pp. 96-106, 2008.
- [13] Y. Li, Q. T. Nguyen, P. Schaezel, C. Lixon-Buquet, L. Colasse, V. Ratiouville and S. Marais, "Proton exchange membranes from sulfonated polyetheretherketone and sulfonated polyethersulfone-cardo blends: Conductivity, watersorption and permeation properties," *Electrochimica Acta*, vol. 111, pp. 419-433, 2013.
- [14] S. Lu, L. Zhang and J. Lu, "Homogeneous blend membrane made from poly(ether sulphone) and poly(vinylpyrrolidone) and its application to water electrolysis," *Journal of Membrane Science*, vol. 300, no. 1-2, pp. 205-210, 2007.
- [15] S. Chen, X. Zhang, K. Chen, N. Endo, M. Higa, K.-i. Okamoto and L. Wang, "Cross-linked miscible blend membranes of sulfonated poly(arylene ether sulfone) and sulfonated polyimide for polymer electrolyte fuel cell applications," *Journal of Power Sources*, vol. 196, no. 23, pp. 9946-9954, 2011.
- [16] Basu, Cano-Odena and Vankelecom, "Asymmetric membrane based on Matrimid® and polysulphone blends for enhanced permeance and stability in binary gas (CO₂/CH₄) mixture separations," *Separation and Purification Technology*, vol. 75, pp. 15-21, 2010.
- [17] W. F. Yong, F. Y. Li, T. S. Chung and Y. W. Tong, "Molecular interaction, gas transport properties and plasticization behavior of cPIM-1/Torlon blend membranes," *Journal of Membrane Science*, vol. 462, pp. 119-130, 2014.
- [18] W. Yong, F. Y. Li, Y. C. Xiao, P. Li, K. P. Pramoda, Y. W. Tong and T. S. Chung, "Molecular engineering of PIM-1/Matrimid blend membranes for gas separation," *Journal of Membrane Science*, Vols. 407-408, pp. 47-57, 2012.
- [19] G. Kapantaidakis and G. Koops, "High flux polyethersulfone-polyimide blend hollow fiber membranes for gas separation," *Journal of Membrane Science*, vol. 204, no. 1-2, pp. 153-171, 2002.
- [20] G. Kapantaidakis, G. Koops and M. Wessling, "Preparation and characterization of gas separation hollow fiber membranes based on polyethersulfone-polyimide miscible blends," *Desalination*, vol. 145, no. 1-3, pp. 353-357, 2002.
- [21] G. C. Kapantaidakis, S. P. Kaldis, G. P. Sakellaropoulos, E. Chira, B. Loppinet and G. Floudas, "Interrelation Between Phase State and Gas Permeation in

Polysulfone/Polyimide Blend Membranes," *Journal of Polymer Science: Part B: Polymer Physics*, vol. 37, no. 19, pp. 2788-2798, 1999.

- [22] S. S. Madaeni, A. Farhadian and V. Vatanpour, "Effects of Phase Inversion and Composition of Casting Solution on Morphology and Gas Permeance of Polyethersulfone/Polyimide Blend Membranes," *Advances in Polymer Technology*, vol. 31, no. 4, pp. 298-309, 2012.
- [23] C. A. Scholes, C. P. Ribeiro, S. E. Kentish and B. D. Freeman, "Thermal rearranged poly(benzoxazole)/polyimide blended membranes for CO₂ separation," *Separation and Purification Technology*, vol. 124, no. 18, pp. 134-140, 2014.
- [24] S. Rafiq, Z. Man, A. Maulud, N. Muhamad and S. Maitra, "Effect of varying solvents compositions on morphology and gas permeation properties on membranes blends for CO₂ separation from natural gas," *Journal of Membrane Science*, vol. 378, no. 1-2, pp. 444-452, 2011.
- [25] A. L. Khan, X. Li and I. F. J. Vankelecom, "SPEEK/Matrimid blend membranes for CO₂ separation," *Journal of Membrane Science*, vol. 380, no. 1-2, pp. 55-62, 2011.
- [26] A. Ismail, R. Rahim and W. Rahman, "Characterization of polyethersulfone/Matrimid® 5218 miscible blend mixed matrix membranes for O₂/N₂ gas separation," *Separation and Purification Technology*, vol. 63, no. 1, pp. 200-206, 2008.
- [27] X. Cao, L. Jing, Y. Liu, W. Hu, z. Jiang and B. Liu, "Immiscible blends of sulfonated polyetheretherketone and fluorinated polyimide for proton exchange membranes," *High Performance Polymers*, vol. 26, no. 5, pp. 532-539, 2014.
- [28] L. Hao, P. Li and T.-S. Chung, "PIM-1 as an organic filler to enhance the gas separation performance of Ultem polyetherimide," *Journal of Membrane Science*, vol. 453, pp. 614-623, 2014.
- [29] G. Kung, L. Y. Jiang, Y. Wang and T.-S. Chung, "Asymmetric hollow fibers by polyimide and polybenzimidazole blends for toluene/iso-octane separation," *Journal of Membrane Science*, vol. 360, no. 1-2, pp. 303-314, 2010.
- [30] T.-S. Chung, W. F. Guo and Y. Liu, "Enhanced Matrimid membranes for pervaporation by homogenous blends with polybenzimidazole (PBI)," *Journal of Membrane Science*, vol. 271, no. 1-2, pp. 221-231, 2006.
- [31] S. S. Hosseini and T. S. Chung, "Carbon membranes from blends of PBI and polyimides for N₂/CH₄ and CO₂/CH₄ separation and hydrogen purification," *Journal of Membrane Science*, vol. 328, pp. 174-185, 2009.

- [32] S. S. Hosseini, N. Peng and T. S. Chung, "Gas separation membranes developed through integration of polymer blending and dual-layer hollow fiber spinning process for hydrogen and natural gas enrichments," *Journal of Membrane Science*, vol. 349, no. 1-2, pp. 156-166, 2010.
- [33] J. C. Jansen, S. Darvishmanesh, F. Tasselli, F. Bazzarelli, P. Bernardo, E. Tocci, K. Friess, A. Randova, E. Drioli and B. V. d. Bruggen, "Influence of the blend composition on the properties and separation performance of novel solvent resistant polyphenylsulfone/polyimide nanofiltration membranes," *Journal of Membrane Science*, vol. 447, pp. 107-118, 2013.
- [34] P. Garg, R. P. Singh and V. Choudhary, "Selective polydimethylsiloxane/polyimide blended IPN pervaporation membrane formethanol/toluene azeotrope separation," *Separation and Purification Technology*, vol. 76, no. 3, pp. 407-418, 2011.
- [35] H.-J. Lee, H. Suda, K. Harya and S.-H. Moon, "Gas permeation properties of carbon molecular sieving membranes derived from the polymer blend of polyphenylene oxide (PPO)/polyvinylpyrrolidone (PVP)," *Journal of Membrane Science*, vol. 296, no. 1-2, pp. 139-146, 2007.
- [36] H.-J. Lee, H. Suda and K. Haraya, "Preparation of Carbon Membranes Derived from Polymer Blends in the Presence of a Thermally Labile Polymer," *Separation Science and Technology*, vol. 42, no. 1, pp. 59-71, 2007.
- [37] P. S. Rao, M.-Y. Way, H.-H. Tseng, I. A. Kumar and T.-H. Weng, "A comparison of carbon/nanotube molecular sieve membranes with polymer blend carbon molecular sieve membranes for the gas permeation application," *Microporous and Mesoporous Materials*, vol. 113, no. 1-3, pp. 499-510, 2008.
- [38] Y. K. Kim, H. B. Park and Y. M. Lee, "Carbon molecular sieve membranes derived from thermally labile polymer containing blend polymers and their gas separation properties," *Journal of Membrane Science*, vol. 243, no. 1-2, pp. 9-17, 2004.
- [39] E. M. Maya, M. Sanchez, A. Marcos, J. G. d. l. Campa and J. d. Abajo, "Preparation and Properties of Catalyzed Polyimide/Dicyanate Semi-Interpenetrating Networks for Polymer Gas Membrane with Suppressed CO₂-Plasticization," *Journal of Applied Polymer Science*, vol. 124, pp. 713-722, 2012.
- [40] S. Shishatskiy, C. Nistor, M. Popa, S. P. Nunes and K. V. Peinemann, "Polyimide Asymmetric Membranes for Hydrogen Separation: Influence of Formation Conditions on Gas Transport Properties," *Advanced Engineering Materials*, vol. 8, no. 5, pp. 390-397, 2006.

- [41] T. Visser, N. Masetto and M. Wessling, "Materials dependence of mixed gas plasticization behavior in asymmetric membranes," *Journal of Membrane Science*, vol. 306, no. 1-2, pp. 16-28, 2007.
- [42] J. Krol, M. Boerrigter and G. Koops, "Polyimide hollow fiber gas separation membranes: preparation and the suppression of plasticization in propane/propylene environments," *Journal of Membrane Science*, vol. 184, no. 2, pp. 275-286, 2001.
- [43] Z. Horák, I. Fortelný, J. Kolařík, D. Hlavatá and A. Sikora, "Polymer Blends," in *Encyclopedia Of Polymer Science and Technology*, Wiley, 2005.
- [44] O. Olabisi, L. M. Robeson and M. T. Shaw, *Polymer-Polymer Miscibility*, New York : Academic Press, 1979.
- [45] D. R. Paul and J. W. Barlow, "Polymer Blends," *Polymer Reviews*, vol. 18, no. 1, pp. 109-168, 1980.
- [46] D. R. Paul and S. Newman, *Polymer Blends*, New York: Academic Press, 1978.
- [47] L. M. Robeson, *Polymer Blends: A Comprehensive Review*, Munich, Germany: Hanser Publications, 2007.
- [48] S. Shishatskiy, C. Nistor, M. Popa, S. P. Nunes and K. V. Peinemann, "Polyimide Asymmetric Membranes for Hydrogen Separation: Influence of Formation Conditions on Gas Transport Properties," *Advanced Engineering Material*, vol. 8, no. 5, pp. 390-397, 2006.
- [49] T. Visser and M. Wessling, "Auto and mutual plasticization in single and mixed gas C3 transport through Matrimid-based hollow fiber membranes," *Journal of Membrane Science*, vol. 312, no. 1-2, pp. 84-96, 2008.
- [50] J. C. Carson, J. P. Stanford and M. E. Rezac, "Polymeric Membranes and Gas Separation: Homogenous Blends of Matrimid@5218 and P84," <http://cse.ksu.edu/REU/S13/jccarson/>, 2013.
- [51] A. Bondi, "van der Waals Volumes and Radii," *The Journal of Physical Chemistry*, vol. 68, no. 3, pp. 441-451, 1964.
- [52] J. Y. Park and D. R. Paul, "Correlation and prediction of gas permeability in glassy polymer membrane materials via a modified free volume based group contribution method," *Journal of Membrane Science*, vol. 125, no. 1, pp. 23-39, 1997.

- [53] V. Krevelen and t. Nijenhuis, "Part VII comprehensive tables: Table IX Survey of group contributions in additive molar quantities," in *Properties of Polymers*, Elsevier Science , 2009, pp. 946-952.
- [54] A. Bos, I. G. M. Punt, M. Wessling and H. Strathmann, "Plasticization-resistant glassy polyimide membranes for CO₂/CH₄ separations," *Separation and Purification Technology*, vol. 14, no. 1-3, pp. 27-40, 1998.
- [55] L. Y. Jiang and T. S. Chuang, "β-Cyclodextrin containing Matrimid® sub-nanocomposite membranes for pervaporation application," *Journal of Membrane Science*, vol. 327, no. 1-2, pp. 216-225, 2009.
- [56] X. Qiao and T.-S. Chung, "Diamine Modification of P84 Polyimide Membranes for Pervaporation Dehydration of Isopropanol," *AIChE Journal*, vol. 52, no. 10, pp. 3462-3472, 2006.
- [57] A. Bos, I. Punt, M. Wessling and H. Strathmann, "CO₂-induced plasticization phenomena in glassy polymers," *Journal of Membrane Science*, vol. 155, no. 1, pp. 67-78, 1999.
- [58] P. S. Rao, M.-Y. Wey, H.-H. Tseng, I. A. Kumar and T.-H. Weng, "A comparison of carbon/nanotube molecular sieve membranes with polymer blend carbon molecular sieve membranes for the gas permeation application," *Microporous and Mesoporous Materials*, vol. 113, no. 1-3, pp. 499-510, 2008.
- [59] Y. Shen and A. C. Lua, "Structural and transport properties of BTDA-TDI/MDI co-polyimide (P84)-silica nanocomposite membranes for gas separation," *Chemical Engineering Journal*, vol. 188, p. 199, 2012.
- [60] J. Ploegmakers, S. Japip and K. Nijmeijer, "Mixed matrix membranes containing MOFs for ethylene/ethane separation Part A: Membrane preparation and characterization," *Journal of Membrane Science*, vol. 428, pp. 445-453, 2013.
- [61] Y. Xiao, T.-S. Chung, M. L. Chng, S. Tamai and A. Yamaguchi, "Structure and Properties Relationships for Aromatic Polyimides and Their Derived Carbon," *J. Phys. Chem. B*, vol. 109, no. 40, pp. 18741-18748, 2005.
- [62] H. H. Yong, H. C. Park, Y. S. Kang, J. Won and W. N. Kim, "Zeolite-filled polyimide membrane containing 2,4,6-triaminopyrimidine," *Journal of Membrane Science*, vol. 188, no. 2, pp. 151-163, 2001.
- [63] N. Mehio, S. Dai and D.-e. Jiang, "Quantum Mechanical Basis for Kinetic Diameters of Small Gaseous Molecules," *The Journal of Physical Chemistry*, vol. 118, no. 6, pp. 1150-1154, 2014.

- [64] L. M. Robeson, "The upper bound revisited," *Journal of Membrane Science*, vol. 320, no. 1-2, pp. 390-400, 2008.
- [65] L. Shao, L. Liu, S.-X. Cheng, Y.-D. Huang and J. Ma, "Comparison of diamino cross-linking in different polyimide solutions and membranes by precipitation observation and gas transport," *Journal of Membrane Science*, vol. 312, no. 1-2, pp. 174-185, 2008.
- [66] Y. Xiao, Y. Dai, T.-S. Chung and M. D. Guiver, "Effects of Brominating Matrimid Polyimide on the Physical and Gas Transport Properties of Derived Carbon Membranes," *Macromolecules*, vol. 38, no. 24, pp. 10042-10049, 2005.
- [67] P. Tin, T. Chung, Y. Liu, R. Wang, S. Liu and K. Pramoda, "Effects of cross-linking modification on gas separation performance of Matrimid membranes," *Journal of Membrane Science*, vol. 225, no. 1-2, pp. 77-90, 2003.
- [68] T.-S. Chung, S. S. Chan, R. Wang, Z. Lu and C. He, "Characterization of permeability and sorption in Matrimid/C60 mixed matrix membranes," *Journal of Membrane Science*, vol. 211, no. 1, pp. 91-99, 2003.
- [69] P. S. Tin, T.-S. Chung, S. Kawi and M. D. Guiver, "Novel approaches to fabricate carbon molecular sieve membranes based on chemical modified and solvent treated polyimides," *Microporous and Mesoporous Materials*, vol. 73, no. 3, pp. 151-160, 2004.
- [70] F. Li, Y. Li, T.-S. Chung and S. Kawi, "Facilitated transport by hybrid POSS®-Matrimid®-Zn²⁺ nanocomposite membranes for the separation of natural gas," *Journal of Membrane Science*, vol. 356, no. 1-2, pp. 14-21, 2010.
- [71] L. M. Robeson, "Polymer Blends in Membrane Transport Process," *Ind. Eng. Chem. Res.*, vol. 49, no. 23, pp. 11859-11865, 2010.
- [72] W. Yave, A. Car, K.-V. Peinemann, M. Q. Shaikh, K. Rätzke and F. Faupel, "Gas permeability and free volume in poly(amide-b-ethylene oxide)/polyethylene glycol blend membranes," *Journal of Membrane Science*, vol. 339, no. 1-2, pp. 177-183, 2009.
- [73] S. Feng, J. Ren, H. Li, K. Hua, X. Li and M. Deng, "Polyvinyl acetate/poly(amide-12-b-ethylene oxide) blend membranes for carbon dioxide separation," *Journal of Energy Chemistry*, vol. 22, no. 6, pp. 837-844, 2013.
- [74] A. Morisato, H. C. Shen, S. S. Sankar, B. D. Freeman, I. Pinnau and C. G. Casillas, "Polymer characterization and gas permeability of poly(1-trimethylsilyl-1-propyne) [PTMSP], poly(1-phenyl-1-propyne) [PPP], and PTMSP/PPP blends," *Journal of Polymer Science Part B: Polymer Physics*, vol. 34, no. 13, pp. 2209-2222, 1996.

- [75] S. Feng, J. Ren, K. Hua, H. Li, X. Ren and M. Deng, "Poly(amide-12-b-ethylene oxide)/polyethylene glycol blend membranes for carbon dioxide separation," *Separation and Purification Technology*, vol. 116, pp. 25-34, 2013.
- [76] B. Duncan, J. Urquhart and S. Roberts, "Review of measurement and modelling of permeation and diffusion in polymers," NPL Report DEPC MPR 012, 2005.
- [77] I. Mamaliga and C. Negoescu, "Some Aspects of Two Stage Diffusion in Polymer Films and Membranes," *Environmental Engineering and Management Journal*, vol. 11, no. 11, pp. 2091-2099, 2012.
- [78] G. Q. Chen, C. A. Scholes, C. M. Doherty, A. J. Hill, G. G. Qiao and S. E. Kentish, "Modeling of the sorption and transport properties of water vapor in polyimide membranes," *Journal of Membrane Science*, Vols. 409-410, pp. 96-104, 2012.
- [79] T. T. Wang and T. K. Kwei, "Diffusion in Glassy Polymers. Reexamination of Vapor Sorption Data," *Diffusion in Glassy Polymers*, vol. 6, no. 6, pp. 919-921, 1973.
- [80] Y. Sun, "Sorption/desorption properties of water vapour in poly(2-hydroxyethyl methacrylate): 2. Two-stage sorption models," *Polymer*, vol. 37, no. 17, pp. 3921-3928, 1996.
- [81] J. S. VRENTAS, C. M. JARZEBSKI and J. L. DUDA, "A Deborah number for diffusion in polymer-solvent systems," *AIChE Journal*, vol. 21, no. 5, pp. 894-901, 1975.
- [82] A. Berens and H. Hopfenberg, "Diffusion and relaxation in glassy polymer powders: 2. Separation of diffusion and relaxation parameters," *Polymer*, vol. 19, no. 5, pp. 489-496, 1978.
- [83] F. A. Long and D. Richman, "Concentration Gradients for Diffusion of Vapors in Glassy Polymers and their Relation to Time Dependent Diffusion Phenomena," *J. Am. Chem. Soc.*, vol. 82, no. 3, pp. 513-519, 1960.
- [84] S. Joshi and G. Astarita, "Diffusion-relaxation coupling in polymers which show 2-stage sorption phenomena," *Polymer*, vol. 20, no. 4, pp. 455-458, 1979.
- [85] J. Crank, *The mathematics of diffusion* 2nd ed., New York: Oxford University Press, 1975.
- [86] J. Barrie and B. Plait, "The Diffusion and Clustering of Water Vapour in Polymers," *Polymer*, vol. 4, no. 3, p. 303, 1963.
- [87] D. A. Edwards, "Skinning during Desorption of Polymers: An Asymptotic Analysis," *Society for Industrial and Applied Mathematics*, vol. 59, no. 3, pp. 1134-1155, 1999.

- [88] L. Hesse, S. Naeem and G. Sadowski, "VOC sorption in glassy polyimides— Measurements and modeling," *Journal of Membrane Science*, Vols. 415-416, pp. 596-607, 2012.
- [89] W.-H. Lin, R. H. Vora and T. Chung, "Gas Transport Properties of 6FDA-Durene/1,4-phenylenediamine (pPDA) Copolyimides," *Journal of Polymer Science: Part B: Polymer Physics*, vol. 38, no. 21, pp. 2703-2713, 2000.
- [90] Y. Maada and D. R. Paul, "Effect of Antiplasticization on Gas Sorption and Transport. II. Free Volume Interpretation," *Journal of Polymer Science: Part B: Polymer Physics*, vol. 25, no. 5, pp. 1005-1016, 1987.
- [91] Chng, Xiao, Chung and Tamai, "The effects of chemical structure on gas transport properties of poly(aryl ether ketone) random copolymers," *Polymer*, vol. 48, pp. 311-317, 2007.

Appendix A - Physical Properties of Matrimid/P84 Blend Films

A.1 Density

Table A.1 Calibration of Density Gradient Column with Standard Density Beans

Color of Beans	Position of Beans	Density g/cm ³
Red	26.8	1.18
White	32.8	1.20
Blue	47.2	1.24
Green	51.4	1.25
Red	55.8	1.26
Yellow	64.8	1.28
Brown	73.3	1.30
Green	88.0	1.34
Clean	96.0	1.36

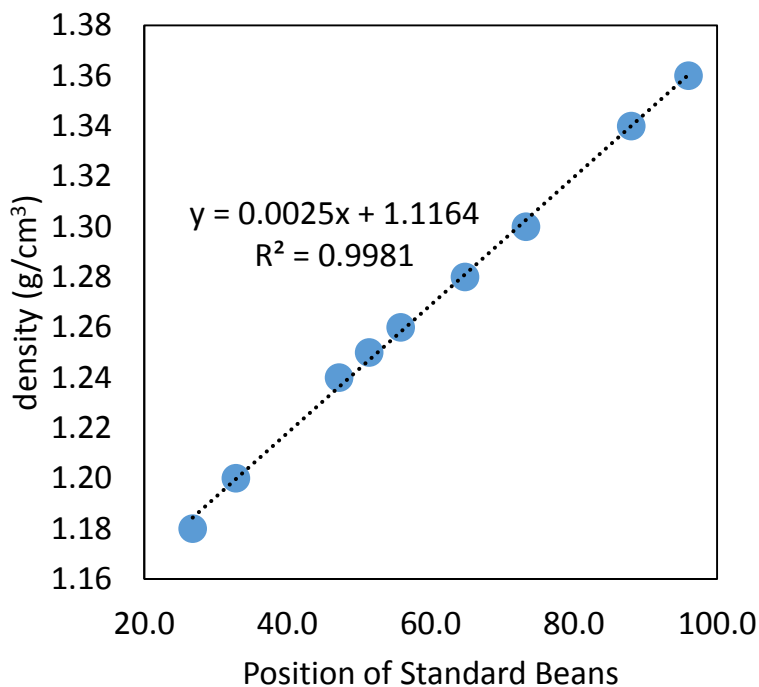


Figure A.1 Calibration of Density Gradient Column

$R^2=0.9981$, is approaching 1, which indicates that the distribution of the standard density beans in the density gradient column are very linear. The column can function in a satisfactory way for the measurement. The absolute error of position reading is ± 0.1 . Then the absolute error of density is $0.0025 \times (\pm 0.1) = \pm 0.00025 \text{ g/cm}^3$, which is very small and can be negligible.

Table A.2 Density of Matrimid/P84 Blend Films

Matrimid wt. %	Position	Density g/cm ³
0	92.0	1.35
25	85.0	1.33
50	76.3	1.31
75	65.0	1.28
100	55.0	1.25

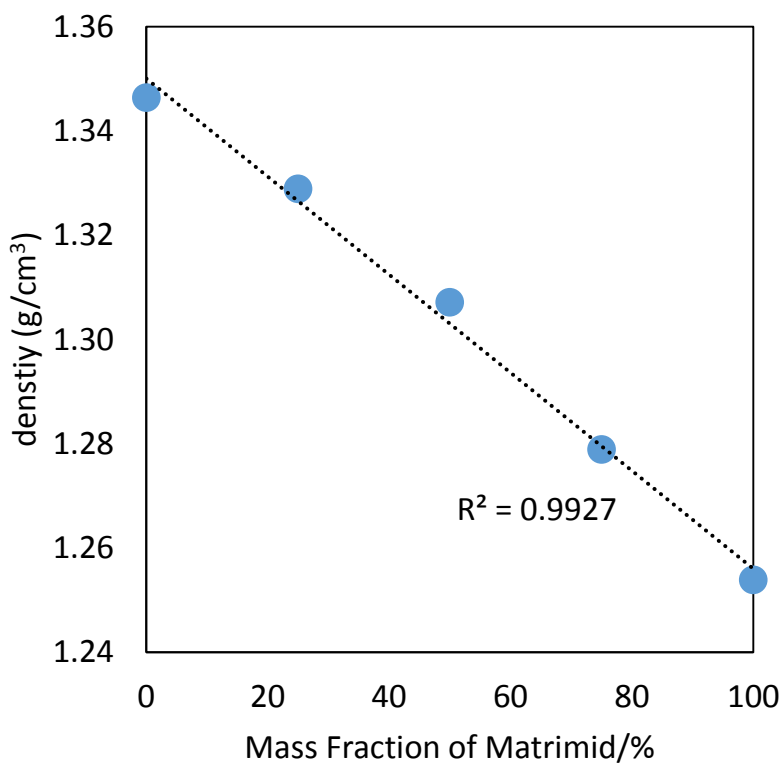


Figure A.2 Density of Matrimid/P84 Blend Films

A.2 FFV

Values of van der Waal's volume of group k were obtained from two resources: van Krevelen and Nijenhuis's book [53] (Resource I), Park and Paul's paper [52] (Resource II). The difference of values of V_w caused difference of calculated fractional free volumes from two resources. Table A.3~A.5 were calculated from the Resource I and Table A.6~A.8 were calculated from Resource II.

Values of van der Waals volumes from the literature were in the unit of cm^3/mol , which were transferred to cm^3/g as below

$$V_w = \frac{\sum(V_w)_k n_k}{\sum(MW)_k n_k} = \frac{cm^3/mol}{g/mol} = cm^3/g$$

The van der Waal's volumes of blends were calculated by the equation [89, 90, 91]

$$(V_w)_{blends} = w_1(V_w)_1 + w_2(V_w)_2 \quad \left[\frac{cm^3}{g}\right]$$

Where w_1, w_2 are the mass fraction of individual polymers, and $(V_w)_1, (V_w)_2$ are the van der Waal's volumes of individual polymers. FFV is calculated from equation (2.1) and equation (2.2).

Below are the chemical structures of Matrimid and P84.

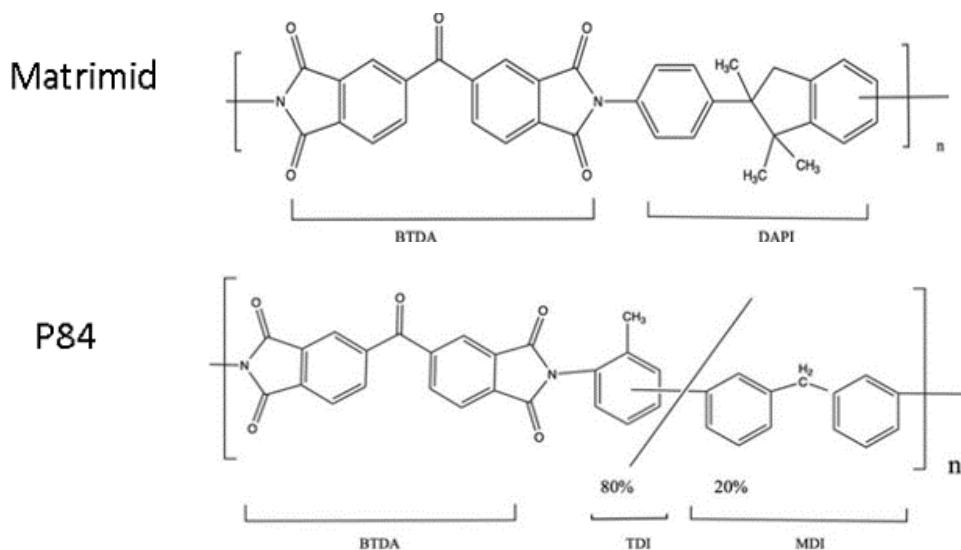


Table A.3 V_w and MW of Groups in Matrimid (Resource I)

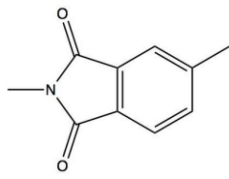
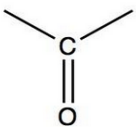

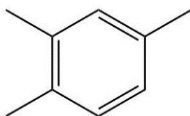
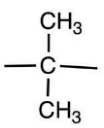
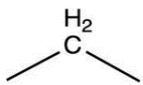
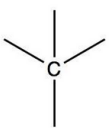
Chemical Formula	Chemical Structure	V_w	MW	n
		cm^3/mol	g/mol	
$\text{C}_8\text{H}_3\text{NO}_2$		69.4	145.11	2
CO		11.7	28.01	1
C_6H_4		43.3	76.10	1
C_6H_3		41.7	75.09	1
C_3H_6		30.7	42.08	1
CH_2		10.23	14.03	1
C		3.3	12.01	1
CH_3	$-\text{CH}_3$	13.67	15.03	1

Table A.4 V_w and MW of Groups in P84 (Resource I)

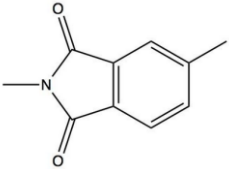
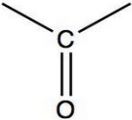
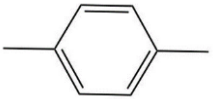
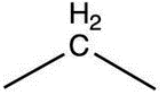
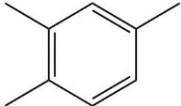
Chemical Formula	Chemical Structure	V_w	MW	n
		cm^3/mol	g/mol	
$\text{C}_8\text{H}_3\text{NO}_2$		69.4	145.11	2
CO		11.7	28.01	1
C_6H_4		43.3	76.10	2X20%
CH_2		10.23	14.03	1X20%
C_6H_3		41.7	75.09	1X80%
CH_3	$-\text{CH}_3$	13.67	15.03	1X80%

Table A.5 FFV of Matrimid/P84 Blend Films (Resource I)

	Matrimid	V _w	MW	V _w	V ₀	Density	V	FFV
	wt. %	cc/mol	g/mol	cc/g	cc/g	g/cc	cc/g	
Reference ^a	0%	194.5	423.6	0.459	0.597	1.336	0.75	0.203
This Study	0%	214.162	423.572	0.506	0.657	1.346	0.74	0.115
	25%			0.512	0.666	1.329	0.75	0.116
	50%			0.518	0.674	1.307	0.77	0.119
	75%			0.525	0.682	1.279	0.78	0.128
	100%	293.4	552.57	0.531	0.690	1.254	0.80	0.134
Reference ^a	100%	273.1	568.6	0.480	0.624	1.241	0.81	0.225

Reference ^a is from [57].

Table A.6 FFV of Matrimid/P84 Blend Films (Resource II)

	Matrimid	V _w	MW	V _w	V ₀	Density	V	FFV
	wt. %	cc/mol	g/mol	cc/g	cc/g	g/cc	cc/g	
Reference ^a	0	194.5	423.6	0.459	0.597	1.336	0.75	0.203
This Study	0	208.5	423.6	0.492	0.640	1.35	0.74	0.136
	25			0.499	0.649	1.33	0.75	0.137
	50			0.506	0.658	1.31	0.76	0.138
	75			0.513	0.667	1.28	0.78	0.146
	100	287.6	552.5	0.520	0.677	1.25	0.80	0.154
Reference ^a	100	273.1	568.6	0.480	0.624	1.241	0.81	0.225

Reference ^a is from [57].

Table A.7 V_w and MW of Groups in Matrimid (Resource II)

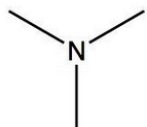
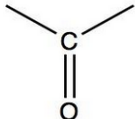
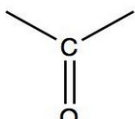
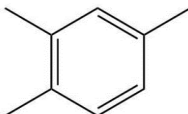

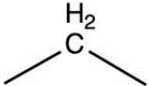
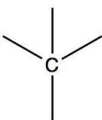
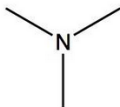
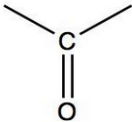
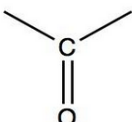
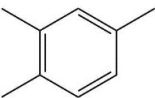
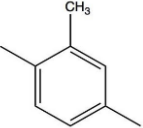
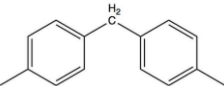
Chemical Formula	Chemical Structure	V_w	MW	n
		cc/mol	g/mol	
N		4.33	14.01	2
CO(aromatic)		11.7	28.01	4
CO(aliphatic)		8.5	28.01	1
C_6H_3		40.8	75.08	3
C_6H_4		43.32	76.09	1
CH_2		10.23	14.03	1
C		3.33	12.01	2
CH_3	- CH_3	13.67	15.03	3

Table A.8 V_w and MW of Groups in P84 (Resource II)

Chemical Formula	Chemical Structure	V_w	MW	n
		cc/mol	g/mol	
N		4.33	14.01	2
CO(aromatic)		11.7	28.01	4
CO(aliphatic)		8.5	28.01	1
C_6H_3		40.8	75.08	2
C_7H_6		54.47	90.12	0.8
$C_{13}H_{10}$		96.87	166.21	0.2

Appendix B - Permeability of Matrimid/P84 Blend Films

Each sample were tested for three times to get the average permeability and average error. For each [gas, composition] group, there were three samples tested (except for 50%Matrimid, four samples were tested). Below are the kinetic diameters of gas molecules and the summaries of the permeabilities of gases for various composition.

Table B.1 Kinetic Diameters and Molecular Weights of Gases

Gas	kinetic diameter	MW
	Å	g/mol
CH4	3.80	16.044
N2	3.64	28.0134
Ar	3.40	39.948
CO2	3.30	44.01
H2	2.89	2.016
He	2.60	4.002602

Table B.2 Summary of Permeability of H₂ in Matrimid/P84 Blend Films

Matrimid wt. %	P	Relative Error	Absolute Error	\bar{P}
	barrer		barrer	barrer
0	6.38	± 12.08%	± 0.770	5.99 ± 0.499
	5.20	± 2.49%	± 0.129	
	6.38	± 9.39%	± 0.599	
25	7.29	± 10.85%	± 0.790	6.96 ± 0.627
	7.22	± 8.24%	± 0.595	
	6.37	± 7.79%	± 0.497	
50	8.16	± 7.16%	± 0.584	7.60 ± 0.620
	7.16	± 9.09%	± 0.651	
	7.43	± 3.51%	± 0.260	
	7.65	± 12.87%	± 0.985	
75	11.4	± 1.72%	± 0.196	11.8 ± 0.887
	12.0	± 11.09%	± 1.33	
	11.9	± 9.49%	± 1.13	
100	12.1	± 3.04%	± 0.368	14.0 ± 0.765
	13.8	± 3.34%	± 0.461	
	16.1	± 9.10%	± 1.46	

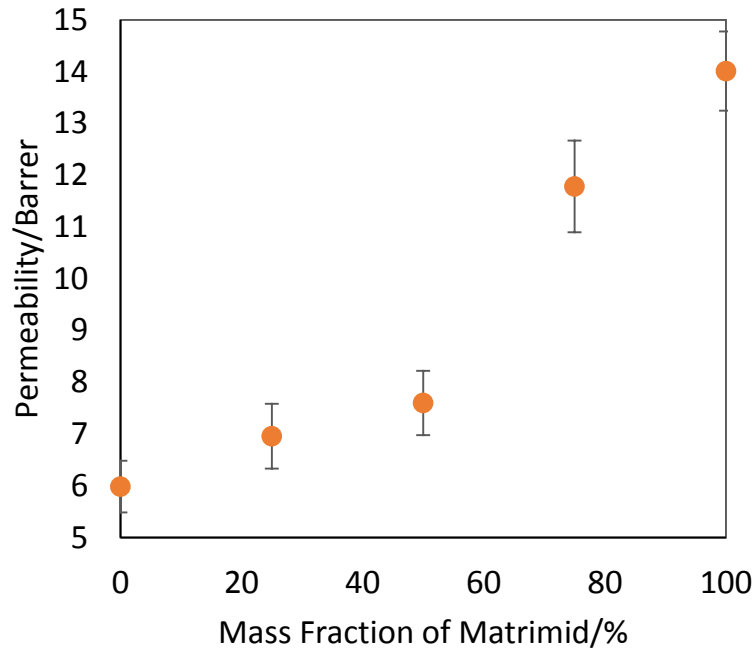


Figure B.1 Permeability of H₂ vs. Matrimid Mass Fraction for Matrimid/P84 Blend Film

Table B.3 Summary of Permeability of He in Matrimid/P84 Blend Films

Matrimid wt. %	P	Relative Error	Absolute Error	\bar{P}
	barrer		barrer	barrer
0	7.16	± 12.08%	± 0.864	6.72 ± 0.560
	5.85	± 2.49%	± 0.145	
	7.15	± 9.39%	± 0.671	
25	8.39	± 8.24%	± 0.692	7.91 ± 0.714
	7.01	± 7.79%	± 0.546	
	8.33	± 10.85%	± 0.904	
50	8.18	± 8.24%	± 0.674	8.28 ± 0.774
	8.67	± 7.16%	± 0.621	
	7.78	± 9.09%	± 0.708	
	8.49	± 12.87%	± 1.093	
75	12.5	± 9.49%	± 1.184	12.1 ± 0.922
	12.5	± 11.09%	± 1.39	
	11.4	± 1.72%	± 0.20	
100	15.5	± 9.11%	± 1.414	13.9 ± 0.750
	12.1	± 3.04%	± 0.367	
	14.0	± 3.34%	± 0.47	

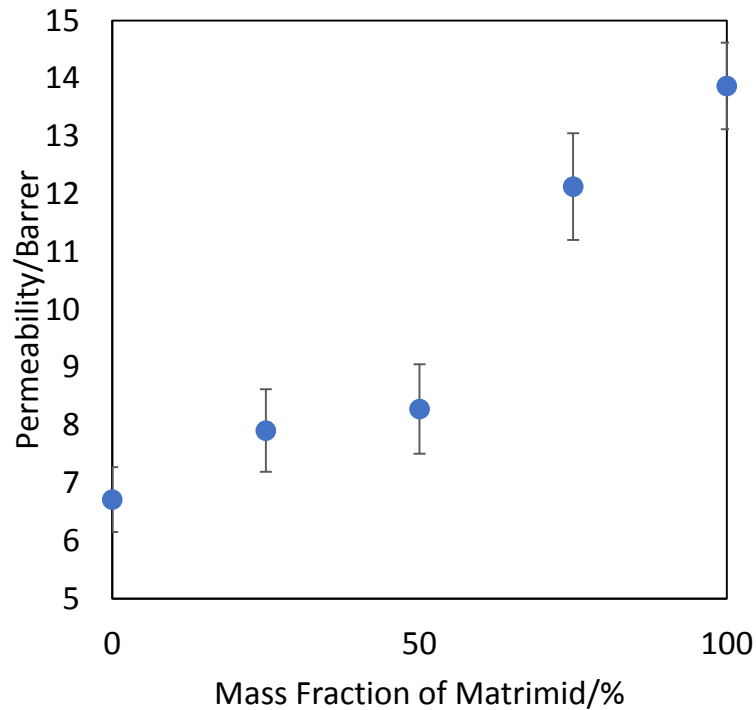


Figure B.2 Permeability of He vs. Matrimid Mass Fraction for Matrimid/P84 Blend Film

Table B.4 Summary of Permeability of CO₂ in Matrimid/P84 Blend Films

Matrimid wt. %	P	Relative Error	Absolute Error	\bar{P} barrer
	barrer		barrer	
0	1.58	± 7.79%	± 0.123	1.54 ± 0.105
	1.34	± 2.49%	± 0.033	
	1.68	± 9.39%	± 0.158	
25	1.97	± 8.24%	± 0.162	1.81 ± 0.162
	1.63	± 7.79%	± 0.127	
	1.82	± 10.85%	± 0.197	
50	1.70	± 3.51%	± 0.060	2.16 ± 0.181
	2.17	± 7.16%	± 0.156	
	2.80	± 9.09%	± 0.254	
	1.98	± 12.87%	± 0.254	
75	3.4	± 9.49%	± 0.326	3.5 ± 0.261
	3.6	± 11.09%	± 0.40	
	3.5	± 1.72%	± 0.06	
100	5.3	± 9.10%	± 0.483	4.9 ± 0.261
	4.7	± 3.04%	± 0.143	
	4.7	± 3.34%	± 0.16	

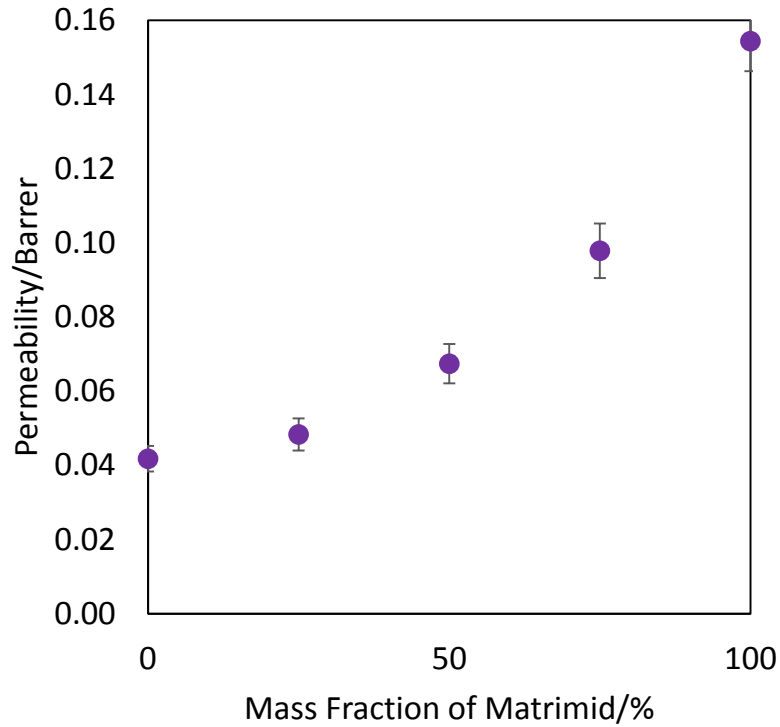


Figure B.3 Permeability of CO₂ vs. Matrimid Mass Fraction for Matrimid/P84 Blend Film

Table B.5 Summary of Permeability of Ar in Matrimid/P84 Blend Films

Matrimid wt. %	P barrer	Relative Error	Absolute Error barrer	\bar{P} barrer
0	0.13	$\pm 12.08\%$	± 0.016	0.13 \pm 0.010
	0.13	$\pm 2.49\%$	± 0.003	
	0.13	$\pm 9.39\%$	± 0.012	
25	0.15	$\pm 8.24\%$	± 0.012	0.16 \pm 0.015
	0.16	$\pm 7.79\%$	± 0.013	
	0.18	$\pm 10.85\%$	± 0.019	
50	0.14	$\pm 3.51\%$	± 0.005	0.19 \pm 0.016
	0.19	$\pm 7.16\%$	± 0.014	
	0.25	$\pm 9.09\%$	± 0.023	
	0.17	$\pm 12.87\%$	± 0.022	
75	0.3	$\pm 9.49\%$	± 0.027	0.4 \pm 0.035
	0.6	$\pm 11.09\%$	± 0.07	
	0.3	$\pm 1.72\%$	± 0.01	
100	0.6	$\pm 9.11\%$	± 0.054	0.5 \pm 0.023
	0.4	$\pm 3.34\%$	± 0.01	

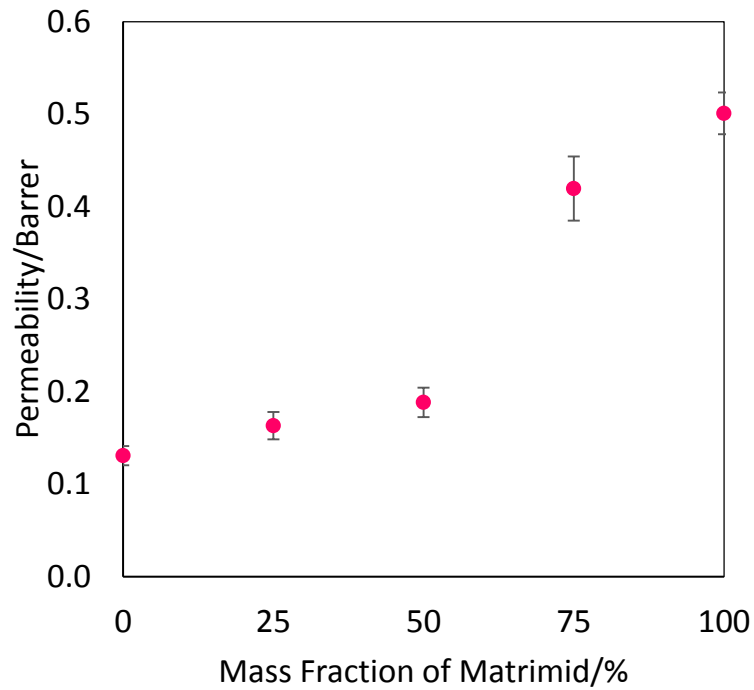


Figure B.4 Permeability of Ar vs. Matrimid Mass Fraction for Matrimid/P84 Blend Film

Table B.6 Summary of Permeability of N₂ in Matrimid/P84 Blend Films

Matrimid wt. %	P	Relative Error	Absolute Error	\bar{P}
	barrer		barrer	barrer
0	0.06	± 12.08%	± 0.007	0.06 ± 0.005
	0.05	± 2.49%	± 0.001	
	0.06	± 9.39%	± 0.006	
25	0.07	± 8.24%	± 0.006	0.07 ± 0.006
	0.06	± 7.80%	± 0.005	
	0.07	± 10.85%	± 0.007	
50	0.06	± 3.51%	± 0.002	0.08 ± 0.007
	0.08	± 7.16%	± 0.006	
	0.11	± 9.09%	± 0.010	
	0.08	± 12.87%	± 0.010	
75	0.1	± 9.49%	± 0.011	0.1 ± 0.010
	0.2	± 11.09%	± 0.02	
	0.1	± 1.72%	± 0.00	
100	0.2	± 9.10%	± 0.017	0.2 ± 0.011
	0.3	± 3.04%	± 0.010	
	0.2	± 3.34%	± 0.01	

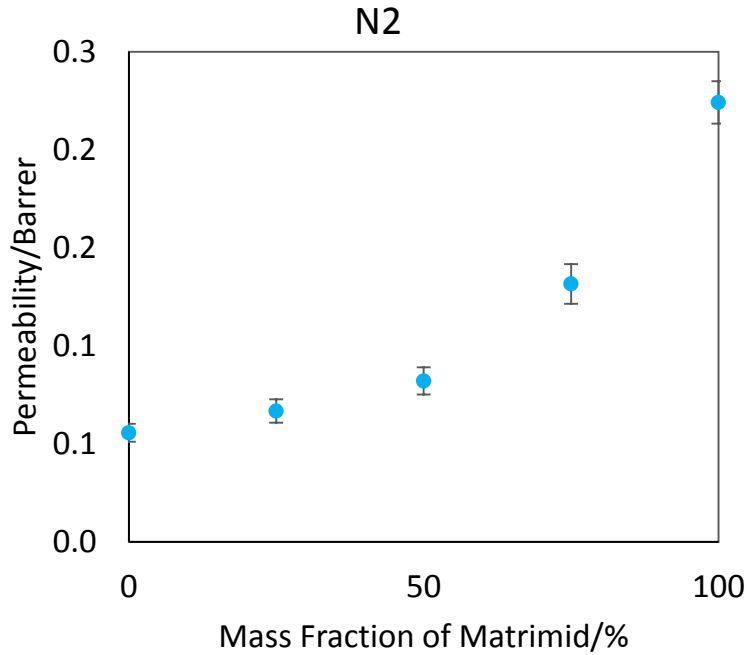


Figure B.5 Permeability of N₂ vs. Matrimid Mass Fraction for Matrimid/P84 Blend Film

Table B.7 Summary of Permeability of CH₄ in Matrimid/P84 Blend Films

Matrimid wt. %	P	Relative Error	Absolute Error	\bar{P}
	barrer		barrer	barrer
0	0.04	± 12.08%	± 0.005	0.04 ± 0.003
	0.04	± 2.49%	± 0.001	
	0.05	± 9.39%	± 0.005	
25	0.05	± 8.24%	± 0.004	0.05 ± 0.004
	0.05	± 7.79%	± 0.004	
	0.05	± 10.85%	± 0.005	
50	0.04	± 3.51%	± 0.001	0.07 ± 0.005
	0.07	± 7.16%	± 0.005	
	0.10	± 9.09%	± 0.009	
	0.06	± 9.39%	± 0.006	
75	0.1	± 9.49%	± 0.009	0.1 ± 0.007
	0.1	± 11.09%	± 0.01	
	0.1	± 1.72%	± 0.00	
100	0.2	± 9.10%	± 0.015	0.2 ± 0.008
	0.2	± 3.04%	± 0.005	
	0.1	± 3.34%	± 0.00	

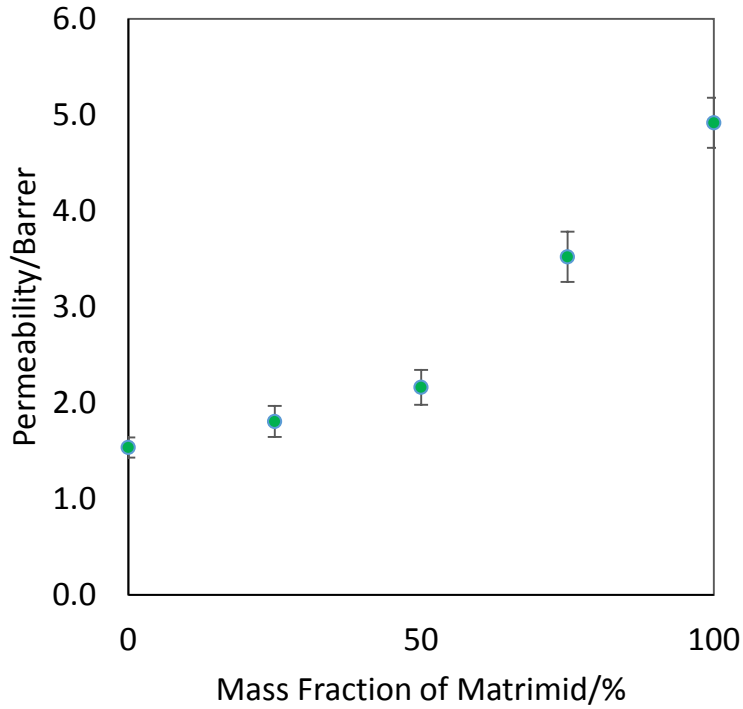


Figure B.6 Permeability of CH₄ vs. Matrimid Mass Fraction for Matrimid/P84 Blend Film

Table B.8 Summary of Selectivity for Matrimid/P84 Blend Films

Matrimid wt.%	0	25	50	75	100
He/CH ₄	90.3	124	123	163	161
He/N ₂	62.1	91.7	101	118	121
He/Ar	27.7	28.8	44.0	48.5	51.3
He/CO ₂	2.84	3.46	3.83	4.37	4.36
He/H ₂	0.993	1.03	1.09	1.14	1.12
H ₂ /CH ₄	90.9	121	113	144	143
H ₂ /N ₂	62.5	89.4	92.6	104	108
H ₂ /CO ₂	2.86	3.37	3.52	3.85	3.89
H ₂ /Ar	27.9	28.1	40.4	42.7	45.7
CO ₂ /CH ₄	31.8	35.8	32.0	37.4	36.8
CO ₂ /N ₂	21.9	26.5	26.3	27.1	27.6
CO ₂ /Ar	9.78	8.33	11.5	11.1	11.8
Ar/CH ₄	3.25	4.29	2.79	3.37	3.13
Ar/N ₂	2.24	3.18	2.29	2.44	2.35
N ₂ /CH ₄	1.45	1.35	1.22	1.38	1.33

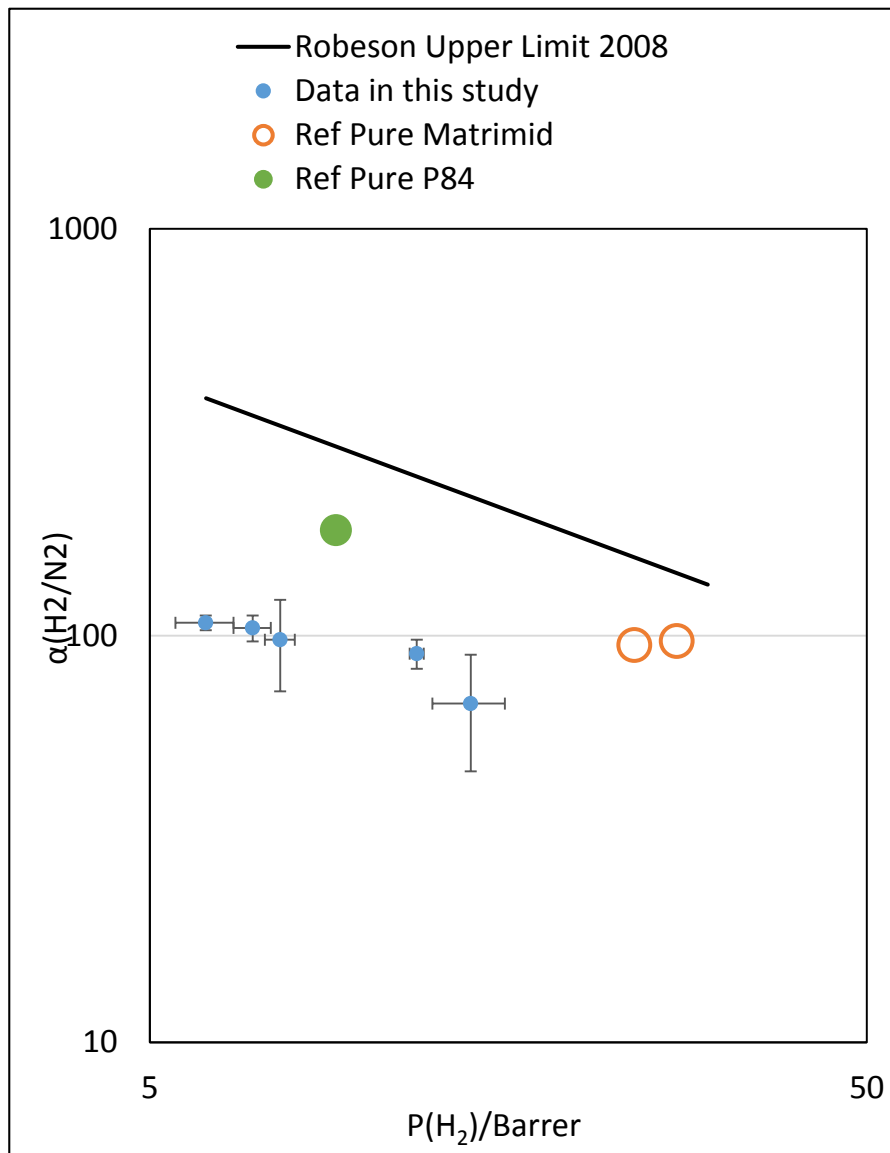


Figure B.7 Selectivity vs. $P(H_2)$ for H_2/N_2 Gas Pair in Comparison with Reference and Robeson Upper Limit Line. Each data in this study is the average value with error bars, from left to right, the content is from 0%Matrimid to 100%Matrimid

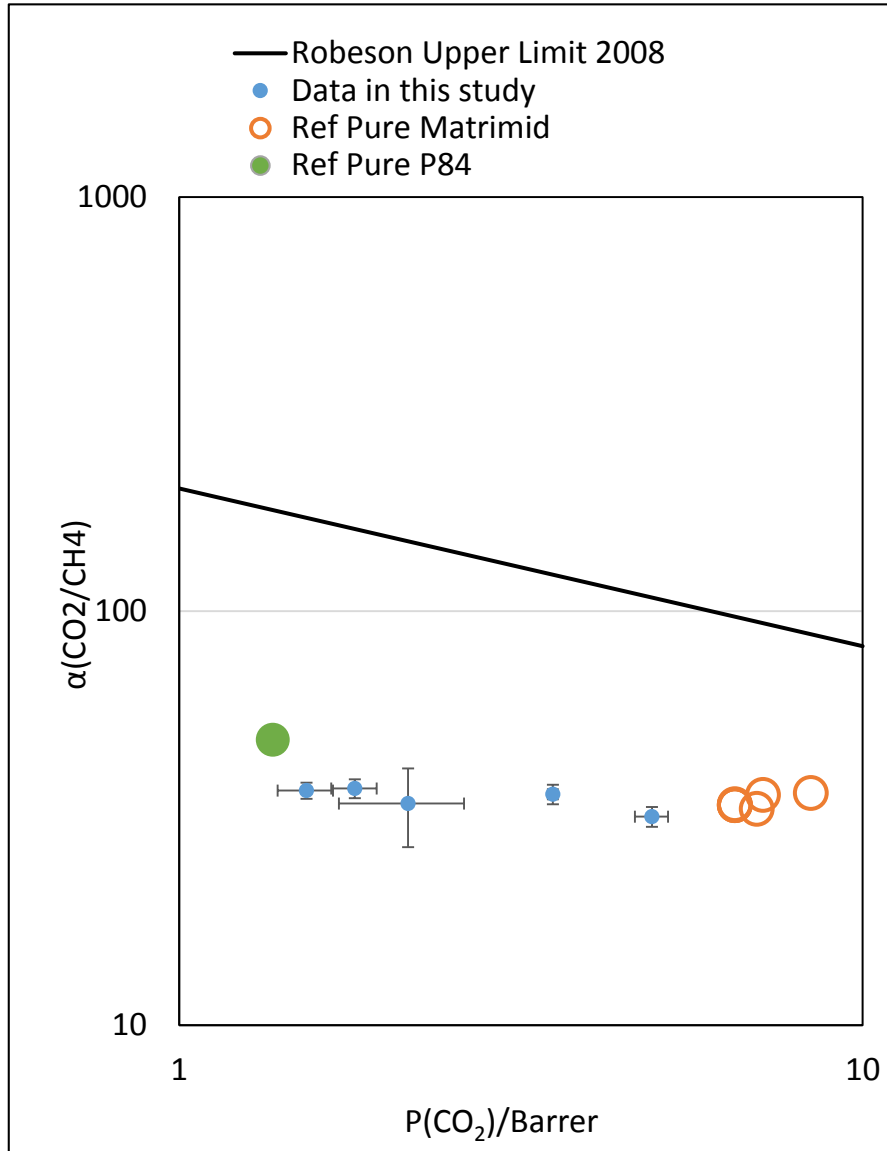


Figure B.8 Selectivity vs. $P(\text{CO}_2)$ for CO_2/CH_4 N_2 Gas Pair in Comparison with Reference and Robeson Upper Limit Line. Each data in this study is the average value with error bars, from left to right, the content is from 0%Matrimid to 100%Matrimid

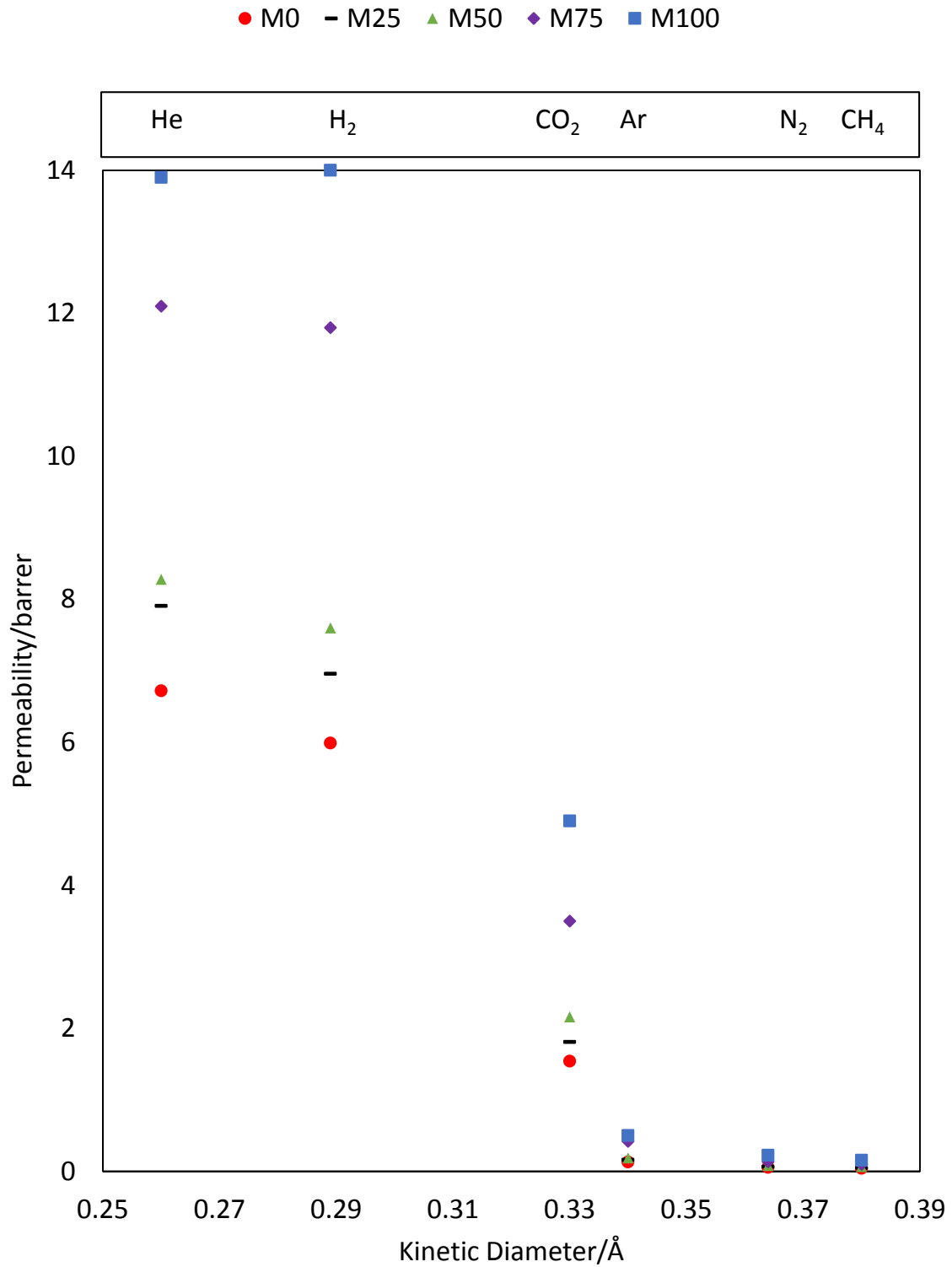


Figure B.9 Permeability versus Kinetic Diameter of Gas Molecules

Appendix C - Matrimid/PBI Blend Films

C.1 The Preparation of Matrimid/PBI Blend Films

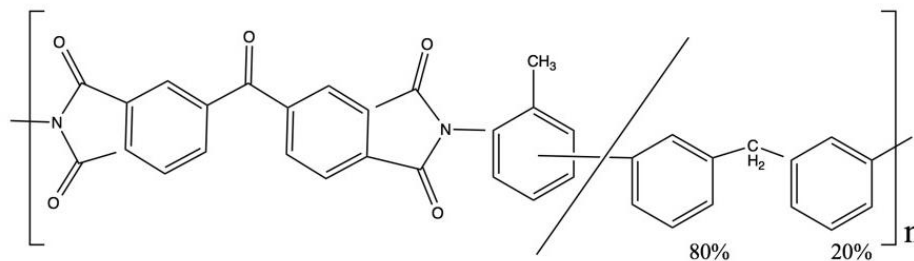


Figure C.1 Chemical Structure of PBI

PBI has high thermal stability, and was added to Matrimid to produce a blend film with high transport performance and thermal stability.

The films were prepared by a casting method. Polymer solutions (20 wt. % polymer/80 wt. % NMP) with various compositions of 0/100, 10/90, 25/75, 50/50, 75/25, 90/10, 100/0 wt. % were prepared from Matrimid and PBI according to the following steps.

Firstly, 18.5 wt. % polymer powders and 1.5 wt. % LiCl, were dried under vacuum at 120 °C overnight before used. Then 1.5 wt. % LiCl were dissolved in 80 wt. % NMP and stirred at 150 °C until totally dissolved. 18.5 wt. % polymer powders were added to the solution and was capped and stirred at 250 °C for 24 hours.

The hot solution was cast on a glass plate, which was preheated at 92.3 °C for at least one hours. The thickness was set to 600 μm. Films were dried in a vacuum oven at 92.3 °C for 12 hours.

The films were taken out of the oven, let cool down and peeled off the glass plate with a bit of water after cooling down to room temperature. The films were wiped with soft tissues and kept in the oven at 100 °C overnight to remove any water residues. Naturally cooled films were conserved in a container with desiccant inside.

C.2 TGA in Air for Matrimid/PBI Blend Membrane

The blend samples were immersed in methanol for 30 min for 3 times and immersed in hexane for 30min for 3 times and dried in a vacuum oven at 120 °C for two days before used in TGA test.

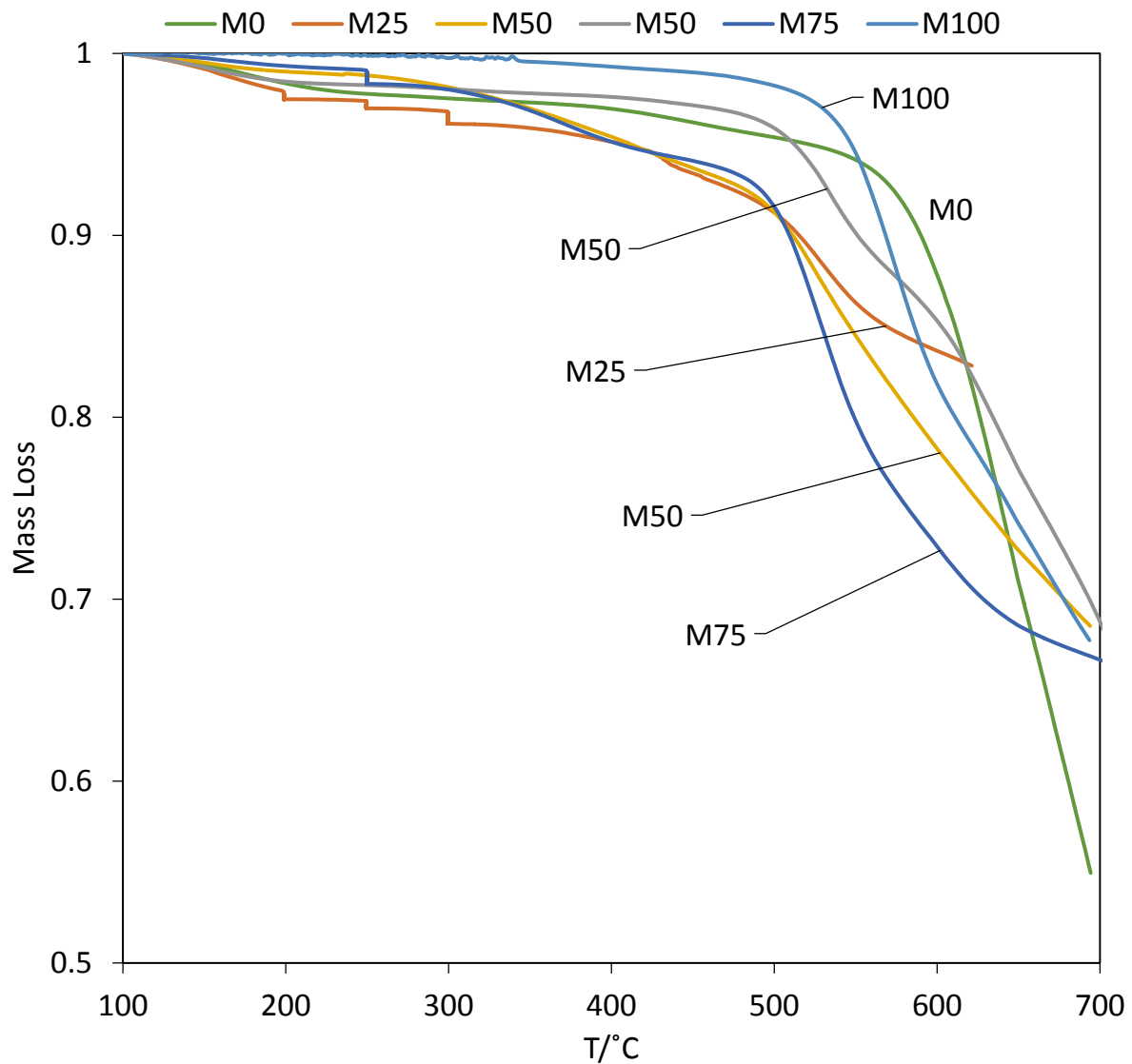


Figure C.2 TGA Mass Loss Curve in air for Matrimid/PBI Blend Film. The mass loss shifts at 200, 250, 300 °C were because of the samples had been hold at those temperature for half an hour

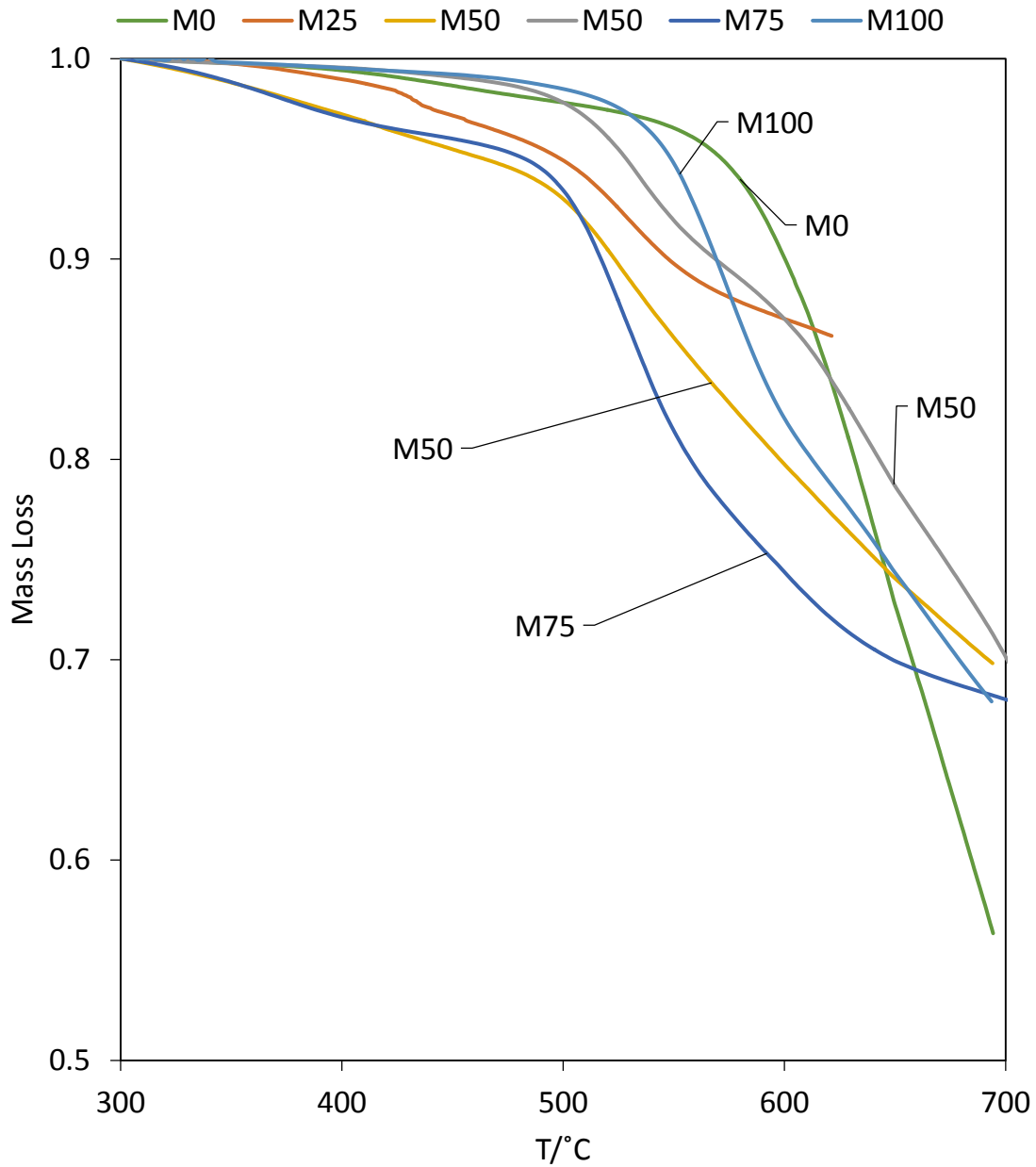


Figure C.3 TGA Mass Loss Curve in air for Matrimid/PBI Blend Film. The mass loss of Figure C.2 was normalized to be 1 at 300 °C